CHARACTERIZATION OF NANOCARBON-REINFORCED AND NEAT ADHESIVES IN BONDED SINGLE LAP JOINTS UNDER STATIC AND IMPACT LOADINGS

by

Babak Soltannia

Submitted in partial fulfilment of the requirements
for the degree of Master of Applied Science

at

Dalhousie University
Halifax, Nova Scotia
August 2013

Dedicated to my parents Iran and Davood and my lovly wife, Safa who taught me the value of unconditional love.

TABLE OF CONTENT

LIST OF TABLES

LIST OF FIGURES

ABSTRACT

Crashworthiness, damage tolerance, energy absorption capability and safety are all important factors in the design of light-weight composite structures. Furthermore, in order to make such structures lighter and more resilient and to avoid stress concentrations that can occur with mechanical fasteners such as bolted or welded joints, it is preferable to mate the structure's various components with adhesively bonded joints. However, a comprehensive understanding of the response of bonded joints subjected to loadings with various rates is of paramount importance in developing reliable structures.

In the first part, the effects of high loading rates (HLR) on the performance of nano-reinforced adhesively bonded single-lap joints (SLJs) with composite adherends are systematically investigated, and will be compared to the static and quasi-static results. The results of the impact tests revealed the loading rate sensitivity of the adhesive/joints, as well as the positive influence of nano- reinforcement.

In next part, the effects of nano reinforcement on the mechanical response of adhesively-bonded SLJs with composite adherends, subjected to different loading (strain) rates are systematically investigated. The results are then compared to those of neat thermoset resin and thermo-plastic adhesive. More specifically, in both parts, nano-reinforced and neat resin bonded joints mating carbon/epoxy and glass/epoxy adherends were subjected to tensile loadings under 1.5 and 3 mm/min and tensile impacts at a loading rate of 2.04E+5 mm/min. In some cases, additional tests were conducted under 15, 150, and 1500 mm/min to obtain additional properties gained using the nano-reinforcements for use in the further numerical investigations. In both parts, the HLR tests were conducted, using a modified instrumented pendulum equipped with a specially designed impact load transfer apparatus. The dispersion of nanoparticles was facilitated using a mechanical stirrer and a three-roll mill machine. The results of the impact tests revealed the positive influence of nano reinforcements on the loading rate sensitivity of the joints. In all, the overall stiffness and strength of the joints increased as the nano reinforcement and loading rates were increased. In both parts, the failure surfaces were then examined with a scanning electron microscope to observe the distribution of the nanoparticles, and study the failure mechanism.

ACKNOWLEDGEMENTS

I would like to express my sincere feelings of gratitude towards the merciful God for His blessing galore upon me, and His gracious kindness by giving me a wonderful family, professional and supportive supervisor and many more things which He gave them to me that I cannot count them one by one.

I would like to gratefully express my appreciation towards my thesis supervisor Professor Taheri, for his invaluable supports and assistance through this study. I am heartily thankful to him, whose encouragement, guidance and support from the initial to the final level enabled me to develop an understanding of the subject. I am also grateful to him for careful reading and minute criticism of this thesis.

My gratitude goes to my committee members, Dr. T. Koko, and Dr. M. Smith, for their direction, dedication, and their invaluable advice along this thesis. Also, I would like to thank the faculties and staff and lab technicians of the department. The Natural Science and Engineering Research Council of Canada's financial support for this research work is gratefully acknowledged. In addition I wish to thank all friends and colleagues for their supportive friendship and help, and fruitful discussions in particular.

I wish to express my gratitude to my parents Iran and Davood, and my lovely wife Safa, and my brother Mohammad Reza for their moral supports and understanding, and for their solid supports in not leaving me alone in any aspects, facing and solving all obstacles, and to whom, I owe debt of gratitude.

Last but not least, I would like to express my gratefulness and regards to all of those who supported me in any aspect during the completion of the research and my appreciations always stay with them.

CHAPTER 1 INTRODUCTION

Most structures are comprised of several elements that have been more or less effectively mated to carry the requisite load, all the while aiming to prevent undesirable concentrations of stresses. The analysis, design, and construction of adhesively-bonded joints (ABJs) with fiber-reinforced polymer (FRP) composite adherends is more detailed undertaking compared to other forms of mechanical fasteners such as bolted or welded joints. Nowadays, the main thrust of research and industry is to use nano-particles to improve the mechanical properties of adhesives used to form ABJs. However, the use of these relatively novel materials adds greater complexity to the general study of the characteristics of ABJs. As a direct result of this complexity, the mode and failure mechanisms of ABJs – and especially those of nano-reinforced ABJs – remain relatively under-investigated.

Generally speaking, structural joints fall under three categories, according to their joining mechanism (i.e., adhesively-bonded, mechanically-fastened welded and bolted joints). This study focuses on the loading-rate (strain rate) effects and influence of various types of nano particles on the response of adhesively-bonded joints, investigated by experimental methods.

1.1 Introduction

Adhesively-bonded joints (ABJs) are becoming increasing popular for use in the oil and gas industry as well as in marine, offshore, and automotive industries. Their primary purpose in these fields is to effectively and efficiently join either metallic or FRP structural components. Adhesively-bonded FRPs provide numerous benefits, chief among which are superior strength and stiffness-to-weight ratios, excellent fatigue and corrosion resistance, controllable damage tolerance, and high energy absorption capabilities. These characteristics make ABJs more desirable means in joining FRP components in comparison to alternative mechanical fasteners [1-3]. Of vital importance in the design of structures that are primarily light-weight is that they also be crashworthy and have strong damage tolerance as well as energy absorption capabilities. Such safety requirements are particularly necessary for consideration in transportation applications. Nevertheless, the

use of adhesives in these and other applications has been hampered by the lack of available information related to the performance of ABJs at high and extremely high (e.g., impact) loading (strain) rates. It should be noted that the mechanical characterization of ABJs at high loading rates is immensely important in the design aspect of the technology [4].

As stated earlier, an emerging research area in this field in recent years has involved the effective application of nanoparticles to improve performance of adhesives. Although carbon nanofibers (CNFs) are both less expensive and more readily available, the nanoparticles most often discussed in today's scientific literature have been carbon nanotubes (CNTs). Ceramic nanotubes (e.g., zirconia, tungsten disulfide), and even whiskers (e.g., silicon nitride, silicon carbide, and alumina), which are used in various applications.

Iijima who is considered as the inventor of carbon nanotubes, attracted a great deal of interest in his work published in 1991. He mentioned that carbon nanotubes are basically sheets of graphite formed into tubes [18, 19]. Currently, there are two primary types of carbon nanotubes: single-walled nanotubes (SWNTs) and multi-walled nanotubes (MWNTs). SWNTs are composed of a single layer of graphene in a cylinder format, with a diameter of 1-2 nm and hemispherical end caps [19, 20]. MWNTs, as their name implies, have multiple coaxial graphene cylinders, each of which has an end cap and an outer diameter of 3-10 nm. Weak Van der Waals forces between the layers necessitates that the tension loads be carried solely by the outer layer of the MWNTs [21]. The strength of individual MWNTs is gauged at around 150 GPa and their elastic modulus at approximately 900 GPa [22]. This is surprisingly robust, given their high degree of flexibility perpendicular to their longitudinal axis [23]. In addition, their desirable mechanical characteristics and length-to-diameter ratio make CNTs ideal candidates for composite reinforcement. However, to reap the greatest advantage in utilizing carbon nano-tubes, a strong interfacial bonding between the polymer matrix and CNTs would be a prerequisite [24].

Hsiao et al. [25]. showed that a joint's mechanical properties could be improved by inclusion of CNTs within an adhesive. For instance, the shear stress was more effectively transferred to the adherends (cohesive failure) simply by adding 5 wt% MWNT to an epoxy adhesive and thus enhancing the average shear strength of their ABJs by 45.6%. In ABJs hosting SWNTs, the adhesive layer provided the site for failure initiation and development.

1.2 Thesis Objective

Despite the large body of works conducted on the subject of adhesive bonding, to the best knowledge of the author no attempt has yet been made to address the subject of the loading rate effects of nano-reinforced, adhesively-bonded joints using graphene nano-platelets. The work undertaken in this thesis intends primarily to address this issue, with the aim of improving the current level of understanding of the mechanical behavior of adhesively-bonded joints, especially those made with adhesive that host nanoparticles.

In brief the overall goal of our study is to develop a relatively inexpensive and strong adhesive for common engineering applications where relatively thicker bond-lines are required (unlike in aerospace-related applications). Moreover, another objective was to explore the viability of nanoparticles as cost-effective reinforcements for strengthening and stiffening adhesives.

1.3 Thesis Organization

This thesis is divided into five chapters. It should be noted that this thesis is in "publishable/published manuscript" form. As a result, since each manuscript is formatted as a stand-alone journal publication, it may contain duplicate information that may appear in other parts of the thesis/manuscripts. . Moreover, the descriptions and information that were not appropriate to be included in a journal paper are provided in below.

Chapter Two contains a brief overview of the body of literature dealing with the subject of adhesively-bonded joints. The discussion begins with a review of the experimental works on the subject, with a focus on designing and analyzing adhesively-bonded joints and investigating the mechanical properties of adhesives.

Chapter Three discusses the loading rate effects on the mechanical behavior of adhesively-bonded joints. Details of the experimental program and the influence of the loading rate are presented in this chapter. The effect of different loading rates on adhesives and adhesively bonded joints are compared to the static loading rate (i.e., the baseline test).

In Chapter Four, the influence of nano-reinforcement on the performance of adhesives and adhesively-bonded joints is discussed. The analysis of the experimental results is based on the inclusion of the different weight percentages of three types of nano-particles. The results of the nano-reinforce adhesives and ABJ are compared against those of the neat adhesives used in this study.

The number of manufactured plates for preparing the dog-bone and rectangular shaped coupons and the single-lap-joints used in the project are reported in Tables 1.1-1.3.

Table 1.1 Number of manufactured plates used to prepare the single-lap

Plates			
Dimension	**Adherend**	**Adhesive**	**no. of specimen**
(35 X 35 X 0.5) cm^3	CFRP/ Epoxy	Huntsman	8
	Glass/Epoxy		8
	Quasi-Isotropic		1
Total Number of Specimens:			17

Table 1.2 Number of dog-bone shape tensile coupons tested under different loading rates.

Tensile Dog-bone Coupons		
Adhesive	**Strain Rate (mm/min)**	**no. of specimen**
WS 20% wt Q-Cell	1.5	3
WS 10% wt Q-Cell	1.5	3
WS 5% wt Q-Cell	1.5	3

Tensile Dog-bone Coupons		
Adhesive	**Strain Rate (mm/min)**	**no. of specimen**
WS With 0.5% wt CNF	1.5	3
WS With 0.5% wt CNT	1.5	3
Neat WS	1.5-15 -150 -1500	12
WS With 0.25% wt GNP	1.5-15 -150 -1500	12
WS With 0.5% wt GNP	1.5 -15 -150 -1500	15
WS With 1.0% wt GNP	1.5-15 -150 -1500	12
Total Number of Tests		66

Table 1.3 Number of single-lap-joint specimens tested under different loading rates.

Single Lap Joints			
Adherend	**Adhesive**	**Strain Rate (mm/min)**	**no. of specimen**
CFRP	WS 20% wt Q-Cell	1.5 -3.0	6
	WS 10% wt Q-Cell	1.5 -3.0-2.04E5	9
	WS 5% wt Q-Cell	1.5 -3.0-2.04E5	9
	WS With 0.5% wt CNF	1.5 -3.0-2.04E5	9
	WS With 0.5% wt CNT	1.5 -3.0-2.04E5	9
	Neat WS	1.5 -3.0-15 -150 -1500 -2.04E5	21
	WS With 0.25% wt GNP	1.5-15 -150 -1500	12
	WS With 0.5% wt GNP	1.5 -3.0-15 -150 -1500 -2.04E5	21
	WS With 1.0% wt GNP	1.5-15 -150 -1500	12
	Plastic Welder	1.5 -3.0-2.04E5	9
GFRP	WS 20% wt Q-Cell	1.5 -3.0	6

Single Lap Joints			
Adherend	**Adhesive**	**Strain Rate (mm/min)**	**no. of specimen**
	WS 10% wt Q-Cell	1.5 -3.0-2.04E5	9
	WS 5% wt Q-Cell	1.5 -3.0-2.04E5	9
	WS With 0.5% wt CNF	1.5 -3.0-2.04E5	9
	WS With 0.5% wt CNT	1.5 -3.0-2.04E5	9
	Neat WS	1.5 -3.0-15 -150 -1500 -2.04E5	21
	WS With 0.25% wt GNP	1.5-15 -150 -1500	12
	WS With 0.5% wt GNP	1.5 -3.0-15 -150 -1500 -2.04E5	21
	WS With 1.0% wt GNP	1.5-15 -150 -1500	12
	Plastic Welder	1.5 -3.0-2.04E5	9
Total Number of Tests:			234

Finally, the summary and conclusions of the results are outlined in Chapter Five, where recommendations for future work are also proposed.

CHAPTER 2 LITERATURE REVIEW

2.1 Introduction

Throughout human history, adhesives have been used in various technological applications. Most adhesive were historically derived from natural products, such as skin, bones, and plants; however, since the 1900s, adhesives have been mainly based on chemical products like synthetic polymers. Today, nearly all industrial applications use adhesives and sealants for bonding purposes [1].

One of the most important outcomes in the use of adhesives for forming adhesively bonded joints (ABJ) is the elimination of stress concentrations associated with bolted and welded joints. There are three primary considerations in producing an ABJ. The first involves getting the adhesive into a semi-solid phase in order to spread the adhesive and "wet" the adherend's surface properly. In this phase, an intimate molecular contact is formed between the adhesive and adherends. The second consideration is to ensure that adhesives are in the form of monomers, as their molecular weight will increase after being polymerized into polymers. The third consideration when producing an ABJ is to keep in mind that the overlap region requires external pressure to ensure better consolidation of the adhesive. The loading capacity of the joints and their durability depend on various factors such as joint configuration, applied loads, and environmental conditions. Therefore, to obtain optimal results with adhesive bonding technology, developers should have in-depth knowledge in various scientific fields such as mechanical engineering, material engineering, chemistry, and physics of polymers [2].

As stated earlier, adhesively bonded joints are increasingly being used in engineering applications as an alternative to conventional mechanical fasteners. ABJs offer many advantages over mechanical joints, such as higher stiffness and load transmission, weight reduction, and the provision of more uniform stress distribution along the bonded areas. The polymeric basis of adhesives also enhances the damping properties of ABJs and results in higher fatigue strength. In addition, ABJs can mate dissimilar materials, even those with different coefficients of thermal expansion because of their inherent flexibility

in compensating for the difference. Although their strength is much lower than that of metals, structural adhesives can efficiently bond thin plates, which is one of their major applications. The joint design is also tailorable, and thus new materials and approaches can be considered. A good example of this technology is fiber-reinforced sandwich structures, which consist of a honeycomb core and a laminate composite skin. Since ABJs do not require holes for rivets or bolts, they produce extremely smooth surfaces. They also forge strong contact between bonded surfaces and resist corrosion, all of which is highly advantageous from a structural perspective.

Despite their numerous advantages, ABJs do have some deficiencies that need to be addressed in future research and technological developments. For instance, the peeling stress needs to be decreased, as the inherent stress concentration within small areas in ABJs reduces their strength. Some other disadvantages of ABJs include their poor resistance to hygrothermal and cryogenic conditions and the fact that bonding will not occur instantaneously, requiring specific jigs to keep the adherends aligned during the bonding process. A further economical disadvantage of some adhesives is the required heat for their curing process.

Surface preparation, which usually involves mechanical abrasion and chemical treatments, plays a significant role in ensuring a durable joint and suitable interfacial strength. Since they are not separable, ABJs require a more rigorous inspection procedure compared to mechanically fastened joints. For this reason, nondestructive methods are often used to ensure the appropriate quality is achieved. Furthermore, there are no simple rules of thumb in designing ABJs, as is the case with welded, bolted and riveted joints. This fact alone makes ABJs more complicated overall [1].

In summary, ABJs are used in numerous industries and have a wide range of applications. In addition to their many perceived benefits such as superior fatigue strength, ABJs also have a few disadvantages, like delayed bonding time. Nevertheless, ABJs are increasingly used in aerospace, automotive and rail industries as well as in electronics and infrastructures that require technology that is lighter, stronger, and more durable.

2.2 Adhesives

As stated earlier, adhesives in various formats have been utilized for bonding purposes since the dawn of recorded history. However, highly effective methods of bonding have only been developed since the mid-1940s as a result of the evolvement of synthetic polymers as a precursor for technological applications. Synthetic polymers are capable of adhering most materials and enable the transfer of considerable magnitudes of load. The oldest definition of adhesives is attributed to Kinloch, who defined adhesives as a material that joins adherends and resists the dismantling of the adherends [3]. Among adhesives, those that can carry significant loads and in some cases improve the stiffness and strength of the structures are referred to as structural adhesives [4].

Adhesives are available in a wide range of strengths, from 5 MPa to 50 MPa, and in a variety of materials, from polyurethane to epoxy. Prior to being bonded, surfaces are called substrates; after bonding, they are referred to as adherends. Both sealants and adhesives are based on the concept of adhesion. More specifically, while cohesion describes the intermolecular forces inside one material, adhesion involves intermolecular forces established between the interfaces of two substances. These intermolecular and cohesion forces are mainly Van der Waals-type forces [5]. Substances bonded with adhesives or sealants work through either interface or cohesion, or a combination of them. The interphase refers to the zone enclosed by the adhesive and the adherend in general, whereas the interface refers to the contact surface of the adhesive and adherend within the interphase. Mechanical and chemical properties of the interphase differ from those of the adherend or neat adhesive and thus play a significant role in determining the adhesive bond's strength.

2.2.1 Adhesive Types

Structural adhesives include epoxies (thermal resistant and with high strength), acrylics (versatile adhesives with fast bonding capability, requiring less surface treatment), cyanoacrylates (able to cure plastic and rubber quickly but weak resistance to temperature and moisture), polyurethanes (flexible at low temperatures and fatigue-resistant), anaerobics (suitable for bonding cylindrical substrates), silicones (excellent sealant for

low stress applications, offering high temperature resistance and a high degree of flexibility), and high-temperature adhesives (polyimides, bismaleimides, and phenolics). The increasing use of high-temperature resin-matrix systems for composite materials has required the evolvement of compatible and equally thermally stable adhesive systems. Epoxies that are commonly used as composite matrices are also very frequently used to bond composites because of the compatibility between the resin and adhesive [1].

To acquire a perfect bond, an appropriate adhesive must be used. Choosing a proper adhesive is usually a rigorous process due to the wide range of available options. There is as yet no universal adhesive that would be suitable for all applications. Hence, the choice of an adhesive depends on several factors, such as expected stresses and environmental conditions that the joint might undergo during its service life, gel-time, curing process, adhesive application method, and type of substrates and its material characteristics. The cost of an adhesive is an especially critical factor in adhesive selection.

Monitoring tests should be performed to analyze and assess different adhesion characteristics before an adhesive is allocated for an application, especially in the case of structural adhesives, where failures can have disastrous consequences. Adhesive properties can differ considerably; therefore, to evaluate the stresses and strains in ABJs that come in a variety of configurations, an adhesive's mechanical properties should be determined. These include the stress-strain curve, the modulus of elasticity, and the failure load and strain [6]. There are two approaches for evaluating an adhesive's mechanical properties: (i) conducting a series of base-line tests, which result in the evaluation of the neat adhesive properties, and (ii) utilizing the specially designed joint configuration with a thin bond-line.

A wide range of tests with specific specimens are needed to achieve adhesive properties, with the specified parameters being failure load and strain. The surface preparation should be adequate to ensure cohesive failure in the adhesive layer, and the test geometry should establish a pure state of stress, uniformly distributed across the contact surface and without stress concentrations through the bond-line [7].

Several ISO and ASTM standards have been developed recently to specify and empirically determine the characteristics of adhesives. The developed test methods are generally used to obtain peel, shear, tensile, compression strength, fatigue, and dynamic properties. For example, the conventional test method used for evaluating fracture toughness is the double cantilever beam (DCB) test (ASTM D3433), the lap shear test assesses strength, and the wedge tests evaluates resistance to solvents [35-42].

There are several test methods for characterizing the shear properties of adhesives, such as the butt torsion test (in the form of a napkin ring or solid specimen), torsion of neat adhesive, the notched beam shear method (Iosipescu), the notched plate shear method (Arcan), and the thick-adherend shear test method (TAST) [1, 35-42]. The TAST (ISO 11003-2:1993) is usually the preferred method for characterizing design parameters, since thick and rigid adherends decrease (but do not eliminate) the peel stresses. The state of stress is predominantly shear, but there are also peel stresses at the end of the overlap. Hence, as stated earlier, to implement the TAST method for characterizing the shear properties, the most commonly used adhesive bond test configuration is the single-lap tension test.

2.2.2 Surface treatment

In general, surface treatment refers to the physical and chemical processes that are required to prepare the regions of substrates receptive to the adhesive. A substrate's surface quality plays a significant role in the bond strength and is probably the main factor affecting the integrity of an ABJ [8]. Proper surface treatment enhances the mechanical properties of ABJs and results in achieving maximum mechanical strength. In this regard, chemical treatments affect the durability of ABJs by augmenting surface integrity [9].

Davis and Bond studied the parameters influencing the endurance of ABJs, utilizing the 'clean surface concept' approach. The most popular misconception in surface treatment is that the only necessity for obtaining an appropriate bond is a clean surface. Certainly, a clean surface is a primary condition for adhesion, but it is not an adequate condition for

bond durability. Structural adhesives often function as a result of the chemical bonding formation between the adhesive components and substrate surfaces [3]. These chemical bonds will transmit the load between the adherends. Poor manufacturing processes (e.g., inappropriate surface preparation) are often the primary reason for the failure of ABJs [9].

Regular surface preparation consists of conventional abrasion/solvent cleaning methods for thermoset composites. However, thermoplastic composites need chemical treatment and surface topographical changes to assure desirable bond strength. For these composites, the essential objective of surface preparation is to enhance the surface energy of the substrates. Proper surface preparation increases surface tension and reduces the water contact angle, thus improving the bond strength [10].

A wide range of surface preparations have been suggested with varying levels of success with respect to enhanced surface tension. The two main preparations are: (i) changing the surface chemistry, and (ii) increasing the surface roughness. Abrasion/solvent cleaning, grit blasting, acid etching, tear-ply, peel-ply, laser treatment, and plasma treatment are the most common types of surface treatments. Since an epoxy surface bonds well to other epoxies, no chemical treatment is needed, and the required abrasion should only remove the surface of the resin without damaging the fibers [9].

2.2.3 Nanocomposite adhesives

Since the advent of "nanotechnology", nanocomposite adhesives have been increasingly used in many advanced applications in naval, automotive, aerospace, construction, and medical industries. Kim and Reneker reported that Young's modulus of the nanofiber-reinforced composite was ten times greater than that of the neat adhesive [11]. However, there are as yet only limited studies on the mechanical properties of nanofiber adhesives and nanofiber composites [12].

Since the adherends are usually much stronger than the adhesives used to bond them, one option for enhancing joint properties is to reinforce and toughen the adhesives. Qian et al.

mentioned that nanotubes (CNTs) could enhance the composite strength by as much as 25% [13]. However, Yu et al. reported that multi-wall nanotubes (MWNTs) were restricted in their usages due to poor inter-shell interaction [14], and that single-wall nanotubes (SWCNTs) are expensive and difficult to produce. Other types of reinforcement for nanocomposites consist of carbon nanofibers (CNFs) and graphite nanoplatelets (GNPs). CNFs also have excellent characteristics and can be implemented as reinforcements in various types of matrices.

Rothon and Hancock pointed out the fallacy of the widespread assumption that nanoparticles are expensive and polymers are cheap [15]. As nanoparticle production expands, nanoparticles are increasingly available in large quantities and at a reasonable price. The cost of nanoparticles greatly depends on the type and purity of the material. Nano-clays can cost as little as $7/kg [16]; however, a kilogram of carbon nanotubes costs between $8,000 and $100,000, while graphene nano platelets (GNPs) cost $2/kg [17].

2.2.3.1 Nanotubes and Nanofibers

The cylindrical nanoparticles most widely discussed in the scientific literature are carbon nanotubes (CNTs), although carbon nanofibers (CNFs), which have a larger diameter, are less expensive and available in greater amounts than carbon nanotubes. Ceramic nanotubes (e.g. zirconia, tungsten disulfide) or whiskers (e.g., silicon nitride, silicon carbide, and alumina) are also available.

The application of carbon nanotubes (CNTs) was first investigated by Iijima in 1991 and later by Iijima and Ichihashi in 1993. CNTs are sheets of graphite rolled into tubes [18, 19]. There are two main kinds of carbon nanotubes. The first are single-walled nanotubes (SWNTs), which consist of a single graphene layer typically wrapped into a cylindrical shape and having a diameter of 1-2 nm and hemispherical end caps [19, 20]. The second type of carbon nanotubes are multi-walled nanotubes (MWNTs). These contain a number of coaxial graphene cylinders, each with an end cap and an outer diameter of 3-10 nm. Due to weak Van der Waals forces between the layers, tension loads are carried only by the outer layer of an MWNT, and consequently the stress will not be transferred to the

inner layers [21]. Even though they are quite flexible perpendicular to their longitudinal axis [23], the strength of MWNTs is estimated to be up to 150 MPa and their elastic modulus up to 1 TPa [22]. Furthermore, their superior mechanical characteristics and optimal length-to-diameter ratio make CNTs highly appropriate candidates for composite reinforcement. To completely benefit from the exceptional mechanical properties of CNTs, however, a strong interfacial bonding between the polymer matrix and CNTs is essential [24].

Hsiao et al. demonstrated that utilizing CNTs in conjunction with an adhesive could improve the mechanical properties of the joint. By adding 5 wt% MWNT to the epoxy adhesive, the shear load was efficiently transferred to the adherends (cohesive failure), and thereby the average shear strength of the bonding increased by 45.6%. In the case of SWNTs, failure initiated and developed within the adhesive layer [25].

An important factor to consider in the design of lightweight vehicles with fiber-reinforced polymer composites (FRPs) is the vehicles' crashworthiness. In other words, the structural joints should have the ability to absorb a large amount of energy to accommodate the required safety factors. Currently, there is a noticeable increase in the application of ABJs in the automotive industry, specifically with the aim of improving passenger safety. Therefore it is also necessary to study the dynamic response of the ABJs used in such applications. The study of the effect of loading rate on the response of ABJs would enable the design of structures that would not fail unexpectedly and catastrophically when subjected to high loading rates.

The dynamic behavior of ABJs made of graphite/epoxy unidirectional plies was studied by Galliot et al. A drop weight machine was used to subject the specimens to a suddenly-applied tensile load (impact). The results were compared to the results of quasi-static tests in order to establish the rate-sensitivity of the adhesive. An average increase of more than 50% in strength was observed in favor of the specimens that were subjected to impact load, showing that the absorbed energy, the failure load, and the stiffness intensified with

increasing loading rate. Nevertheless, the joint behavior remained qualitatively the same under the quasi-static and dynamic loading cases [26].

Harris and Adams used a modified Izod pendulum in their impact tests to associate the geometry of single-lap joints (SLJs) with aluminum adherends. Single-lap joints formed by various types of adhesives were tested under quasi-static and impact, at a velocity of 1.4 m/s. The results indicated that the joint strength was not considerably influenced by the loading rate, and that for the majority of the tested adhesives, the impact strength was insignificantly higher than the static load [27]. However, Gilliot et al. observed that the adhesive did not apparently contribute to the energy absorption of their ABJs, and that the deformation of the adherend material absorbed the energy. Baseline quasi-static loading tests were also conducted on a universal tensile machine (Instron) at a loading rate of 0.3 mm/min (5×10E-6 m/s) [26].

Goglio and Rosetto used the instrumented pendulum to study the effects of geometrical parameters on the mechanical response of adhesively-bonded steel joints. In their investigation, they joined the specimen to a swinging hammer while the striker was clamped. The results indicated that joint strength evolved under the dynamic condition. They also demonstrated the significant effects of their adhesive's thickness [28].

Ger et al. implemented a "slingshot-type" high velocity loading machine to validate the dynamic tensile behavior of FRPs. The results indicated that the dynamic loading rate resulted in a catastrophic failure. They also mentioned that the dynamic failure load was higher than that under the quasi-static test [29].

Using a drop weight tower to develop high loading rate and to conduct quasi-static tests, Brown et al. showed that the compression and tensile strengths and modulus of elasticity were enhanced by the increasing loading rate. The tests were performed on an Instron™ electro-mechanical universal test machine at a crosshead speed of 5 $mm.min^{-1}$ [30].

Hsiao et al. experimentally investigated CNTs' effect on the performance of ABJs consisting of carbon fiber reinforced composites. They reported that, by adding only 1 wt% of MWNT in epoxy adhesive, the shear strength of joint was increased by 31.2%, and that by adding 5 wt% MWNT, the shear strength was increased by 45.6% [25].

It is important to mention here that there is an optimum amount of nanofiller at which the adhesive properties can be maximized. At higher contents, the properties actually degrade due to the change in the failure mode of the joints. Commonly, the bonded joints with neat adhesives fail at the interface, while nano-reinforced adhesively bonded joints fail mainly in cohesive failure mode (which occurs in adherends). However, at relatively high quantities of nano-reinforcement, the joint failure mode becomes interfacial again. It is clear that MWNT particles enhance the strength and toughness of epoxies because nano particles strengthen the polymeric chains of the resin and resist crack initiation and propagation [31].

In 2011, Srivastava investigated the effects of adding 3% MWNT to ABJs with similar and dissimilar substances as adherends. The results generally showed that the toughness and strength of the epoxy resin were increased. In particular, the interface bonding strength of the ABJs with similar adherends was much higher than those with dissimilar adherends [32].

2.2.3.2 Graphene nanoplatelets

Graphene nanoplatelets (GNPs) generally consist of piled platelets that are exfoliated or intercalated by a polymer during processing. The thickness of these plate-like particles is approximately 1nm and their lateral dimensions can vary from 25 nm to a micron, which indicates that they have large aspect ratios [33, 34]. A regular Van der Waals gap, called the "gallery" or "interlayer" [24], has been observed in between the layers. To make GNPs, the graphite is intercalated by a special acid treatment process, followed by exfoliation prompted by a thermal shock applied at a temperature of around 600°C.

To obtain a reinforced adhesive with the best properties, the nanoparticles should be well dispersed within it, and each particle should be immersed properly in the polymer. This is

a very challenging process, because the formation of agglomerations can act as defect regions, reducing performance instead of enhancing it.

2.3 Adhesively bonded joints

As stated earlier, adhesive bonding technology is increasingly being used to make structural components. Single-lap joints, double lap joints, L-joints and T-joints are some of the conventional joint configurations for joining structural elements. Single- and double-sided repair configurations can also be conducted when adhesive bonding is applied to reinforce or repair structural damages and defects [1]. Figure 2.1 illustrates various types of adhesively bonded joints.

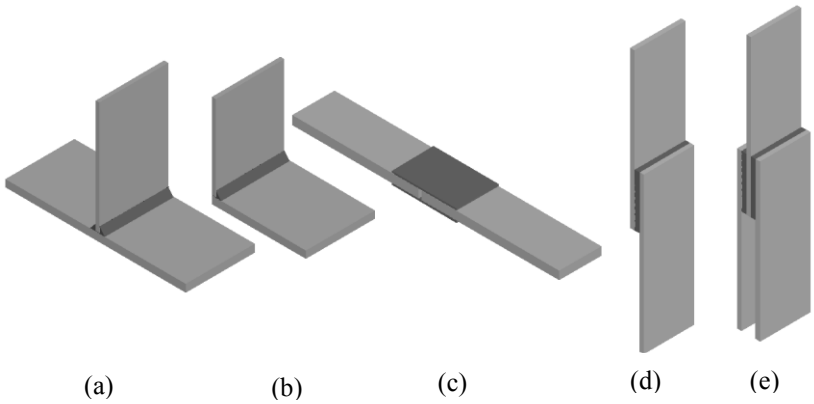

Fig. 2.1 Different types of adhesively bonded joints, (a) T-joint, (b) L-joint, (c) double strap joint, (d) single-lap joint, (e) double lap joint.

Although, when being analyzed, lap-type joints can be modeled as two-dimensional (2D), stress variations in such joints are three-dimensional (3D) in nature. Numerical methods, such as the finite element method (FEM), have been used to effectively model 3D problems of adhesively bonded structures. Nevertheless, closed-form solutions are essential for preliminary designs, as they can produce meaningful results in a timely manner. Hence, several attempts have been made to improve the analytical approaches for evaluating stress distribution in ABJs.

An adhesive layer usually has a thickness measured in fractions of a millimeter. For instance, a bond-line thickness of about 0.2 mm is commonly used in aerospace ABJs. The stress state in the adhesive layer is relatively complex in 2D or 3D problems, and

though adherends are usually modeled as beams or plates, the adhesive layer is much thinner in practical ABJs in comparison to the adherends. Consequently, the adhesive layer is typically modeled by an infinite number of springs or an appropriate interface, with the assumption that only normal (through-thickness) and shear stresses exist within the adhesive layer, and that they remain constant across the thickness and change only along the bond-line length. This assumption is used to develop 1D analytical solution.

A single-lap joint (SLJ) is considered the simplest geometric configuration for adhesively bonding structural components. The SLJ configuration has been extensively used as a standard test specimen to investigate the responses of ABJs and has been shown to be representative in modeling the influence of the fundamental properties and main factors in bonded lap joints [1].

2.3.1 Modeling adhesive stresses

Various models have been recommended to estimate stresses in the adhesive layer of ABJs. The simplest is the average shear stress model, which assumes that the adhesive is a continuous shear spring and the substrates are rigid bars. This assumption arises from the fact that adherends are generally thick and stiff and do not deform significantly, and that only the adhesive deforms, as it is relatively softer.

The results can be extended to the plane strain state by altering the relevant parameters. Here, symmetric composite adherends are assumed to have the same stacking sequences. The results can be directly used for joints with equivalent properties or isotropic adherends. The shear lag model offered by Volkersen is based on the above assumptions. In this model, the shear stress is not constant along the overlap (bond) length and increases at the ends of the overlap region [35].

Goland and Reissner suggested an adhesive-beam model for SLJs in which the elastic medium and Euler beam theory were used to model the adhesive and adherends, respectively. It is necessary to mention that Goland and Reissner's stress analysis is only applicable to ABJs formed by isotropic materials [36].

For thin layer adhesives (i.e., <0.3 mm), a model with constant peel and shear stresses can be implemented to express the overall structural performance of ABJs. In other words, since the adhesive stresses are not uniform throughout the thickness (even in very thin adhesive cases), the peel and shear stresses should be considered as an approximation of those in the adhesive mid-plane.

In contrast, the constant adhesive model should not be applied for modeling a relatively thick adhesive layer, as the peel and shear stresses are not constant within the overlap region and thus and the axial stress may not be neglected [37, 38]. To evaluate the stress variation across the adhesive thickness and free edge stress in the adhesive ends, a 2D elastic model should be implemented. Allman, and later Chen and Cheng, applied a constant shear stress and linear variation assumption for the peel stress through the adhesive thickness [39, 40]. Ojalvo and Eidinoff, followed by Carpenter, assumed constant peel stress and linear variation of shear stress across the adhesive thickness [37, 41]. A few decades later, Luo and Tong adopted linear and higher order variations of peel, shear, and axial normal stresses through the adhesive thickness [38].

Adams and Mallick and Zhao and Lu proposed analytical models for ABJs based on the 2D elastic theory by assuming that both adherends and adhesive are considered as elastic media. Although these models can be used for joints with thick adhesive, this type of analytical solution is quite complex and essentially impractical [42, 43]. Therefore, it should be mentioned that by using different methods, analytical solutions for ABJs can be obtained with or without consideration of geometrical nonlinearity.

The eccentric load path is one of the most unique and complex features of SLJs. It may result in geometric nonlinearity that would require an iterative solution (load updating). Goland and Reissner performed an uncoupled analysis for the load update and adhesive stresses. In their proposed formulation, the overlap was assumed as an isotropic beam for the purpose of the load updating [36]. However, in most studies, researchers have included end tabs to eliminate the eccentricity.

In their study of SLJs, Harris and Adams applied a geometrically nonlinear finite element analysis (NFEA). They recognized a small inconsistency in the shear stress but large discrepancies in the adhesive edge moment and peel stress by comparing the numerical results of Goland and Reissner with those of the NFEA.

2.3.2 Analytical approaches for treating ABJs with material nonlinearity

In the strength analysis and design of ABJs, material nonlinearity should also be taken into consideration, since ductile or soft adhesive materials behave elastic-plastically. In addition, as a result of singular features and the stress concentration of ABJs, stresses near the edges of the overlap region may go beyond the elastic range. Hence, when analyzing ABJ, including a nonlinear material model is imperative. In fact, accounting for material nonlinearity is usually done for all ABJ constituents, though based on the usually lower strength of adhesives, the stress-strain response of adherends would be within the linear regime, in which case just the adhesive material nonlinearity is usually considered.

Hart-Smith modeled the response of single-lap joints by considering linear material property for the adherends and adhesive peel stress, and the linearly elastic-perfectly plastic model to simulate the adhesive's shear stress-strain relationship [44]. Grant and Teig conducted multiregional material nonlinearity for their adhesive by dividing it into several zones and applying the shear lag model to each zone. The resulting governing equations were solved numerically [45].

Delale et al. considered a strain energy function to identify stress-strain relationships when performing their nonlinear analyses of SLJs [46]. Nonlinear material analyses of unbalanced lap joint under general loading conditions were also carried out by Bigwood and Crocombe. In their study, adhesive material was analyzed based on the plastic deformation theory, and the adherends were assumed as linearly elastic plates. The stress-strain curve of their adhesive was described using a piece-wise continuous mathematical formulation, with the adhesive yielding considered to follow the von Mises yield

criterion. They constructed a system of six simultaneous nonlinear differential equations (NDE) in agreement with the predefined stress-strain relationship and solved the NDEs by the finite difference method (FDM) [47].

Yang et al. derived an analytical formulation to describe the adhesive stress and strain relationship. Based on their model, adherends were assumed as a laminated anisotropic plate and the adhesive governing equation was developed using the elastic-perfectly plastic constitutive model. The von Mises yield criterion was also implemented in the adhesive plastic deformation. They constructed and numerically solved coupled differential equations of their single-lap joints and also conducted the nonlinear material FEA for comparison [48]. A few years later, Lee and Kim derived a closed-form analytical solution for the analysis of symmetric single-lap joints with material nonlinearity considerations. They investigated the use of the elastic-perfectly plastic material model for the adhesive and analyzed the peel and shear stresses independently [49].

2.4 Finite element modeling

The advancement in accurate design and predictive techniques has gradually resulted in the more effective use of adhesives and FRPs. To design ABJs optimally and thereby to increase their use in joining structural components, it is essential to be able to accurately analyze them. This means that stresses and strains should be evaluated under given loading conditions, and approximate failure limits need to be estimated. There are two basic mathematical models for the analysis of ABJs: numerical methods (i.e., mainly the finite-element analyses) and closed-form solutions (i.e., analytical methods) [1].

Nowadays, advancements in numerical modeling have resulted in the development of accurate numerical models for capturing the response of ABJs. For example, cohesive zone models (CZMs) have been developed to simulate damage (crack) initiation and propagation and to predict the failure mode of ABJs [50, 51]. The virtual crack closure technique (VCCT) has also been widely implemented in numerical approaches to evaluate the strain energy release rate (SERR) in ABJ [52, 53]. The main benefit of a

cohesive element is that it can be designated to a zero or near-zero thickness without causing any computational issue (i.e., a singularity that would be created as a result of using a zero-dimension element) [54].

Shahin and Taheri developed a comprehensive analytical model to specify the SERR in ABJs with different geometries (i.e., SLJs and double cantilever beam specimens), based on Irwin's virtual crack closure integral (VCCI) and the asymptotic analysis of adhesive layer stresses. Their results were used to explain the effects of edge shear force on total SERR, and their solution provided fairly accurate predictions that were in good agreement with their finite element analysis [55].

Mehrabadi also studied the failure modes of adhesively bonded composite joints experimentally and numerically. The mentioned model used to simulate the response of the adhesive was an elastic-traction material, which recorded the failure of the cohesive elements. The adhesive joint was simulated with the Abaqus cohesive type element (COH3D8). The vital constitutive law expressing the cohesive elements failure mode is called the "traction-separation" (maximum tearing-separation force), which permits taking into account the effects of both failure caused by tangential interaction and normal (tearing) interaction. The obtained results, based on numerical analysis, were in good agreement with the experimental results [56].

Karkkainen and Yen derived a cohesive element-based model for simulating interface failure in the context of a butterfly-type Hopkinson Bar interface specimen. The modeling enabled an understanding of the crack propagation and dynamic in-situ stress state under impact loading and also helped determine the material response of high loading rates. An effective failure criterion was employed that provided good agreement with their experimental results obtained at multiple loading rates [54].

Several traction-separation cohesive laws were also implemented to cohesive elements based on FEM conducted by Lundsgaard et al. in order to model different bond states in end-notch flexural specimens [57]. Their results showed the significance of rate

dependency. Anvari et al. [58] investigated the influence of loading rate and triaxiality in terms of the variation in plasticity and stress state at higher energy states in a traction-separation formulation. In the same vein, Zavattieri et al. designed a cohesive interface between elastic-plastic solids with modified viscosity cohesive zone model of Xu-Needleman, identifying factors that prevented crack propagation and enhanced interfaces [59, 60].

The traction-separation model in the Abaqus finite element code [61] considers primarily linear elastic behavior followed by the inception and propagation of damage. Ma et al. used the zero thickness cohesive elements (COH3D8) of the Abaqus to model the delamination between the adherend layers, and conducted a traction-separation constitutive law to simulate the adhesive interfacial bonds. They developed an innovative stiffness reduction approach in consideration of the brittle and toughness properties of the fiber and matrix, respectively, to estimate the energy absorption characteristics and the relevant failure modes of composites. The results were in good agreement with their experimental data [62].

Broughton and Hinopoulos applied the finite element method (FEM) to demonstrate the influences of adherend characteristics, specimen geometry, and hygrothermal conditions on stiffness of ABJs and the stress state within the adhesive layer. Their parametric study showed that the strain and stress distributions were governed by the adhesives' thickness, adherends' material properties and thickness, and the applied load. They also noted that by increasing the joint stiffness (i.e. by increasing the adherends' thickness or the elastic modulus), the peak stresses at the ends of the overlap were decreased [63].

A model for the demonstration of the strain energy release rate (SERR) in ABJs with optional cracked laminate composite adherends using the beam theory was developed by Qin and Dzenis. The integrity of their proposed model was experimentally verified, with the results showing that SLJs were delamination tolerant. In other words, as the crack length increased, the magnitude of the maximum SERR decreased [64].

2.4.1 General considerations in analyzing ABJs

As mentioned earlier, several analytical techniques are currently used in the analysis of ABJs [35, 36, 65]. However, these techniques are restricted in their application based on the simplifying assumption made in their load condition, geometry, and material properties. Also as mentioned earlier, adherends and adhesives may present noticeable plastic deformation prior to failure, so one should use an appropriate non-linear material model for their analysis. In SLJs, adherend rotation occurs during loading, mainly near the overlap region, so nonlinear geometrical analysis should be conducted to accurately model the state of stress. Polymeric adhesives may also have a time-dependent response under loading. Thus, under specific situations a viscoelastic-plastic material model may be needed to demonstrate their response to loading.

In predicting the failure of ABJs, more traditional failure criteria such as the maximum-stress-and-strain-based failure criteria have been used. For example, Harris and Adams used these criteria to estimate the failure of SLJs, where a nonlinear FE analysis incorporating an elasto-plastic material model for the adherends and adhesive was performed. The selection of the strain- or stress-based failure criterion was dependent on the tensile uniaxial results. For a toughened adhesive in which the failure was ductile, the maximum-strain criterion was implemented, whereas a brittle failure was recognized for an un-toughened adhesive and thus the maximum stress criterion was incorporated. It should be noted that these criteria fall short of producing accurate results when stress singularities or highly localized stress concentrations are developed in ABJs [66].

To prevent the issues caused by localized stresses and to predict the strength of ABJs more accurately, Crocombe provided a standard yielding criterion. As such, joint failure was specified when a region of adhesive along the overlap deformed plastically and no further increase in the applied load could be sustained by that region. This phenomenon was conducted to simulate failure in SLJs lap shear test joints and double lap joints, and a good agreement between numerical and experimental results was obtained. The failure of the adhesive layer was characterized when the adhesive layer region became plastic and

was not able to carry a load. Thus, the proposed criterion may not be appropriate in joints that may undergo localized failure [67].

Dorn and Liu implemented a cumulative plastic strain-based criterion for predicting the strength of SLJs. A critical zone was specified and the maximum cumulative practical plastic strain in the critical zone was applied as a factor of strength estimation [68].

Failure methods based on strength are quite simple to implement in FEM. However, as they are mesh convergence-sensitive, a general mesh refinement study should be conducted to obtain accurate results. In problems with localized stress singularities, the failure criteria selection is more challenging. To solve this issue, one of the recommended solutions is to assign a fixed failure value for all elements in a specified area or to average over an area. Wahab et al. (2001) compared a large number of failure criteria, applying both the averaging and fixed-value methods [69].

2.4.2 Failure analysis of ABJs

Failure in ABJs can occur in the adherends within the adhesive layer (also referred to as cohesive failure) or at the interface of adhesive and adherends (interfacial failures).

The cohesive zone model (CZM) is a modeling approach for failure prediction that relies on hybrid concepts of fracture mechanics and stress analysis. CZM has been extensively applied in recent years to model crack initiation, growth and failure based on a traction-separation constitutive law. CZM permits multiple cracks to be simulated and it is not necessary to know the crack growth direction in advance. However, cohesive zone elements must be assigned to all potential crack paths regions. The most common shapes for the traction-separation law used for fracture prediction are the bilinear, exponential, and trapezoidal shape curves, as depicted in Figure 2.2.

As it is often difficult to specify the shape of the traction-separation law empirically, the variation of traction versus crack face separation is simplified and pre-assumed. Based on the nature of the problem, the influence of a traction-separation curve depends on

material behavior and specimen geometry. The shape of a traction-separation curve also affects the numerical performance of the simulation. It is worth noting here that using a trapezoidal traction-separation curve would create more convergence difficulties in FEA in comparison with a bilinear curve. Therefore, the selection of a CZM should be based on all aforementioned influencing parameters. A trapezoidal CZM is usually more practical for ductile materials, while a bilinear traction-separation shape is mostly assigned to composite and brittle materials. In a bilinear CZM, the primary response of the cohesive zone is elastic until a critical traction is approached and reached, after which the stiffness begins to degrade until failure. Fracture toughness refers to the area under the traction-separation curve known as the cohesive energy [1].

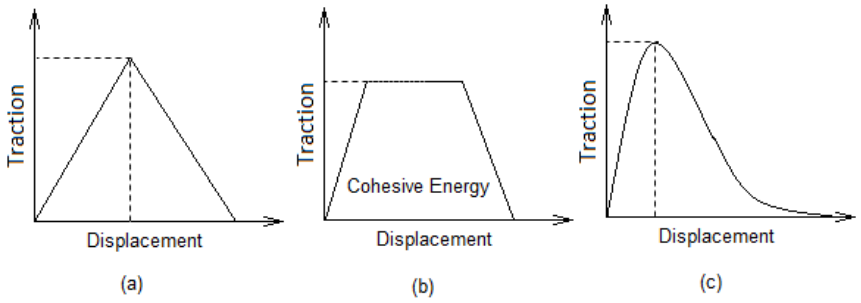

Fig. 2.2 Different types of cohesive zone damage models (a) Linear (b) Trapezoidal (c) Exponential [1].

As stated, one of the major restrictions of a CZM is that cohesive elements must exist on the crack path. This model is appropriate for crack or interfacial failure when the fracture does not depend on the substrates failure. Although many techniques have been proposed to calibrate the traction-separation laws, there is still no one standard method. Liljedahl et al. applied a method to demonstrate CZM parameters based on numerical and experimental results. A mixed-mode flexural specimen was tested under three-point bending conditions. A fracture mechanics-based FEM, along with the experimental results, were implemented to identify the adhesive's fracture energy, after which empirically specified fracture energy was applied to a CZM and the critical value of the tripping traction obtained by fitting the experimental data. Specified CZM factors were then employed to predict the behavior of the crack in SLJs. In this technique, joint geometry does not influence the developed CZM factors [70].

CHAPTER 3 STATIC, QUASI-STATIC, AND HIGH LOADING RATE EFFECTS ON GRAPHENE NANO-REINFORCED ADHESIVELY BONDED SINGLE-LAP JOINTS

Babak Soltannia[1] and Farid Taheri[1]

Department of Civil and Resource Engineering, Dalhousie University, PO Box 15000, 1360 Barrington Street, Halifax, NS, B3H 4R2, Canada

Submitted to the Journal of Reviews of Adhesion and Adhesives, August 2013

3.1 Abstract

Crashworthiness, damage tolerance, energy absorption capability and safety are all important factors in the design of light-weight composite structures. Furthermore, in order to make such structures lighter and more resilient and to avoid stress concentrations that can occur with mechanical fasteners such as bolted or welded joints, it is preferable to mate the structure's various components with adhesively bonded joints. However, a comprehensive understanding of the response of bonded joints subjected to loadings with various rates is of paramount importance in developing reliable structures. In this paper, the effects of high loading rates on the performance of nano-reinforced adhesively bonded single-lap joints with composite adherends are systematically investigated, and will be compared to the static and quasi-static results. Bonded joints mating carbon/epoxy and glass/epoxy adherends were subjected to tensile loadings under 1.5, and 3 mm/min, and the tensile impacts at a loading rate of 2.04E+5 mm/min. The high loading rate tests were conducted using a modified instrumented pendulum, equipped with a specially designed impact load transfer apparatus. The results of the impact tests revealed the loading rate sensitivity of the adhesive/joints, as well as the positive influence of nano-reinforcement. In all, that overall stiffness and strength of the joints were increased with increasing loading rates and nano reinforcement. It was also recognized that the effect of nano reinforcement in few cases overcame the effect of loading rate, meaning that even small increases in the amount of nano-particles can overcome enormous increases in loading rates using the same epoxy resin base. The observed failure mechanisms were examined with a scanning electron microscope.

Keywords
Graphene nanoplatelets; Nano composites; Loading rate; Impact; Single-lap joints.

3.2 Introduction

Adhesively bonded joints (ABJs) are increasingly being used in automotive, marine, offshore, and oil and gas industries to mate both metallic and fiber-reinforced polymer composite (FRP) structural components. Adhesively bonded FRPs offer numerous advantages, including high strength and stiffness-to-weight ratios, good fatigue and corrosion resistance, controllable damage tolerance, and high energy absorption capability, all of which makes them more efficient compared to other types of mechanical fasteners [1-9]. Crashworthiness, improved damage tolerance, energy absorption capability, and safety requirements are important factors in the design of light-weight composite structures, especially in automotive and marine vessel applications. However, a major concern in the use of adhesives in these applications has been the lack of an adequate database with regards to the performance of ABJ at high rates of loading and impact loads. Therefore, the mechanical characterization of ABJs at high loading rates is vital for achieving reliable designs.

The cylindrical nanoparticles that are most widely discussed in the scientific literature are carbon nanotubes (CNTs), despite the fact that carbon nanofibers (CNFs), which have a larger diameter and are less expensive, are more widely available. Ceramic nanotubes (e.g., zirconia, tungsten disulfide) or whiskers (e.g., silicon nitride, silicon carbide, and alumina) can also be used in these applications.

The use of carbon nanotubes, which are effectively sheets of graphite rolled into tubes [10, 11], was first proposed by Iijima in 1991 and later by Iijima and Ichihashi in 1993. There are two main kinds of carbon nanotubes. One type is single-walled nanotubes (SWNTs), which consist of a single graphene layer typically wrapped into a cylinder with a diameter of 1-2 nm and hemispherical end caps [11, 12]. The other type, known as multi-walled nanotubes (MWNTs), contains a number of coaxial graphene cylinders, each of which has an end cap and an outer diameter of 3-10 nm. Due to weak Van der Waals forces between the layers, the tension loads are carried only by the outer layer of

an MWNT, and thus stress will not be transferred to the inner layers [13]. The strength of an MWNT has been estimated to be up to 150 GPa and their elastic modulus up to 900 GPa [14], even though they are quite flexible perpendicular to their longitudinal axis [15]. Their superior mechanical characteristics and desirable length-to-diameter ratio make CNTs highly desirable for composite reinforcement. Nevertheless, to completely benefit from the exceptional mechanical properties of CNTs, a strong interfacial bonding between the polymer matrix and CNTs is essential [16].

Hsiao et al. demonstrated that utilizing CNTs in conjunction with an adhesive could improve the mechanical properties of the joint. By adding 5 wt% MWNT to the epoxy adhesive, the shear load was more efficiently transferred to the adherends (cohesive failure), thereby increasing the average shear strength of the bonding by 45.6%. In SWNTs, failure initiated and developed within the adhesive layer [17].

An important factor in the design of lightweight vehicles is the crashworthiness of composite structures. In particular, the structural joints should have the ability to absorb a large amount of energy to accommodate the safety factors and improve passenger safety. To accomplish this, the dynamic behavior of the adhesively bonded joints used in such applications need to be studied, as the effect of loading rate on the response of ABJ would enable us to design structures that would not fail unexpectedly and catastrophically when subjected to high loading rates.

Harris and Adams used a modified Izod pendulum for impact tests to associate the geometry of SLJs with aluminum adherends. Single-lap joints formed by various types of adhesives were tested under quasi-static and impact at a velocity of 1.4 m/s. The results indicated that joint strength was not considerably influenced by high loading rate, and that, for the majority of adhesives, the impact strength was not significantly higher than the static load [18].

The dynamic behavior of ABJs made of graphite/epoxy unidirectional plies was studied by Galliot et al. A drop weight machine was used to subject the specimens to a suddenly-

applied tensile load (impact) in order to compare the results to quasi-static test results. The intent was to find the rate-sensitivity of the adhesive. In contrast to the work of Harris and Adams, an average increase of more than 50% in strength was recognized by comparing the impact and quasi-static test results. They showed that the absorbed energy, the failure load, and the stiffness were intensified with increasing loading rate. Nevertheless, the joint behavior remained qualitatively the same under the quasi-static and dynamic loading cases. They noted that the adhesive did not apparently contribute to the energy absorption of the ABJ and that the deformation of the adherend material absorbed the energy. Baseline quasi-static loading tests were also conducted on a universal tensile machine (Instron) at a loading rate of 0.3 mm/min (5×10E-6 m/s). [19]

Goglio and Rosetto used the instrumented pendulum to study the effect of geometrical parameters on the mechanical properties of adhesively-bonded steel joints. In this investigation, they joined the specimen to a swinging hammer while the striker was clamped. The results indicated evolved joint strength under dynamic conditions and showed the significant effect of adhesive thickness [20].

Ger et al. implemented a "slingshot type" high velocity loading machine to validate the dynamic tensile behavior of composite laminates. The results indicated that the dynamic loading rate could lead to drastic failure. They also mentioned that the dynamic failure load was higher than the quasi-static one [21].

By using a drop weight tower to develop a high loading rate and by conducting quasi-static tests, Brown et al. showed that the compressive and tensile strengths and the modulus were enhanced by increasing loading rates. The tests were performed on an Instron™ electro-mechanical universal test machine at a crosshead speed of 5 $mm.min^{-1}$ [22].

Hsiao et al. experimentally investigated the effect of CNTs on the performance of ABJs consisting of carbon fiber-reinforced composites. They reported that, by adding only 1 wt% of MWNT in epoxy adhesive, the shear strength of the joint was increased by

31.2%; furthermore, by adding 5 wt% MWNT, the shear strength was increased by 45.6% [17].

It is important to note that there is an optimum amount of nanofiller for which adhesive properties can be maximized. At a higher content, the properties degrade due to changes in the failure mode of the joints. Commonly, the bonded joints with neat adhesives fail at the interface, while nano-reinforced adhesively bonded joints exhibit a cohesive failure mode that occurs within the adhesive. However, at relatively high quantities of nano-reinforcement, the joint failure mode becomes interfacial again. It is clear that MWNT particles enhance the strength and toughness of epoxies because nano-particles strengthen the polymeric chains of the resin and resist crack initiation and propagation [23].

In 2011, Srivastava investigated the effect of adding 3% MWNT to ABJs using a variety of substances as adherends. The results generally showed that the toughness and strength of the epoxy resin had increased; however, it was also demonstrated that the interface bonding strength of ABJs with similar adherends was much higher than those with dissimilar adherends [24].

As the overall goal of our study is to develop a relatively inexpensive and strong adhesive for common engineering applications where relatively thicker bond-lines are required (unlike the aerospace related applications), various aspects of such ABJ will be investigated. In this work, the effect of high loading rate on the mechanical response of nano-reinforced adhesively bonded single-lap joints with composite adherends subjected to a tensile impact load at 2.04E+5 mm/min is investigated and results will be compared with those one obtained from static and quasi static tests under 1.5 and 3.0 mm/min. Unidirectional graphite epoxy and E-glass fiber reinforced epoxy laminate were used to fabricate the adherends. The high loading rate tests were accomplished using a modified instrumented pendulum equipped with a specially designed tension impact apparatus. The static and quasi static tests were conducted on a servo universal tensile machine (Instron).

The observed failure mechanisms obtained from the scan electron microscopic study of the failed specimens will also be presented.

3.3 Experimental Plan

3.3.1 Fixture design

The tensile impact fixture's elements are illustrated in Fig. 3.1, and the actual fixture is shown in Fig. 3.2.

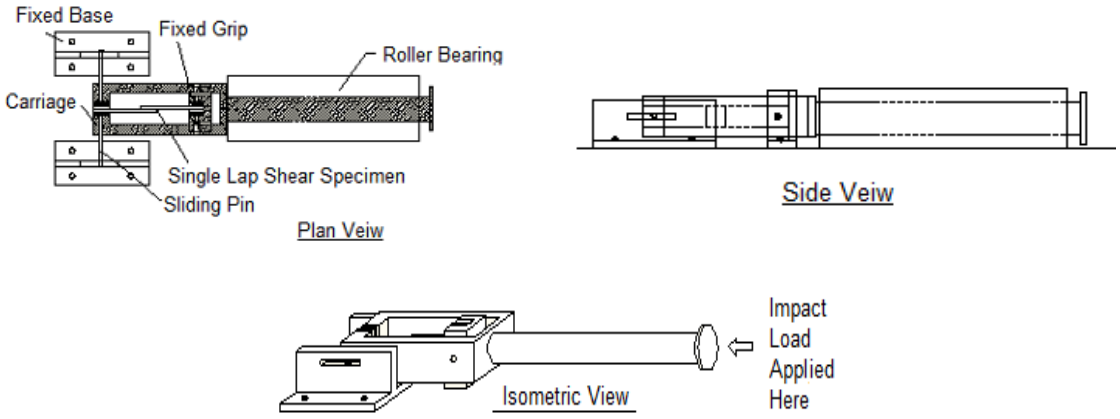

Fig. 3.1 Various views of the fixture used to apply a tensile impact load to the ABJ.

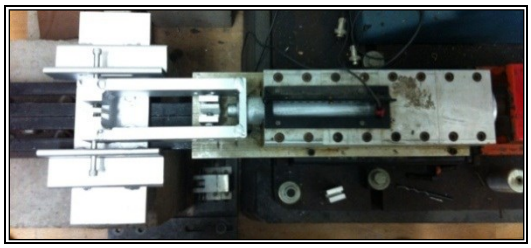

Fig. 3.2 Plan view of the tensile impact fixture.

As can be seen, the rod which has been designed to transfer the tensile impact load is aligned within several ball-bearings. To reduce the errors related to undesirable friction during the impact test, the height of each bolt was adjusted. Furthermore, to avoid unwanted torsions or bending moments, the system was designed with just one degree of freedom and axial movement capability only.

A jig was also designed and fabricated to make ABJs consistent and accurately aligned, as shown in Fig. 3.3. Shims were used to obtain the required thickness of the bond-line (i.e., 0.25 mm). This thickness was selected based on ASTM D5868-01standards [35].

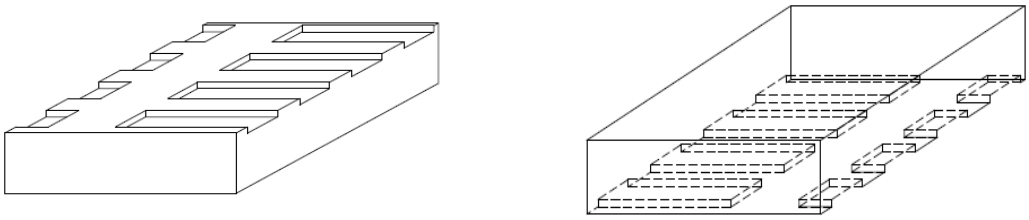

Fig. 3.3 Two halves of the jig made to facilitate fabrication of consistent single-lap joints.

3.3.2 Specimen preparation

3.3.2.1 Q-Cell reinforced adhesive

To prepare single-lap joints (SLJs), a commonly used thermoset epoxy resin (i.e., West System's 105 resin and 206 hardener [Bay City, MI]) was used as the baseline adhesive, due mainly to its common use and relatively low cost. However, as the viscosity of 105 resin is very low, it must be thickened (i.e., become paste-like) in order to be able to form practical bonded joints. To accomplish this, Q-Cell filler (obtained from Rayplex, Toronto, ON) was used to thicken the resin. Q-Cell is relatively inexpensive and lightweight filler that consists of white hollow inorganic microspheres with low bulk density. It is commonly added to resins at ratios of 0.5% - 10% (by weight). Although it is commonly known that the inclusion of filler will degrade a resin's mechanical properties, nevertheless no factual information or data on the actual level of resin degradation resulting from the addition of Q-Cell filler could be obtained from either the vendor or the literature.

Therefore, in order to establish the level of degradation in the resin properties that the addition of Q-Cell filler would cause, influence of three concentrations of the filler (i.e., 0%, 5%, and 10% by weight Q-Cell) in the resin were investigated. These ratios were selected based on the ease of applying the resin/adhesive in practical applications, especially when adhesives have to be applied on vertical surfaces.

To get a better feeling for and understanding of the strength of the nano-reinforced SLJs, a thermoplastic adhesive (two -part acrylic epoxy) (i.e., Plastic Welder [Devcon, Danvers, MA]) was applied.

3.3.2.2 Nano particle-reinforced adhesive

Since the addition of commonly used fillers like Q-cell is known to degrade the mechanical properties of resins and adhesives, another filler-type material was used with the aim of actually enhancing the resin's mechanical properties. For that, and as a means to economically enhance the mechanical properties of the thermoset resin/adhesive (in our case, West System 105), attempts were made to use various forms of nano-carbons as the filler. However, the uniform dispersion of nano-carbon in resin is quite challenging, time-consuming and thus an added cost. Not only does the dispersion directly govern the mechanical properties of the adhesive, but more importantly, the nano-particles agglomeration causes severe statistical inconsistencies in the strength and performance of adhesives. Therefore, a mechanical stirrer and three-roll mill machine were used to disperse the nano-particles uniformly in the resin.

To enhance dispersion, each roller should revolve with a set constant speed. In this study, the roller speed and calendering frequency were set to the maximum speed of the machine (i.e., 174 RPM). To maximize the quality of dispersion, calendering was conducted seven times. After each round of calendering, the quality of the dispersion was monitored by sampling the mix and assessing the uniformity of the dispersion with a digital microscope, thereby avoiding unwanted agglomerations.

Three different types of nano-particles were selected to be dispersed into the epoxy resin.

(i) Graphene Nano Platelet (GNP-M-25) with an average diameter of 25 μm, a thickness of 6 nm, and a surface area of 100 m2/g (obtained from XG Science Ltd., Lansing, MI).

(ii) Multi-Walled Carbon Nanotubes (MWCNTs) with an outer diameter of 5 to 15 nm and more than 95% purity (obtained from the US Research Nanomaterials, Inc., Houston, TX).

(iii) Graphitized Carbon Nano Fibers (CNF) with an outer diameter of 200 to 600 nm and more than 99.9 % purity (obtained from the US Research Nanomaterials, Inc., Houston, TX).

The nano-particles were first distributed in the resin using a mechanical stirrer set at a speed of 2000 rpm for 10 min.

The next step was to calender the nano-particle resin slurry using the three-roll mill. The roller gap was set at 20 μm using a filler gauge, for a 0.5% (by weight) concentration of CNF, MWCNT, and GNP (see Fig. 3.4). Later, due to required comparisons, other weight percentages of GNP were taken into consideration (i.e., 0.5%).

Fig. 3.4 The three-roll mill equipment used in the calendering process.

As stated, after each calendering, the quality of the dispersion was monitored by taking a small sample and examining the nano-particle dispersion using a digital microscope (see Fig. 3.5).

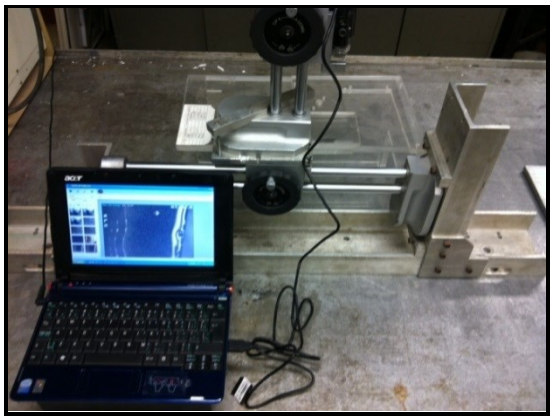

Fig. 3.5 Quality control process using a microscope after each calendering.

After the above procedures, the curing agent or hardener was added to the slurry and mixed in using the stirrer at a speed of 400 rpm for 4 to 6 minutes. The mixture was then degassed under 28" Hg vacuum for 2 to 3 minutes (the degassing duration depends on the gel time of the resin). After degassing, the mixture was poured in appropriately shaped molds and allowed to cure for 12 hours at room temperature. Typical final products in the form of dog-bone coupons, with dimensions as per ASTM D638-94B, are shown in Fig. 3.6 [36].

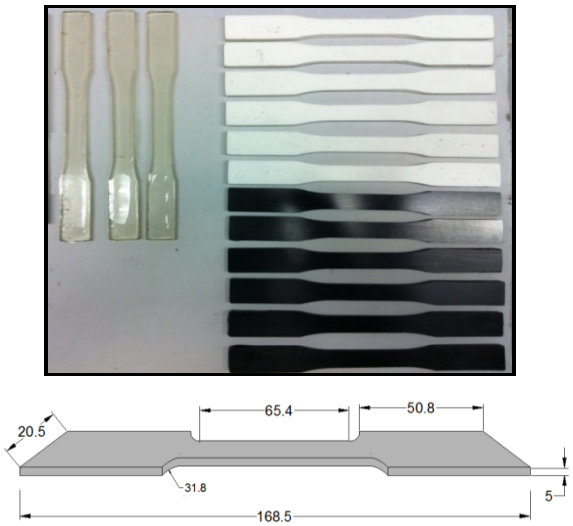

Fig. 3.6 Representatives tensile coupons neat, Q-Cell filler and nano-particle reinforced resins, as per ASTM D 638-94B (dimensions in mm).

3.3.2.3 Adherends preparation

To manufacture the adherends, laminate plates with a dimension of 350 mm × 350 mm were fabricated by the vacuum resin infusion technique (VRIT). Appropriately-sized coupons were then extracted from the plates, followed by the surface preparation process applied to the bonding regions [29-31]. To meet ASTM D5868-01 requirements, the graphite/epoxy and glass/epoxy plates were made from 12 unidirectional plies. Unidirectional graphite and E-glass fabrics and Huntsman's Araldite LY 564 epoxy resin with Aradure 2954 hardener (West Point, GA) were used to fabricate the laminate plates [35].

3.3.2.4 Single-lap Joint preparation

Using the described jig, single-lap joints (SLJs) were prepared from graphite/epoxy, glass/epoxy laminate adherends, and adhesive containing different amounts of micro- and nano-particles. Some typical graphite/epoxy and glass/epoxy SLJ specimens are illustrated in Fig. 3.7.

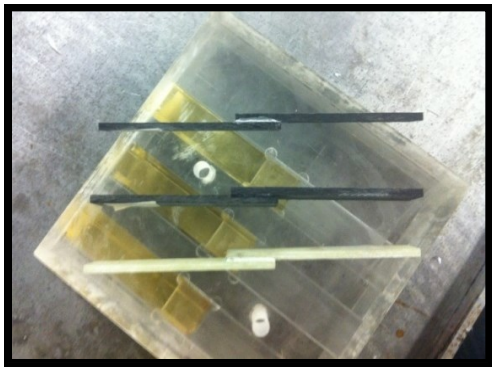

Fig. 3.7 Typical graphite/epoxy and glass/epoxy single-lap joint specimens.

To ensure the adhesive in ABJs would be subjected to concentric load, FRP tabs with appropriate thickness were affixed to adherends' ends (see Fig. 3.8).

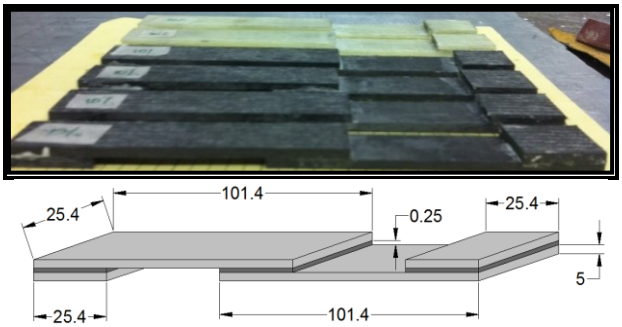

Fig. 3.8 Typical single-lap joint specimens (dimensions in mm).

It should be noted here that for the impact tests (high loading rate tests), modified quasi-isotropic tabs with holes in their centres were used (see Fig. 3.9) to prevent slippage and tearing-off of the adherends (see Fig. 3.10). Details of the static, quasi-static and impact (high-strain) loading for the SLJ specimens are given in next section.

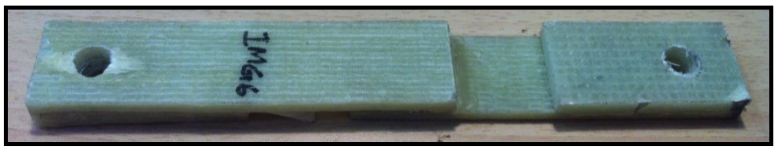

Fig. 3.9 Modified quasi-isotropic tab with holes, designed for tensile impact loadings.

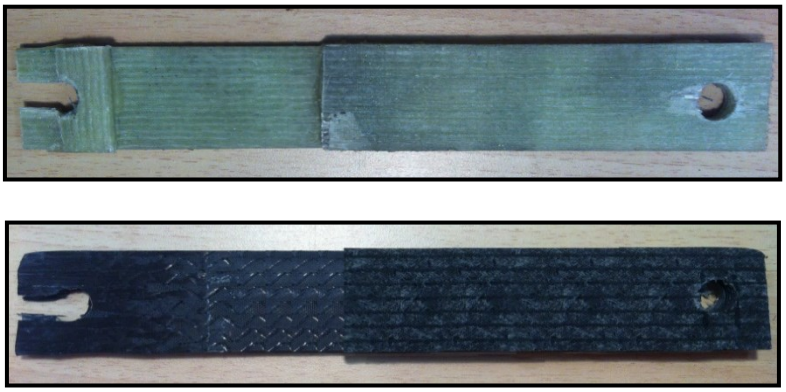

Fig. 3.10 Tearing-off problems in SLJs that were without quasi-isotropic tabs as a result of being subjected to tensile impact loading.

3.3.3 Characterization of the mechanical properties of adhesives

The prepared dog-bone shaped specimens were tested in tension using an Instron servo-hydraulic universal test machine equipped with 8500+ electronics. The specimens were subjected to displacement controlled tensile loading, as per ASTM D638, to establish the stress-strain curve of each adhesive [36]. An Instron extensometer was used to record the gauge-length displacement (hence, the strain) of the specimens. First Tensile tests were performed on the neat resin, at room temperature at cross-head speeds of 1.5, 3, 15, and 150 mm/min (as the baseline tests for the static and quasi-static loading conditions), and at 1500 mm/min (as baseline tests for the high loading rate loading condition), based on ASTM D 897 and ASTM D 950, respectively [39-41]. Subsequently, the reinforced-adhesive specimens underwent similar tests. Using the recorded load and gauge length displacement, the stress-strain curve of each adhesive was constructed and their elastic modulus was evaluated.

3.4 Experimental investigation of ABJs

The experimental part consists of two phases, as discussed below.

3.4.1 Baseline tests

To perform the baseline tests on the ABJs and the dog-bone shaped tensile coupons, the aforementioned loading rates were used. The applied load was recorded directly through the Instron machine's electronics and indirectly using the National Instrument DAQ system equipped with Lab View software. Gauge length displacement was also captured using a laser extensometer through the same DAQ system.

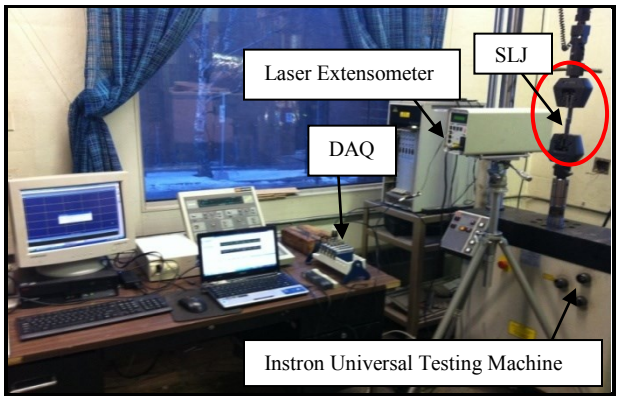

Fig. 3.11 Experimental set-up of static and quasi-static tests.

3.4.2 Impact (high loading rate) tests

In this category of tests, the applied load was measured using a PCB dynamic load cell (Depew, NY), positioned at the tip of the tensile carriage fixture (see Fig. 3.12(b)). The relative displacement of the overlap region was captured by a dynamic linear variable differential transducer - DLVDT (Data Instruments, Acton, MA), as shown in Fig. 3.12(c). The velocity of the impactor was also measured and adjusted using flat proximity sensors (Omron Corporation, Japan), as shown in Fig. 3.12(d).

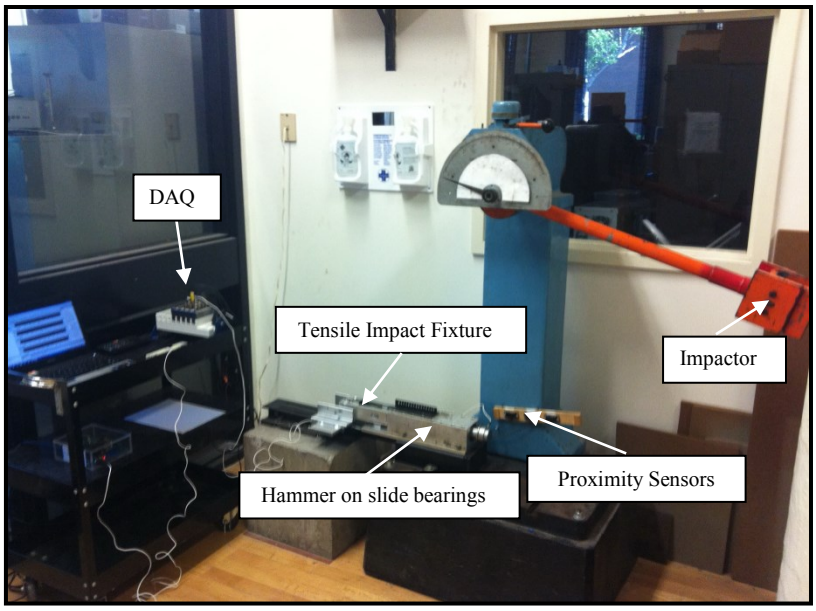

(a) Test set-up for impact (high loading rate) tests.

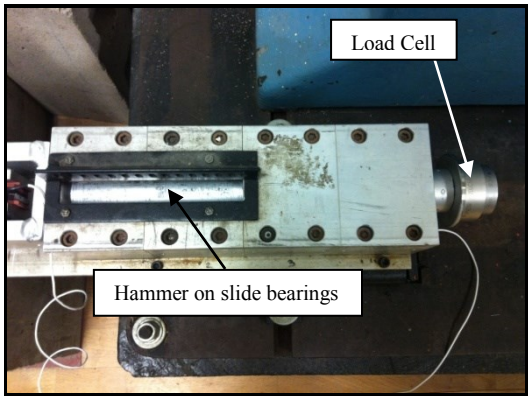

(b) Position of the dynamic load cell to record the impact loads.

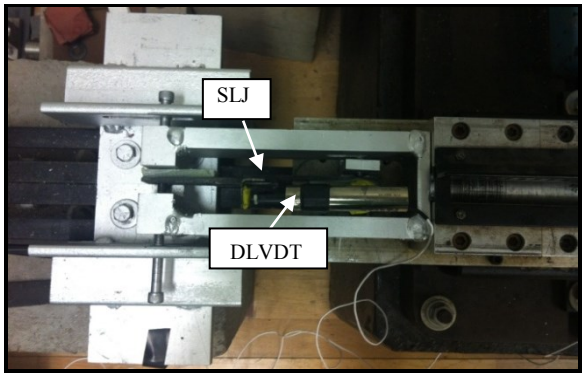

(c) Location of the dynamic LVDT to record the impact-induced displacement.

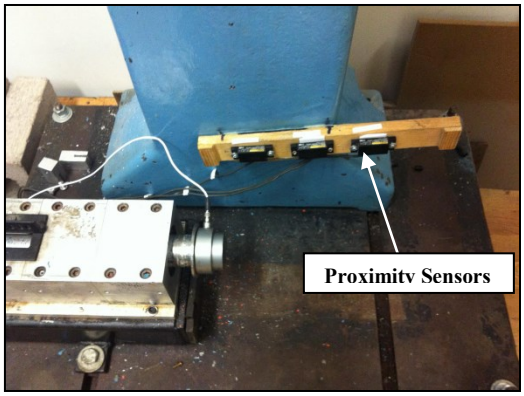

(d) Flat proximity sensors

Fig. 3.12 The experimental test set-up for the high loading rate.

3.5 Results and Discussion

The obtained experimental results related to the mechanical properties of adhesives (base-line tests) are shown in Table 3.1. As indicated, the results can be discussed from two significant points of view.

Table 3.1 Effect of nano reinforcement on the average ultimate tensile stress (MPa) in the West System (WS) epoxy adhesive

Loading Rate (mm/min)	Neat WS	WS with 0.25% wt GNP	WS with 0.5% wt GNP	WS with 1.0% wt GNP
1.5	51.12	54.62	55.84	57.15
15	60.87	66.28	67.24	68.36
150	69.33	76.69	78.16	80.17
1500	75.88	84.68	87.24	90.35

3.5.1 Influence of the micro-filler and nano-particles on the mechanical response of the adhesives

In light of the main objective of this research, and in an attempt to produce a strong and viscous adhesive from a commonly used and relatively inexpensive room-cured resin, Q-Cell filler and various nano-carbons were added to the neat resin (West System 105). The results of the tensile tests showed that although adding Q-Cell filler increased the adhesive's workability (viscosity), however, the mechanical properties of the adhesive

were degraded. The observed decrease in Q-Cell-added adhesive renders the adhesive unsuitable for practical bonding.

In contrast to the above, very good results were obtained when the least expensive type nano-carbon (i.e., graphene nano-platelets - GNP) was added to the resin [33, 34], [43, 44]. Various researchers have also observed that the addition of Carbon Nano Fibers (CNF) or Multi-Walled Carbon Nano Tubes (MWCNTs) to resins have produced enhancement of the resin's mechanical properties and fracture toughness [17-24]. However, very limited data exists for the level of enhancement that could be expected by the addition of GNPs to resins. As stated, GNPs are considerably less expensive than CNFs and MWCNTs. The results indicate that not only does the inclusion of GNPs improve the mechanical properties of this adhesive, it also enhances the resin's viscosity. This makes it suitable for use as an adhesive, especially for marine and other light-weight applications. In fact, the average ultimate tensile strength of the reinforced adhesive with 0.5% GNPs in weight was enhanced by 9% for lower and 15% for higher rates. Also, as shown in Table 1, the average ultimate tensile strength of reinforced adhesive with 1% GNPs in weight was improved by 12% and 19% for the lower and higher loading rates, respectively (see Fig. 3.13).

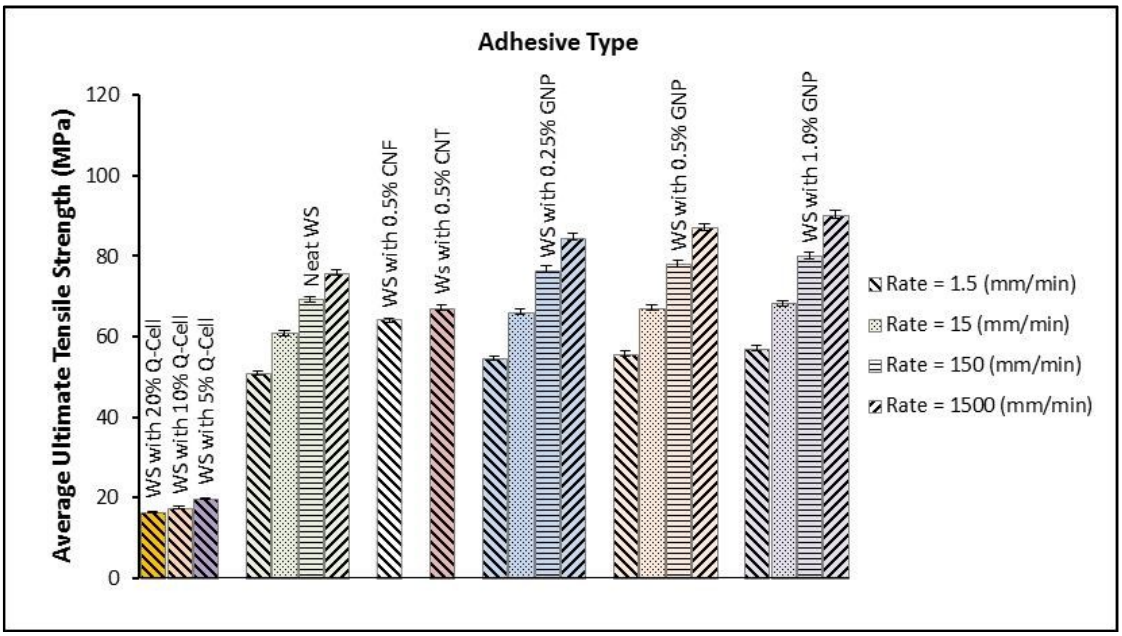

Fig. 3.13 Effects of the Q-Cell and various types of nano-carbon particles on resin's ultimate tensile strength.

Elastomeric particles (fillers or additives) would stretch as they bridge through a propagating crack, resulting in dissipating a portion of the energy required to develop the new surfaces of the growing crack. This, in turn, leads to increased strength under higher rate of loading. Fig. 3.14 (a) illustrates the SEM images of the GNP powder, (b) neat resin as well as (c) the MWCNT and (d) GNP -reinforced resins, respectively. The higher surface aspect ratio of the GNPs offers added strength to micro-cracking. Moreover, in the event of cracking, they effectively bridge the micro-cracks, in contrast to the MWCNTs dispersed in the resin (see Fig. 3.14(e)), and usually are filamentous and furcated, or exfoliated and piled on top of one another, as can be seen in Fig. 3.14(f).

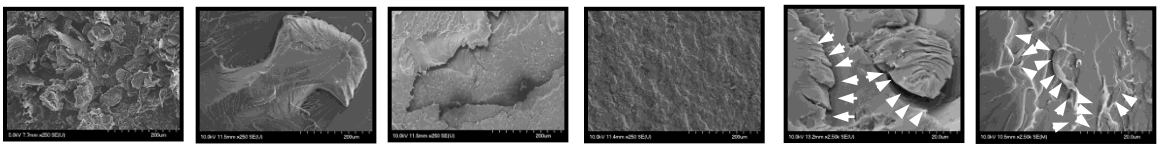

(a) (b) (c) (d) (e) (f)

Fig. 3.14 SEM images of various nanoparticles used in reinforcing the resin.

3.5.2 Influence of loading rate on the mechanical response of nano-particle-reinforced SLJs

As discussed in the previous section (3.3.2.4), the prepared SLJ specimens were tested using a modified instrumented pendulum equipped with a specially designed impact load transfer apparatus, subjected to the tensile impact with a loading rate of $2.04 \cdot 10^5$ mm/min.

The results showed that the inclusion of GNP in the resin could significantly improve the resin's stiffness and strength. The average ultimate shear strength of SLJs with carbon adherends was increased (relative to the neat adhesive) as much as 32% when SLJs were subjected to the high loading rates and about 26% under quasi-static rates (see Fig. 3.15). It was observed that increases in the loading rates affect the average ultimate shear stress of the adhesive in a nonlinear manner. These enhancements changed in the case of SLJs with glass/epoxy adherends. In that case, the average ultimate shear strength was increased by 28% and 22% for higher and lower loading rates, respectively (see Fig. 3.16).

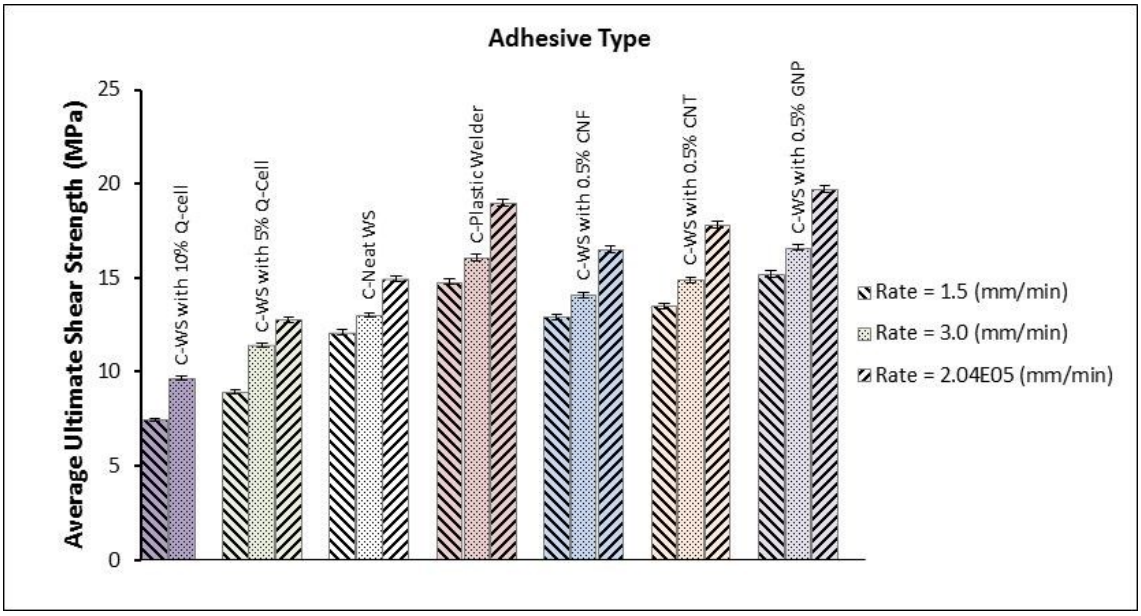

Fig. 3.15 Effects of loading rate on nano-reinforced adhesively bonded single-lap joints with graphite/epoxy adherends.

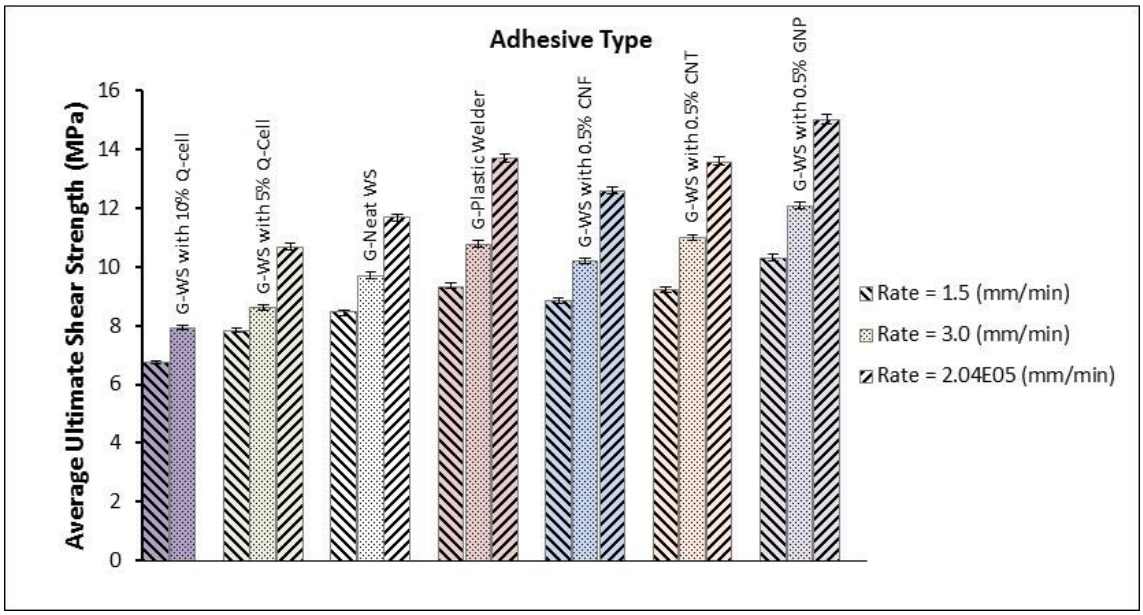

Fig. 3.16 Effects of loading rate on nano-reinforced adhesively bonded single-lap joints with glass/epoxy adherends.

To obtain a better understanding of the strength of nano-reinforced adhesives, a thermoplastic adhesive (two-part acrylic epoxy) was also used to prepare SLJ specimens. These specimens also contained the same fillers with the same weight percentages as used in the case of the thermoset resin.

It should be mentioned here that, from a macro-molecular point of view, loading rates affect failure modes as well. Figure 3.17 illustrates the differences between failure modes in static (quasi-static) and higher loading rates. As is shown, the detached cohesive parts that remained on the adherends in the bonded zone were divided into almost two equal portions and the failure occurred at the middle at static and quasi-static load rates; whereas in the case of higher loading rates (impact), the failure occurred at the end of the bond-line, and so the detached portions are not the same.

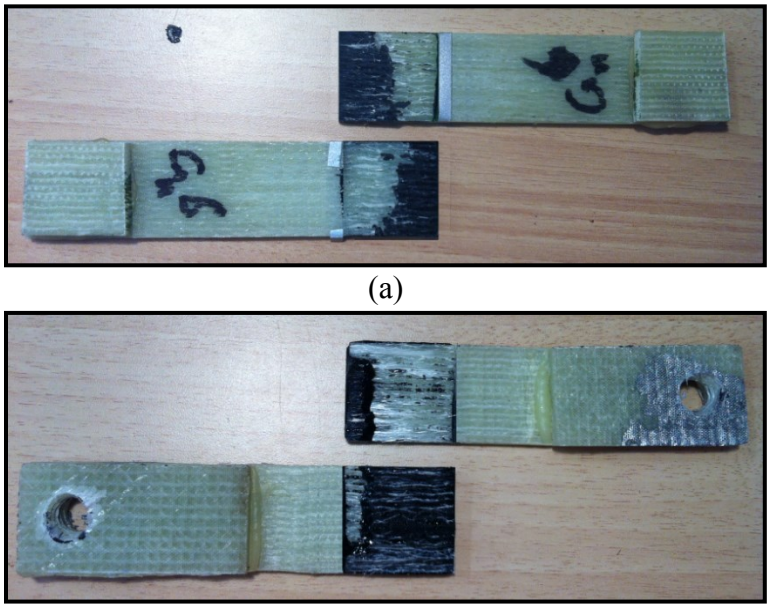

(a)

(b)

Fig. 3.17 Effects of loading rate on failure modes in SLJs (a) typical failure mode observed under static and quasi-static loading rates (b) at the higher loading rate (impact).

Furthermore, as it is shown in Table 3.2, the average ultimate shear stress of SLJs with carbon adherends are generally higher than the one with glass adherends, which can be explained based on higher strength and stiffness of carbon adherends to flexural and bending moments.

Table 3.2 Effect of adherend type on the average ultimate shear stress (MPa) of SLJs under different loading rates.

Adherend Type	Static (1.5 mm/min)					Impact (2.04E05 mm/min)				
	WS* with 5% Q-Cell	Neat WS	WS with 0.5% CNT	WS with 0.5% GNP	PW**	WS with 5% Q-Cell	Neat WS	WS with 0.5% CNT	WS with 0.5% GNP	PW
Graphite/Epoxy	8.95	12.10	13.51	15.20	14.98	14.93	14.93	17.82	19.70	18.23
Glass/Epoxy	7.84	8.44	9.25	10.32	9.35	10.70	11.70	13.60	15.03	13.70

*WS stands for the West System.
**PW stands for the Plastic Welder.

3.6 Conclusions

The results indicated that ABJs tested under the highest loading rates exhibited increased stiffness and strength. It was also observed that 0.25% GNP (in weight) has approximately the same mechanical properties of 0.5% CNF and CNT (in weight) under the same loading rate. It was also shown that 0.5% GNP (in weight) under lower loading rates exhibited similar mechanical behavior as 0.25% GNP (in weight) subjected to the highest loading rate. It was also concluded that ABJs with carbon adherends show higher strength in comparison with the one with glass adherends. Also, it was concluded that by increasing the loading rate, the average ultimate shear and tensile strength and stiffness generally were enhanced. Loading-rate-dependent properties derived from the experimental data will be used in the near future in conjunction with finite element analysis to conduct a parametric study and optimize the performance of such joints.

3.7 Acknowledgement

The financial support of the NSERC in support of this work is gratefully acknowledged.

3.8 References

1. da Silva L. F. M., Ochsner A., Adams R. D. [2011] Handbook of adhesion technology. Springer-Verlag, Berlin, Heidelberg.
2. Petrie E. M. [2000] Handbook of adhesives and sealants. McGraw-Hill, New York.
3. Kinloch A. J. [1987] Adhesion and adhesives: science and technology. Chapman & Hall, London.

4. Adams R. D., Comyn J., Wake W. C. [1997] Structural adhesive joints in engineering, 2nd edition. Chapman & Hall, London.
5. Berthelot J-M. [1999] Composite materials, Mechanical behavior and structural analysis. New York: Springer.
6. Hyer M. W. [1998] Stress Analysis of Fiber-Reinforced Composite Materials. McGraw-Hill Inc., New York.
7. Reddy J. N. [2006] Theory and Analysis of Elastic Plates and Shells CRC, 2nd edition. Taylor & Francis, Philadelphia, PA.
8. Timoshenko S., and Woinowsky-Krieger S. [1959] Theory of Plates and Shells 2nd Ed., McGraw-Hill, New York.
9. Banea M. D., da Silva L. F. M. [2008] Adhesively bonded joints in composite materials: an overview, Journal of Materials: Design and Applications, vol. 233, pp. 1-18.
10. Iijima S. [1991] Helical microtubules of graphitic carbon. Journal of Nature, vol. 354, pp.56-58.
11. Iijima S., Ichihashi T. [1993] Single-shell carbon nanotubes of 1-nm diameter. Journal of Nature, vol. 363, pp. 603-605.
12. Tjong S. C. [2006] Structural and mechanical properties of polymer nanocomposites. Journal of Material Science and Engineering, vol. 53, Issue (3-4), pp. 73-197.
13. Lau K.T., Gu C., Gao G.H., Ling H.Y., and Reid S.R [2004] Stretching process of single- and multi-walled carbon nanotubes for nanocomposite applications. Journal of Carbon, vol. 42, Issue (2), pp. 426-429.
14. Demczyk B. G., Wang Y. M., Cumings J., Hetman M., Han W., Zettl A., Ritchie R. O. [2002] Direct mechanical measurement of the tensile strength and elastic modulus of multiwalled carbon nanotubes. Journal of Material Science and Engineering, vol. 12, pp. 934-935.
15. Saito R., and Dresselhaus G., Dresselhaus M. S. [1998] Physical properties of carbon nanotubes. Imperial College Press, London.

16. Alexandre M., Dubois P. [2000] Polymer-layered silicate nanocomposites: preparation, properties and uses of a new class of materials. Journal of Material Science Engineering Reports, vol. 28, Issue (1-2), pp.1-63.
17. Hsiao K. T., Alms J., and Advani S. G. [2003] Use of epoxy/multiwalled carbon nanotubes as adhesives to join graphite fiber reinforced polymer composites. Nanotechnology, vol. 14, Issue (7), pp. 791-793.
18. Harris J. A., Adams R. [1985] An assessment of the impact performance of bonded joints for use in high energy absorbing structures. Proc International Mechanical Engineering, vol. 199(C2), pp. 121-131.
19. Galliot C., Rousseau J., and Verchey G. [2012] Drop weight tensile impact testing of adhesively bonded carbon/epoxy laminate joints. International Journal of Adhesion and Adhesives, vol. 35, pp. 68-75.
20. Goglio L., Rossetto M. [2008] Impact rupture of structural adhesive joints under different stress combinations. International Journal of Impact Engineering, vol. 35, Issue (7), pp. 635-643.
21. Ger G.S., Kawata K., Itabashi M. [1996] Dynamic tensile strength of composite laminate joints fastened mechanically. Journal of Theoretical and Applied Fracture Mechanics, vol. 24, Issue (2), pp. 147–155.
22. Kevin A., Brown K. A., Brooks R., Warrior N. A. [2010] The static and high strain rate behavior of a commingled E-glass/polypropylene woven fabric composite. Composites Science and Technology, vol. 70, Issue (2), pp. 272-283.
23. Srivastava V. K., Hogg P. J., Moisture [1998] Effects on the toughness, mode-I and mode-II of particles filled quasi-isotropic glass-fibre-reinforced polyester resin composites. Journal of Material Science. vol. 33, Issue (5), pp. 1129–1136.
24. Srivastava V.K. [2011] Effect of carbon nanotubes on the strength of adhesive lap joints of C/C and C/C–SiC ceramic fibre composites. International Journal of Adhesion and Adhesives, vol. 31, Issue (6), pp. 486–489.
25. Jacob G. C., Starbuck J. M., Fellers J. F., Simunovic S. [2004] Strain rate effects on the mechanical properties of polymer composite materials. Journal of Applied Polymer Science, Vol. 94, pp. 296-301.

26. Sierakowski R. L. [1999] Strain rate effects in composites. Journal of Applied Mechanics Review, vol. 50, pp. 741-761.
27. Barre S., Chotard T., Benzeggagh M. L. [1996] Comparative study of strain rate effects on mechanical properties of glass fiber-reinforced thermoset matrix composites. Journal of Composite: Applied Science Manufacturing, vol. 27, pp. 1169-1181.
28. Hamouda M. S. and Hashmi M. S. J. [1998] Testing of composite materials at high rates of strain: advances and challenges. Journal of Material Processing Technology, vol. 7, pp. 327-336.
29. Davis M. J. and Bond D. [1999] Principles and practice of adhesive bonded structural joints and repairs. International Journal of Adhesion and Adhesives, 19(3), 91-105.
30. Molitor P., Barron V., and Young T. [2001] Surface treatment of titanium for adhesive bonding to polymer composites: a review. International Journal of Adhesion Adhesives, vol. 21, Issue (2), pp. 129-136.
31. Kim J. S. and Reneker D. H. [1999] Mechanical properties of composites using ultrafine electrospun fibers. Journal of Polymer Composites, vol. 20, Issue (1), pp. 124-131.
32. J.A. Chambers, [1995] Preloaded Joint Analysis Methodology for Space Flight Systems. NASA TM-106943, December 1995.
33. Rothon R. N. and Hancock M. [1995] General principles guiding selection and use of particulate materials. In: Particulate-filled polymer composites. Rothon R. N. (ed) Longman Scientific and Technical, Harlow, P1.
34. Senguptaa R., Bhattacharyaa M., Bandyopadhyayb S., Bhowmicka A.K. [2011] A review on the mechanical and electrical properties of graphite and modified graphite reinforced polymer composites, Journal Polymer Science, vol. 36, pp. 638-670.
35. ASTM D5868-01, Standard Test Method for Lap Shear Adhesion for Fiber Reinforced Plastic (FRP) Bonding, ASTM International, West Conshohocken.
36. ASTM D638, Standard Test Method for Tensile Properties of Plastics, ASTM International, West Conshohocken.

37. ASTM D907, Terminology of Adhesives, ASTM International, West Conshohocken.
38. ASTM D4896, Guide for Use of Adhesive-Bonded Single-lap-Joint Specimen Test Results, ASTM International, West Conshohocken.
39. ASTM D897, Test Method for Tensile Properties of Adhesive Bonds, ASTM International, West Conshohocken.
40. ASTM D905, Test Method for Strength Properties of Adhesive Bonds in Shear by Compression Loading, ASTM International, West Conshohocken.
41. ASTM D950, Test Method for Impact Strength of Adhesive Bonds, ASTM International, West Conshohocken.
42. ASTM D1002, Test Method for Apparent Shear Strength of Single-Lap-Joint Adhesively Bonded Metal Specimens by Tension Loading (Metal-to-Metal), ASTM International, West Conshohocken.
43. Kaneka, http://www.kaneka.com.Retrieved 9 April 2012.
44. Sigma Aldrich, http//www.sigmaaldrich.com. Retrieved 9 October 2012.

CHAPTER 4 INFLUENCE OF NANO REINFORCEMENT ON THE MECHANICAL BEHAVIOR OF ADHESIVELY-BONDED SINGLE-LAP JOINTS SUBJECTED TO STATIC, QUASI-STATIC AND IMPACT LOADING

B. Soltannia, F. Taheri *
Department of Civil and Resource Engineering, Dalhousie University, 1360 Barrington Street, PO Box 15000 Halifax, NS, B3H 4R2, Canada
* Corresponding author: (Farid.Taheri@dal.ca)

To be submitted to the Journal of Nanotechnology, August 2013

4.1 Abstract

Crashworthiness, damage tolerance, energy absorption capability and safety are all important factors in the design of light-weight composite structures, especially for those with application in transportation industry. In order to make such structures lighter and more resilient and to avoid stress concentrations that are inherent in mechanical fasteners such as bolted or welded joints, it is desirable to mate the structure's various components with adhesively-bonded joints. Therefore, the comprehensive understanding of the response of bonded joints subjected to loadings with various rates is of paramount importance in developing reliable structures. On the other hand, the emergence of nano-technology industry, has offered novel means in enhancing the mechanical properties of numerous structures.

In this paper, the effects of nano reinforcement on the mechanical response of adhesively-bonded single-lap joints with composite adherends, subjected to different loading (strain) rates are systematically investigated. The results are then compared to those of neat thermoset resin and thermo-plastic adhesive. More specifically, nano-reinforced and neat resin bonded joints mating carbon/epoxy and glass/epoxy adherends were subjected to tensile loadings under 1.5 and 3 mm/min and tensile impacts at a loading rate of 2.04E+5 mm/min. In some cases, additional tests were conducted to obtain additional properties gained using the nano-reinforcements for use in the further numerical investigations. The additional loading rates tried were 15, 150, and 1500 mm/min. High loading rate tests were also conducted, using a modified instrumented pendulum equipped with a specially

designed impact load transfer apparatus. The dispersion of nanoparticles was facilitated using a mechanical stirrer and a three-roll mill machine. The results of the impact tests revealed the positive influence of nano reinforcements on the loading rate sensitivity of the joints. In all, the overall stiffness and strength of the joints increased as the nano reinforcement and loading rates were increased. The failure surfaces were then examined with a scanning electron microscope to observe the distribution of the nanoparticles, and study the mode of failure.

4.2 Keywords

Adhesively bonded joints; Single-lap joints; Graphene nanoplatelets; Nano composites; Loading rate; High loading rate.

4.3 Introduction

Adhesively-bonded joints (ABJs) are increasingly being used in automotive, marine, offshore, and oil and gas industries to mate both metallic and fiber-reinforced polymer composite (FRP) structural components. Adhesively-bonded FRPs offer numerous advantages, including high strength and stiffness-to-weight ratios, good fatigue and corrosion resistance, controllable damage mechanism, and high energy absorption capacity, all of which make them more efficient compared to their counterparts (mechanical fasteners)[1-9]. Crashworthiness, improved damage tolerance, energy absorption capability, and safety requirements are important factors in the design of light-weight composite structures, especially in transportation related applications. However, a major concern in the use of adhesives in such applications has been the lack of adequate database with regards to the performance of ABJs at high rates of strain (loading). For design purposes, the mechanical characterization of ABJs at high loading rates is vital.
Moreover, in recent years, several works have been conducted with the aim of strengthening and toughening adhesives. One of the emerging technologies has been the incorporation of nanoparticles in adhesives. It is therefore prudent to provide a brief introduction to the nanoparticles often considered for inclusion in resins.

The nanoparticles that are most widely discussed in the scientific literature are carbon nanotubes (CNTs), despite the fact that carbon nanofibers (CNFs) and graphene

nanoplatelets (GNPs), which have a larger diameter and aspect ratios, are less expensive, and are more widely available. Ceramic nanotubes (e.g., zirconia, tungsten disulfide) or whiskers (e.g., silicon nitride, silicon carbide, and alumina) have also been used for the purpose. The use of carbon nanotubes, which are essentially sheets of graphite rolled into tubes [10, 11], was first proposed by Iijima in 1991 and later by Iijima and Ichihashi in 1993. There are essentially two main types of nanotubes. The first type is single-walled nanotubes (SWNTs), which consist of a single graphene layer, typically wrapped into a cylinder, with a diameter of 1-2 nm and hemispherical end caps [11, 12]. The second type, known as multi-walled nanotubes (MWNTs), contain a number of coaxial graphene cylinders, each of which has an end cap, with an outer diameter of 3-10 nm. Due to the weak Van der Waals forces between the layers, the tension loads are carried only by the outer layer of a MWNT, and thus stress is not transferred to the inner layers [13]. Even though they are quite flexible perpendicular to their longitudinal axis [14], the strength of MWNTs has been estimated to be up to 150 GPa and their elastic modulus up to 900 GPa [15]. Their superior mechanical characteristics and optimal length-to-diameter ratio make CNTs highly desirable for reinforcement of resins. Nevertheless, in order to fully harness the exceptional mechanical properties of CNTs, a strong interfacial bonding between the polymer matrix and CNTs must exist [16].

Hsiao et al. demonstrated that utilizing CNTs in conjunction with an adhesive could improve the mechanical properties of the joint. By adding 5 percent by weight (wt%) MWNT to an epoxy adhesive, the shear stress could be more efficiently transferred to the adherends (cohesive failure), thereby increasing the average shear strength of the joint by 45.6%. In SWNTs, failure was initiated and developed within the adhesive layer [17].

4.3.1 Adhesively-bonded joints

As stated earlier, adhesive bonding technology is increasingly being utilized to join various structural components. Single-lap joints, double-lap joints, L-joints and T-joints are some of the conventional joint configurations used for joining structural elements. Single- and double-sided repair configurations can also be conducted when adhesive

bonding is applied to reinforce or repair structural damages and defects [1]. Fig. 4.1 illustrates various types of adhesively bonded joints.

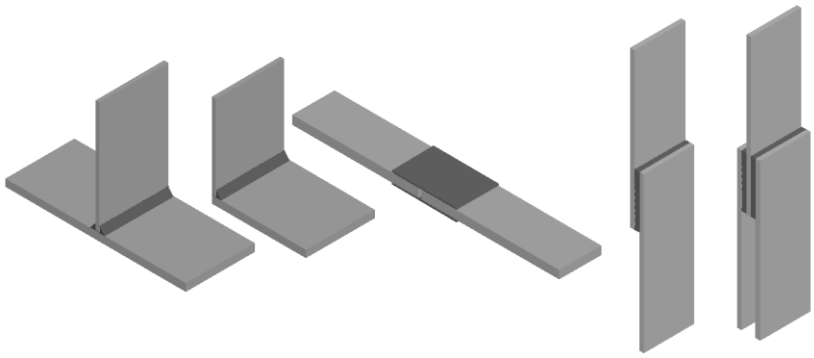

(a) (b) (c) (d) (e)

Fig. 4.1 Different types of adhesively bonded joints, (a) T-joint, (b) L-joint, (c) double strap joint, (d) single-lap joint, (e) double lap joint.

Although, when being analyzed, lap-type joints can be modeled as a two-dimensional (2D) system, the stress variations in such joints are actually three-dimensional (3D) in nature. Numerical methods, such as the finite element method (FEM), have been used to effectively model both 2D and 3D problems of adhesively-bonded joints. Nevertheless, closed-form solutions are essential for preliminary design purposes, as they can produce meaningful results in a timely manner. Hence, several attempts have been made to improve the analytical approaches for evaluating stress distribution in ABJs [45-50].

In several applications (especially in aerospace industry), the thickness of the adhesive layer is usually very thin, measuring in fractions of a millimeter. For instance, a common bond-line thickness in an ABJ application would be approximately 0.2 mm thick. The stress state in the adhesive layer is relatively complex in 2D or 3D problems, and although adherends are usually modeled as beams or plates, the adhesive layer is much thinner in practical ABJs in comparison to the adherends. Consequently, the adhesive layer is typically modeled by an infinite number of springs or an appropriate interface, with the assumption that only normal (through-thickness peel) and shear stresses exist within the adhesive layer, and that they remain constant across the thickness, changing only along the bond-line length. This assumption is used to develop various 1D analytical solutions.

A single-lap joint (SLJ) is considered to be the simplest geometric configuration for bonding structural components. The SLJ configuration has therefore been extensively used as a standard test specimen to investigate the responses of ABJs, and has been shown to be a suitable representative of ABJs in modeling the influence of the fundamental parameters involved in ABJs [1].

4.3.2 High loading rate studies

An important factor considered in the design of lightweight vehicles, especially those made of FRPs is their crashworthiness. In particular, structural joints should have the ability to absorb a large amount of energy to accommodate the safety factors and improve passenger safety. To accomplish this, the dynamic behavior of the adhesively-bonded joints used in such applications should be fully understood, as the effect of the loading rate on the response of ABJs would enable engineers to design structures that would not fail unexpectedly and catastrophically when subjected to high loading loading rates.

Harris and Adams used a modified Izod pendulum for impact tests to associate the geometry of SLJs with aluminum adherends. Single-lap joints formed by various types of adhesive were tested under quasi-static and high velocity of 1.4 m/s. The results indicated that joint strength was not significantly influenced by the high loading rate, and that, for the majority of the adhesives, the strength under high applied loading rate was not significantly higher than that observed under static load [18].

The dynamic behavior of ABJs made of graphite/epoxy unidirectional plies was studied by Galliot et al. A drop-weight machine was used to subject the specimens to a tensile load that was suddenly applied (impact) in order to compare the results to quasi-static test results. The intent was to find the rate-sensitivity of the adhesive. In contrast to the observations of Harris and Adams, an average increase of more than 50% in strength was observed by Galliot et al. when comparing the impact and quasi-static test results, which showed that the absorbed energy, the failure load, and the stiffness were intensified with increasing loading rates. The joint behavior, however, remained qualitatively the same

under the quasi-static and dynamic loading cases. Galliot et al. noted that the adhesive did not apparently contribute to the energy absorption of the ABJs and that the deformation of the adherend material absorbed the energy. Baseline quasi-static loading tests were also conducted using a universal servo-hydraulic test machine (Instron) at a loading rate of 0.3 mm/min (5×10E-6 m/s) [19].

Goglio and Rosetto used the instrumented pendulum to study the effect of geometrical parameters on the mechanical properties of adhesively-bonded steel joints. In this investigation, they joined the specimen to a swinging hammer while the striker was kept stationary. The results indicated evolved joint strength under dynamic conditions and showed the significant effect of adhesive thickness [20].

Ger et al. implemented a "slingshot-type" high velocity loading machine to validate the dynamic tensile behavior of composite laminates. The results demonstrated that the dynamic loading rate could lead to catastrophic failure modes and that the dynamic failure load was higher than the quasi-static one [21].

By using a drop-weight tower to develop a high loading rate and by conducting quasi-static tests, Brown et al. demonstrated that the compressive and tensile strengths and the modulus were enhanced by increasing loading rates. Their tests were performed on an Instron™ electro-mechanical universal test machine at a crosshead speed of 5 $mm.min^{-1}$ [22].

Hsiao et al. experimentally investigated the effect of CNTs on the performance of ABJs mating of carbon fiber-reinforced composites. They reported that, by adding only 1 wt% of MWNT in epoxy adhesive, the shear strength of the joint was increased by 31.2%; furthermore, by adding 5 wt% MWNT, the shear strength was improved by 45.6% [17].

It is important to note that there is an optimum amount of nanofiller by which adhesive properties can be maximized. At a higher content, the properties actually degrade due to changes in the failure mode of the joints. Commonly, the bonded joints with neat

adhesives fail at the interface, while nano-reinforced adhesively-bonded joints exhibit a cohesive failure mode that occurs within the adhesive. However, at relatively high quantities of nano-reinforcement, the joint failure mode becomes interfacial again. It is clear that MWNT particles enhance the strength and toughness of epoxies because nano-particles strengthen the polymeric chains of the resin and resist crack initiation and propagation [23].

In 2011, Srivastava investigated the effect of adding 3% MWNT to ABJs using a variety of materials as adherends. The results generally showed that the toughness and strength of the epoxy resin had increased; however, it was also demonstrated that the interface bonding strength of ABJs with similar adherends was much higher than those with dissimilar adherends [24].

4.3.3 Nanoparticle reinforced adhesives

Since the advent of nanotechnology, nanocomposite adhesives have been increasingly used in many advanced applications in naval, automotive, aerospace, and medical industries. Kim and Reneker reported that the Young's modulus of a nanofiber-reinforced composite was ten times greater than that of a neat adhesive [11]. However, there are as yet only limited studies on the mechanical properties of nanofiber adhesives and nanofiber composites [12].

Since adherends are usually much stronger than the adhesives used to bond them, one option for enhancing joint properties is to reinforce and toughen the adhesives. Qian et al. suggested that nanotubes (CNTs) could enhance the composite strength by as much as 25% [13]. However, Yu et al. reported that multi-wall nanotubes (MWNTs) were restricted in their usages due to poor inter-shell interaction [14], and that single-wall nanotubes (SWCNTs) are expensive and difficult to produce. Other types of reinforcement for nanocomposites consist of carbon nanofibers (CNFs) and graphite nanoplatelets (GNPs). CNFs also have excellent characteristics and can be implemented as reinforcements in various types of matrices. For instance, they can functionalize facile

sites with fillers and additives chemically, resulting in a stronger interfacial bond with the matrix.

Rothon and Hancock pointed out the fallacy of the widespread notion that nanoparticles are expensive and that polymers are inexpensive [15]. As nanoparticle production expands, nanoparticles would become increasingly available in larger quantities, and at a reasonable price. The cost of nanoparticles greatly depends on the type and purity of the material. Nano-clays can cost as little as $7/kg [16]; however, a kilogram of carbon nanotubes costs between $8,000 - $100,000, while graphene nano platelets (GNPs) cost approximately $2/kg [17].

Graphene nanoplatelets (GNPs) generally consist of stocks of platelets that are exfoliated or intercalated by a polymer during processing. The thickness of these plate-like particles is approximately 1nm and their lateral dimensions can vary from 25 nm to a micron, which indicates that they have large aspect ratios [33, 34]. The conventional Van der Waals gap, called the “gallery” or “interlayer” [24], has been observed in between the layers. To make GNPs, the graphite is intercalated by a special acid treatment process, followed by exfoliation prompted by a thermal shock applied at a temperature of around 600°C.

To obtain a reinforced adhesive with the most optimum properties, the nanoparticles should be well dispersed within it, and each particle should be properly immersed in the polymer. This is a very challenging process, because the formation of agglomerations can act as defect regions, reducing the performance instead of enhancing it.

4.4 Motivation and Objectives

The overall goal of our study is to develop a relatively inexpensive and strong adhesive for common engineering applications where relatively thicker bond-lines are required (unlike in aerospace-related applications), therefore, various aspects of ABJs will be investigated. In this work, the effect of high loading rate on the mechanical response of nano-reinforced adhesively-bonded, single-lap joints with FRP adherends, subjected to a

high loading rate of 2.04E+5 mm/min is investigated and the results compared with those obtained from static and quasi-static tests conducted at loading rates of 1.5 and 3.0 mm/min, respectively. Uni-directional graphite epoxy and E-glass fiber-reinforced epoxy laminate were used to fabricate the adherends. The high loading rate tests were accomplished using a modified instrumented pendulum equipped with a specially designed tension impact apparatus. The static and quasi-static tests were conducted on a servo-hydraulic universal test machine (Instron 8500+ equipped with digital electronic control).

The observed failure mechanisms obtained from the scan electron microscopic study of the failed specimens will also be presented.

4.5 Experimental Plan

4.5.1 Fixture design

The tensile impact fixture's elements which are designed to produce the very high loading rate are illustrated in Fig. 4.2 as well as the actual fixture.

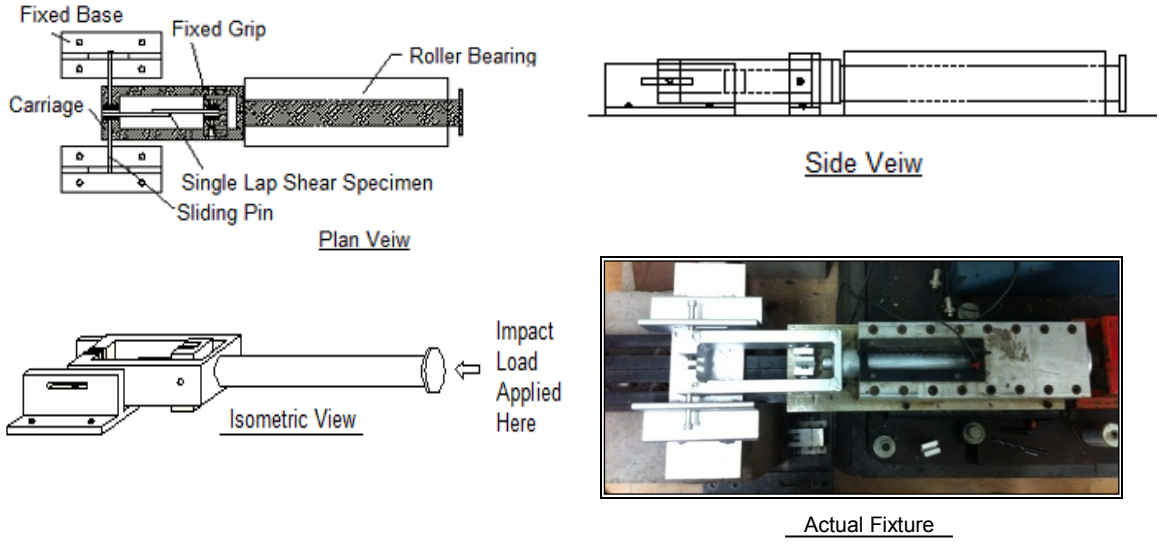

Fig. 4.2 Various views of the fixture used to apply the highest loading rate to the ABJs, including the picture of the actual fixture.

As can be seen, the rod which has been designed to transfer the impact load is aligned within several ball-bearings. To reduce the errors related to undesirable friction during the impact test, the height of each bolt was adjusted. Furthermore, to avoid unwanted

torsions or bending moments, the system was designed with just one degree of freedom (i.e., axial movement only).

A jig was also designed and fabricated for producing the ABJs consistently and accurately aligned, as shown in Fig. 4.3. Shims were used to obtain the required bond-line thickness (i.e., 0.25 mm). This thickness was selected based on ASTM D5868-01standards [35].

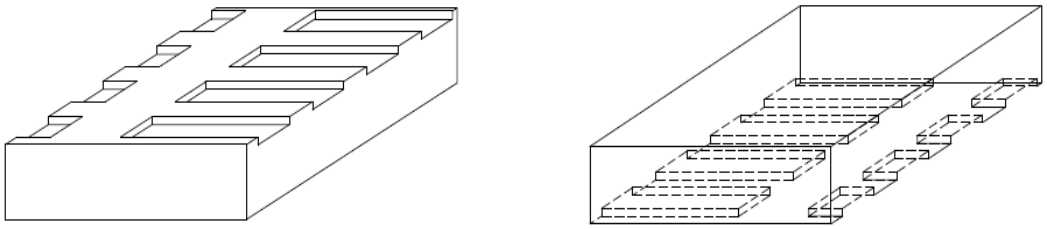

Fig. 4.3 Two halves of the jig made to facilitate fabrication of consistent single-lap joints.

4.5.2 Specimen preparation

4.5.2.1 Q-Cell reinforced adhesive

To prepare the single-lap joints, a commonly used thermoset epoxy resin (i.e., the West System 105 resin and 206 hardener [Bay City, MI]) was used as the baseline adhesive, mainly due to its availability, popularity and relatively low cost. However, as the viscosity of 105 resin is very low, it must be thickened (i.e., become paste-like) in order to be able to form practical bonded joints. To accomplish this, Q-Cell filler (obtained from Rayplex, Toronto, ON) was used to thicken the resin. Q-Cell is inexpensive and lightweight filler that consists of white hollow inorganic microspheres with low bulk density. It is commonly added to resins at ratios of 0.5% - 10% (by weight). Although it is well known that the inclusion of filler will degrade a resin's mechanical properties, no factual information or data on the actual level of resin degradation resulting from the inclusion of Q-Cell filler could be obtained from either the vendor or the literature. Therefore, in order to establish the level of degradation in the resin mechanical properties that the inclusion of Q-Cell filler would cause, the influence of two filler contents (i.e., 5%, and 10% by weight Q-Cell) in the resin was investigated. These ratios were selected based on the ease of application of the resin/adhesive in practical applications, especially when adhesives are applied on vertical surfaces.

To gain a better understanding of the performance of SLJs, a thermoplastic adhesive (a two-part acrylic epoxy; i.e., the Plastic Welder [Devcon, Danvers, MA]) was also used to form SLJs.

4.5.2.2 Nano particle-reinforced adhesive

Since the addition of commonly used fillers like Q-cell is known to degrade the mechanical properties of resins and adhesives, another filler-type material was used, with the aim of enhancing the resin's mechanical properties. For that, and as a means to economically enhance the mechanical properties of the thermoset resin/adhesive (in our case, West System 105), attempts were made to use various forms of nano-carbons as a reinforcing agent. However, the uniform dispersion of nano-carbon in resin is quite challenging and time-consuming, and thus an added cost. Not only does the dispersion directly govern the mechanical properties of the adhesive, but more importantly, the nano-particle agglomeration causes significant statistical inconsistencies in the strength and performance of adhesives. Therefore, a mechanical stirrer and three-roll mill machine were used to disperse the nano-particles uniformly in the resin.

To enhance dispersion, each roller should revolve with a set constant speed. In this study, the roller speed and calendering frequency were set to the machine's maximum speed of 174 RPM. To maximize the quality of dispersion, calendering was conducted seven times. After each round, the quality of the dispersion was monitored by sampling the mix and assessing the uniformity of the dispersion with a digital microscope with the aim of avoiding unwanted agglomerations.

Three different types of nano-particles were selected to be dispersed into the epoxy resin.

(i) Graphene Nano Platelet (GNP-M-25) with an average diameter of 25 μm, thickness of 6 nm, and surface area of 100 m^2/g (obtained from XG Science Ltd., Lansing, MI).

(ii) Multi-Walled Carbon Nanotubes (MWCNTs) with an outer diameter of 5 to 15 nm and more than 95% purity (obtained from the US Research Nanomaterials, Inc., Houston, TX).

(iii) Graphitized Carbon Nano Fibers (CNF) with an outer diameter of 200 to 600 nm and more than 99.9 % purity (obtained from the US Research Nanomaterials, Inc., Houston, TX).

The nano-particles were first distributed in the resin using a mechanical stirrer set at a speed of 2000 rpm for 10 min.

The next step was to calender the nano-particle resin slurry using a three-roll mill. The roller gap was set at 20 μm using a filler gauge, for the 0.5% (by weight) concentration of CNF, MWCNT, and GNP (see Fig. 4.4). Later, due to required comparisons, other weight percentages of GNP were taken into consideration (i.e., 0.25% or 1%).

As stated, after each calendering, the quality of the dispersion was monitored by taking a small sample and examining the nano-particle dispersion under a digital microscope (see Fig. 4.5).

Fig. 4.4 The three-roll mill equipment used in the calendering process (Torrey Hills Technologies LLC, San Diego, CA).

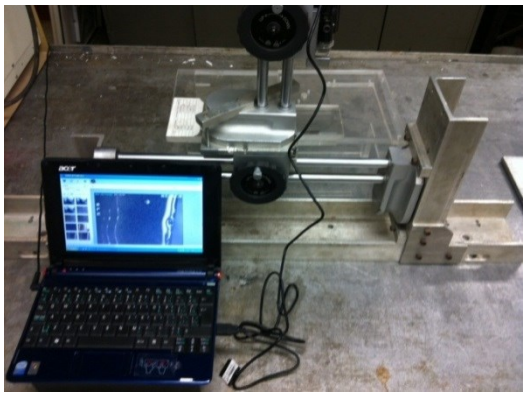

Fig. 4.5 Quality control processing using a digital microscope after each calendering.

Following the above procedures, the curing agent or hardener was added to the slurry and mixed in using the stirrer at a speed of 400 rpm for 4 to 6 minutes. The mixture was then degassed under 28″ Hg vacuum for 2 to 3 minutes (the degassing duration is adjusted based on the gel time of the resin). After degassing, the mixture was poured into appropriately shaped molds and allowed to cure for 12 hours at room temperature. The final products in the form of dog-bone coupons, with dimensions as per ASTM D638-94B, are shown in Fig. 4.6 [36].

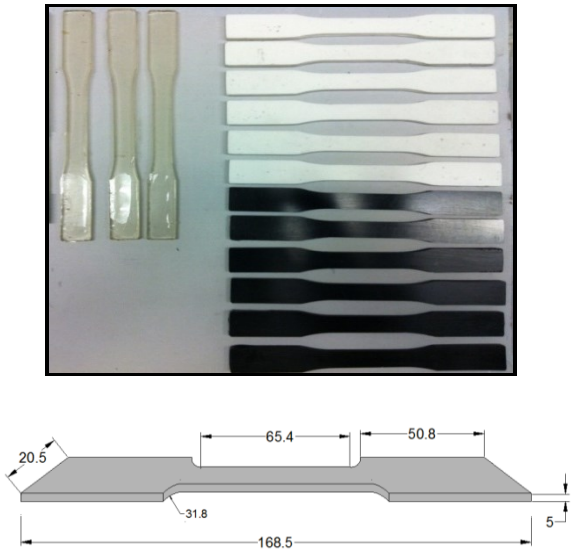

Fig. 4.6 Representative tensile coupons (neat, Q-Cell filler and nano-particle reinforced resins), as per ASTM D 638-94B (dimensions in mm).

4.5.2.3 Adherends preparation

To fabricate the adherends, laminate plates with a dimension of 350 mm × 350 mm were fabricated by the vacuum resin infusion technique (VRIT). Appropriately-sized coupons were then extracted from the plates, followed by the surface preparation process applied to the bonding regions [29-31]. To meet ASTM D5868-01 requirements, the graphite/epoxy and glass/epoxy plates were made from 12 uni-directional plies. Uni-directional graphite and E-glass fabrics and Huntsman's Araldite LY 564 epoxy resin with Aradure 2954 hardener (West Point, GA) were used to fabricate the laminate plates [35].

4.5.2.4 Single-lap joint preparation

Using the described jig, single-lap joints were prepared from graphite/epoxy, glass/epoxy laminate adherends and adhesive containing varying amounts of micro- and nano-particles. Some typical graphite/epoxy and glass/epoxy SLJ specimens are illustrated in Fig. 4.7.

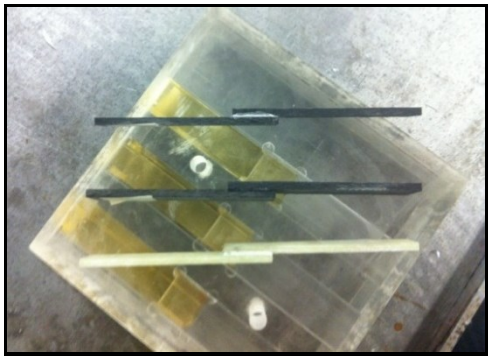

Fig. 4.7 Typical graphite/epoxy and glass/epoxy single-lap joint specimens.

To ensure the adhesive in ABJs would be subjected to concentric load, FRP tabs with appropriate thickness were affixed to the ends of the adherends (see Fig. 4.8).

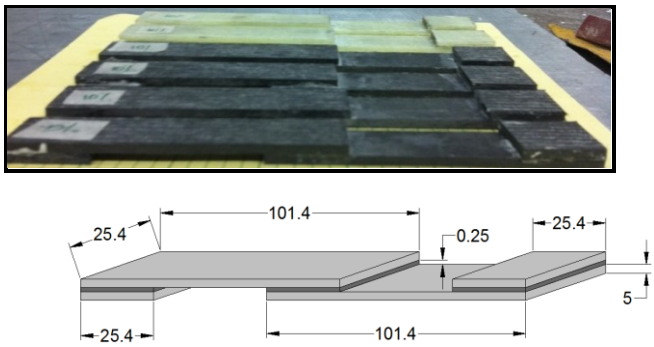

Fig. 4.8 Typical single-lap joint specimens (dimensions in mm; drawing not to scale).

It should be noted that, to prevent slippage and tearing-off of the adherends, tested under very high loading rate, modified quasi-isotropic tabs with holes in their centers were used (see Fig. 4.9). Details of the static, quasi-static and impact (high-strain) loading for the SLJ specimens are given in the next section.

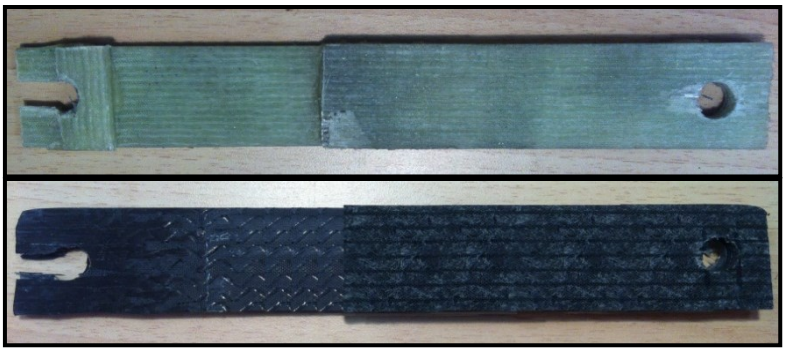

(a)

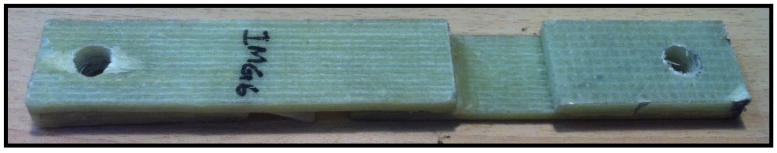

(b)

Fig. 4.9 (a) The failed specimens (with unidirectional tabs); (b) tabbed specimens used in the highest loading rate tests (with quasi-isotropic tabs).

4.5.3 Characterization of the mechanical properties of adhesives

The prepared dog-bone shaped specimens were tested in tension using an Instron servo-hydraulic universal test machine equipped with 8500^{+} electronics. As per the requirements of ASTM D638, the specimens were subjected to displacement controlled tensile loading to establish the stress-strain curve of each adhesive [36]. An Instron extensometer was used to record the gauge-length displacement (hence, the strain) of the specimens tested under static and quasi-static loading rates. First, tensile tests were performed on the neat resin at room temperature, at cross-head speeds of 1.5, 3, 15, and 150 mm/min (as baseline tests for the static and quasi-static loading conditions) and at 1,500 mm/min (as the baseline tests for the high strain rate loading condition), based on ASTM D 897 and ASTM D 950, respectively [39,41]. Subsequently, the reinforced-adhesive specimens underwent similar tests. Using the recorded load and gauge length displacement, the stress-strain curve of each adhesive was constructed and their elastic modulus evaluated.

4.6 Experimental investigation of ABJs

The experimental portion of the study consisted of two phases, as discussed below.

4.6.1 Baseline tests

To perform the baseline tests on the ABJs and the dog-bone shaped tensile coupons, the aforementioned loading rates were used. The applied load was recorded directly through the Instron machine's electronics and indirectly using the National Instrument DAQ system equipped with Lab View software. Gauge length displacement was also captured using a laser extensometer through the same DAQ system.

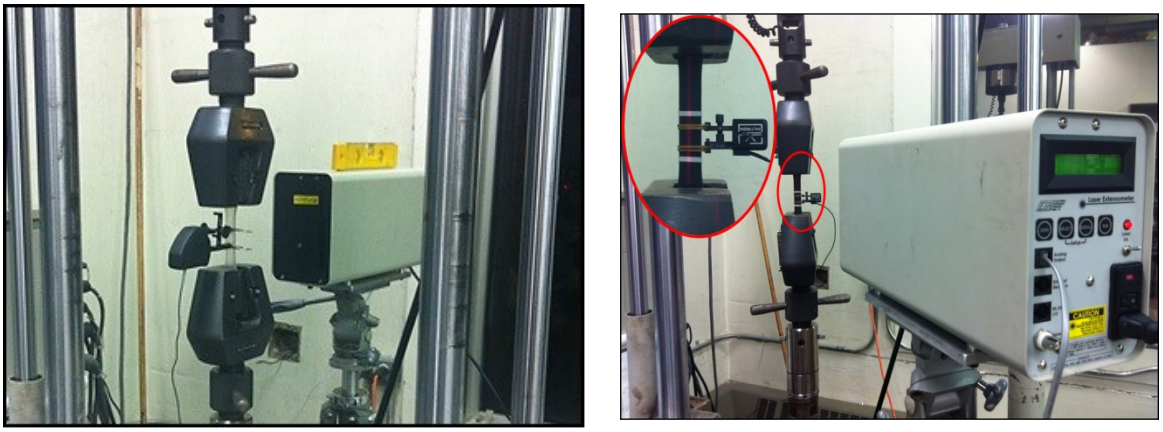

(a) (b)

Fig. 4.10 Experimental set-up of (a) static; (b) quasi-static and higher loading rate tests.

For greater accuracy as well as to obtain more mechanical characteristics of nano-reinforced adhesives (and to be able to use the obtained information in FEA), additional quasi-static and higher loading rate tests (i.e., at loading rates of 15, 150, 1500 mm/min) were conducted on dog-bone shaped tensile coupons using an Instron dynamic axial clip-on Extensometer (Instron Industrial Products, Grove City, PA) and EIR laser Extensometer (Electronic Instrument Research, Irwin, PA), simultaneously, as shown in Fig. 4.10(b). Static tests were also conducted under 1.5 mm/min using an Instron Static Extensometer (Instron Industrial Products, Grove, PA) and EIR Laser Extensometer (see Fig. 4.10(a)).

4.6.2 Impact (high loading rate) tests

In this category of tests, the applied load was measured using a PCB dynamic load cell (Depew, NY) positioned at the tip of the tensile carriage fixture (see Figure 4.11). The relative displacement of the overlap region was captured by a dynamic linear variable

differential transducer - DLVDT (Data Instruments, Acton, MA), with the set up shown in Fig. 4.11. The velocity of the impactor was also measured and adjusted using flat proximity sensors (Omron Corporation, Japan), as shown in Fig. 4.11.

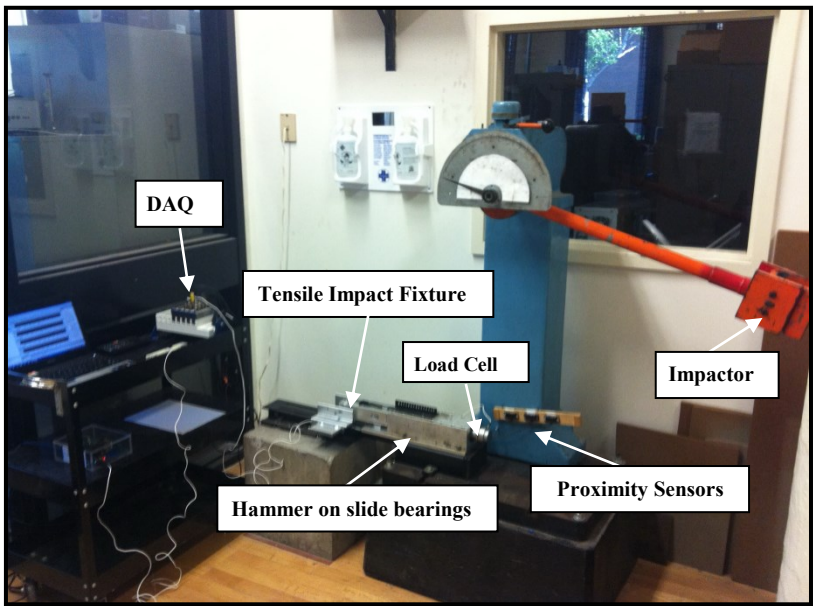

Fig. 4.11 Experimental test set-up for high loading rates.

4.7 Results and Discussion:

The processed experimental data related to the mechanical properties of adhesives (base-line tests) are shown in Fig. 4.12. As indicated, the results can be discussed from two significant points of view.

4.7.1 Influence of the micro-filler and nano-particles on the mechanical response of the adhesives

In light of the main objective of this research, and in an attempt to produce a strong and viscous adhesive from a commonly used and relatively inexpensive room-cured resin, Q-Cell filler and various nano-carbons were added to the neat resin (West System 105). The results of the tensile tests showed that although adding Q-Cell filler increased the adhesive's workability (viscosity), the mechanical properties of the adhesive were degraded. Moreover, the observed decrease in the mechanical properties of the Q-Cell-added adhesive renders the adhesive unsuitable for use in real-life bonding applications.

In contrast to the above, very good results were obtained when the least expensive type of nano-carbon (i.e., graphene nano-platelets [GNPs]) was added to the resin. Several researchers have also observed that the addition of Carbon Nano Fibers (CNF) or Multi-Walled Carbon Nano Tubes (MWCNTs) to resins have enhanced the resin's mechanical properties and fracture toughness [17-24]. However, very limited data currently exists for the level of enhancement that can be expected by the addition of GNPs to resins. As stated, GNPs are considerably less expensive than CNFs and MWCNTs. The results indicate that not only does the inclusion of GNPs improve the mechanical properties of this adhesive, it also enhances the resin's viscosity. This makes it suitable for use as an adhesive, especially for marine and other applications where relatively thick bond-line is used. In fact, the average ultimate tensile strength of the reinforced adhesive with 0.5% GNPs in weight was enhanced by 9% and 15%when specimen subjected to the low and higher loading rates, respectively. Also, as shown in Table 4.1, the average ultimate tensile strength of reinforced adhesive with 1% wt GNPs was improved by 12% and 19% for the lower and higher loading rates, respectively (see Fig. 4.12).

Table 4.1 Effect of nano reinforcement and loading rate on the average ultimate tensile strength (MPa) of adhesives

Loading Rate (mm/min)	Neat WS	WS with 0.25% GNP	WS with 0.5% GNP	WS with 1.0% GNP
1.5	51.12	54.62	55.84	57.15
15	60.87	66.28	67.24	68.36
150	69.33	76.69	78.16	80.17
1500	75.88	84.68	87.24	90.35

*WS stands for the West System.

To study the effect of nano reinforcement on the stiffness of adhesives, new sets of experiments were conducted using the Instron universal test machine, and an Instron clip-on extensometer (Instron Industrial Products, Grove City, PA), as well as a laser extensometer (Electronic Instrument Research, Irwin, PA) were used to extract the stress-strain curves. Additionally, to study the effect of roller gap width on calendering, and hence dispersion of nanoparticles, a roller gap size of 0.030 microns was used, which is larger than the diameter of the GNPs (25 nm or 0.025 microns). This size was chosen to prevent the nano-particles from being damaged while being exfoliated. The number of

calendering rounds was also decreased from 7 to 4. Nonetheless, despite the increase in roller gap size and the decrease in calendering, the results did not show any significant differences or enhancements in the average ultimate tensile strength and modulus of elasticity. This indicates that there is an optimum number for calendering cycles necessary for uniform dispersion of nano particles, and therefore additional efforts (i.e., more calendaring rounds) would be unnecessary. The results also indicated that choosing a gap size slightly larger than the diameter of the GNPs would prevent damage to the particles, while at the same time transferring sufficient shear force to exfoliate the particles. It is postulated that when the nano-particles are dispersed into adhesives, they would be wrapped by monomer molecules; subsequently, the addition of the curing agent would initiate the chemical reaction process of the resin. As a result, the monomer molecules of the resin would surround the GNPs as the resin cures and gets hardened. In addition to mechanical bonding, chemical bonding known as Van der Waals bonds takes place, as there are two different ways of load transfer between GNPs and polymer molecules. The inclusion of nano-particles into resin increases the resin viscosity (thickens the adhesive) by causing their molecular immobility. Consequently, the higher modulus of elasticity of the GNP enhances the stiffness of the nano-reinforced adhesives. Therefore, for exfoliating GNPs into resin efficiently, the gap size should be optimized and adjusted to transfer the required shear load to GNPs. This is because a greater interfacial area of GNPs increases the interactions between the adhesive and nano particles in comparison to other types of nano particles such as CNFs, or CNTs.

As noted, inclusion of GNP into the neat resin improved the stiffness of the adhesives. Table 2 shows that the modulus of elasticity was enhanced by 11%, and 21% for 0.5% GNP (in weight) nano-reinforced composite adhesive evaluated at the lowest, and highest loading rates, respectively. Also, based on these results, one can conclude that the higher weight percentage (i.e., 1% GNP) results in higher stiffness. It can be seen that the modulus of elasticity was enhanced by 19%, and 33% for 1% GNP (in weight) nano-reinforced composite adhesive at the lowest, and highest loading rates respectively.

Table 4.2 Effect of nano reinforcement and loading rate on modulus of elasticity of the resins

Modulus of elasticity values (MPa)				
Loading Rate (mm/min)	Neat WS	WS with 0.25% wt GNP	WS with 0.5% wt GNP	WS with 1.0% wt GNP
1.5	2708	2842.2	3012	3233.6
15	2896.8	3123.1	3349.1	3513.2
150	3007.3	3370.1	3577.1	3799.3
1500	3163.7	3646.1	3843.4	4201.8

*WS stands for the West System.

Fig. 4.12 shows the enhanced values in resins' stiffness and ultimate strength as a function GNP wt%. The chart demonstrates how the nano reinforcement offsets the effects of the loading rate, such that adding a small amount of GNPs plays the same role as the loading rate. In some cases, the addition of GNPs even has a greater influence on the mechanical properties of the adhesive in comparison with the effects of loading rates. As seen, the inclusion of 0.25 wt% of GNP to the resins tested under a static loading rate of 1.5 mm/min produces higher average ultimate tensile strength as well as higher average modulus of elasticity in comparison to the case when 0.5 wt% of CNF was added to the resins. Likewise, the mechanical properties of 0.5 wt% of GNP tested under a loading rate of 1.5 mm/min is higher than the mechanical properties of 0.25 wt% of GNP even when subjected to a loading rate of 15 mm/min.

It should be mentioned that nano reinforcement and loading rate effects appear to be coupled, and competing each other's effect.

Based on a study on the effect of nano particles' type, as it is shown in Fig. 4.12, GNPs indicate better mechanical properties. Also, as it is shown in Fig. 4.13, 1% wt GNP indicated higher performance compared to the other amounts. And at the end, Fig. 4.14 shows the stress-strain curves of the adhesives reinforced with various nanoparticles. As can be seen, the nano-reinforced adhesives strength and stiffness are increased by increasing the loading rate or strain rate.

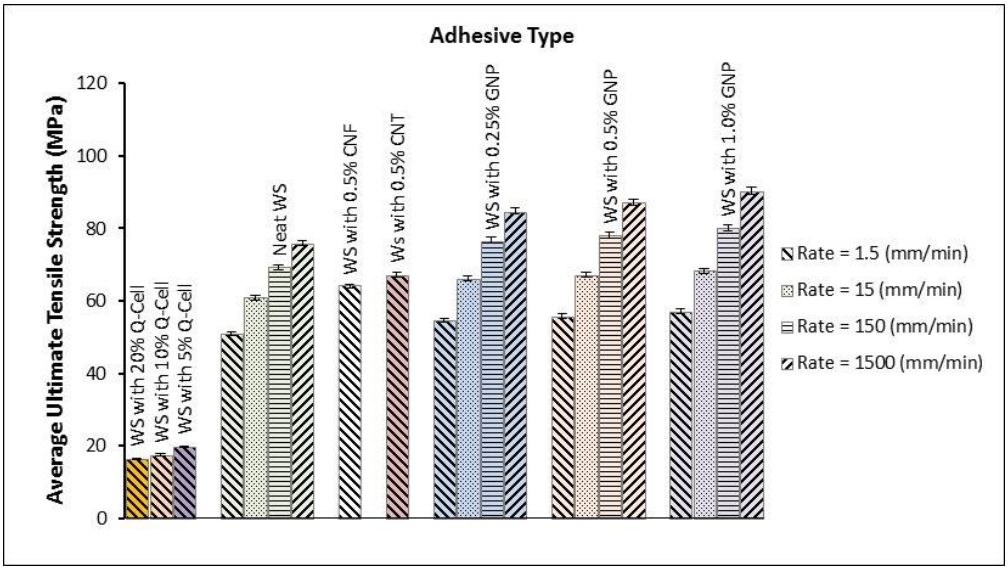

(a)

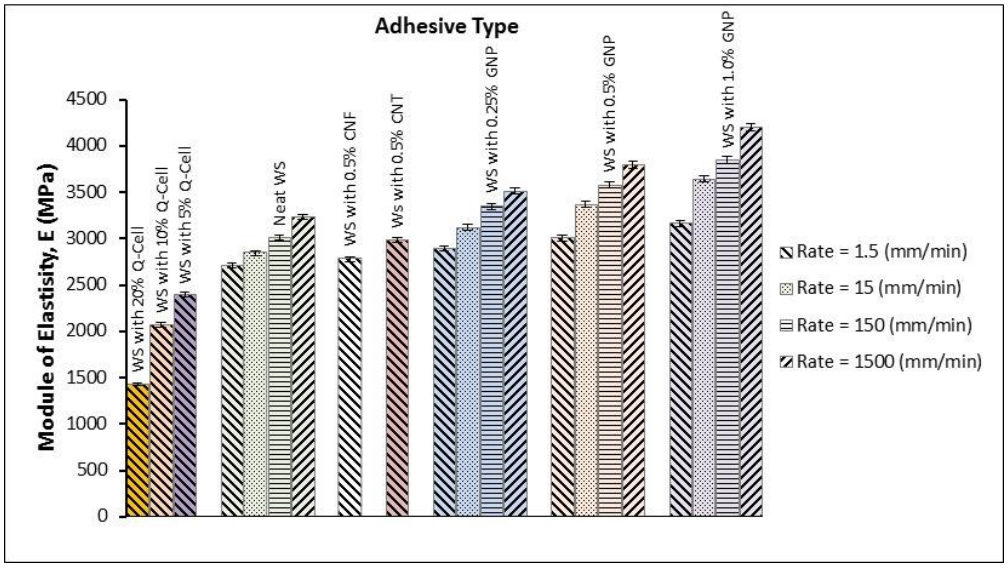

(b)

Fig. 4.12 Effects of the Q-Cell and various types of nano-carbon particles on resin's (a) ultimate tensile strength and (b) modulus of elasticity.

In further illustrating the influence of nanoparticle type on the response of the adhesives, the stress-strain response of the nano composite adhesives are shown in Fig. 4.12. As seen GNP inclusion produces the most optimum enhancement. Moreover, the results illustrated in Fig. 4.13 indicate that the optimum %wt inclusion of GNP is at 1% wt. Finally, the influence of the loading rate on the stress-strain response of GNP-reinforced resin can be seen in Fig. 4.14.

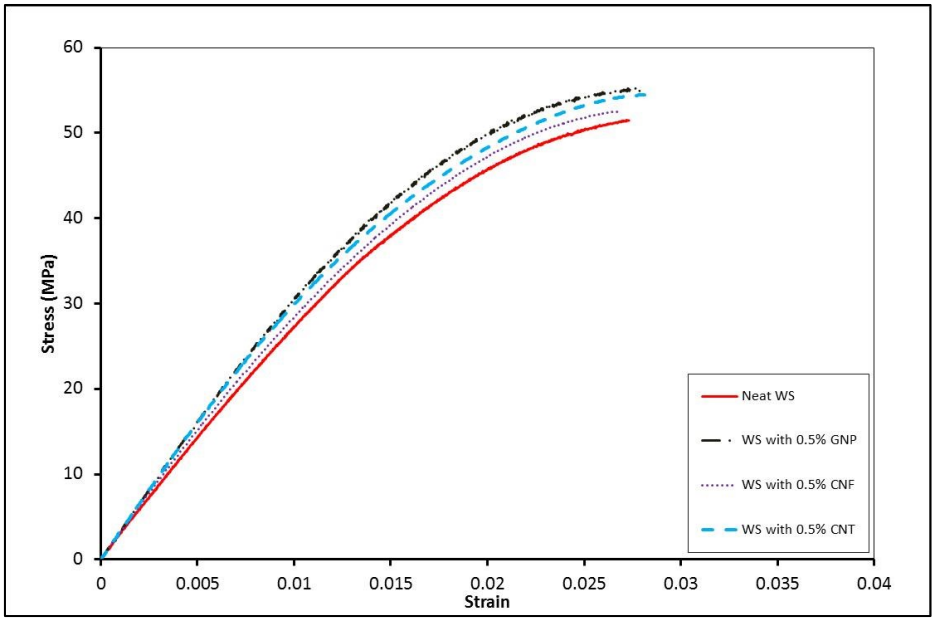

Fig. 4.13 Stress-strain curves of West System resins reinforced with various nanoparticles (Loading Rate =1.5 mm/min)

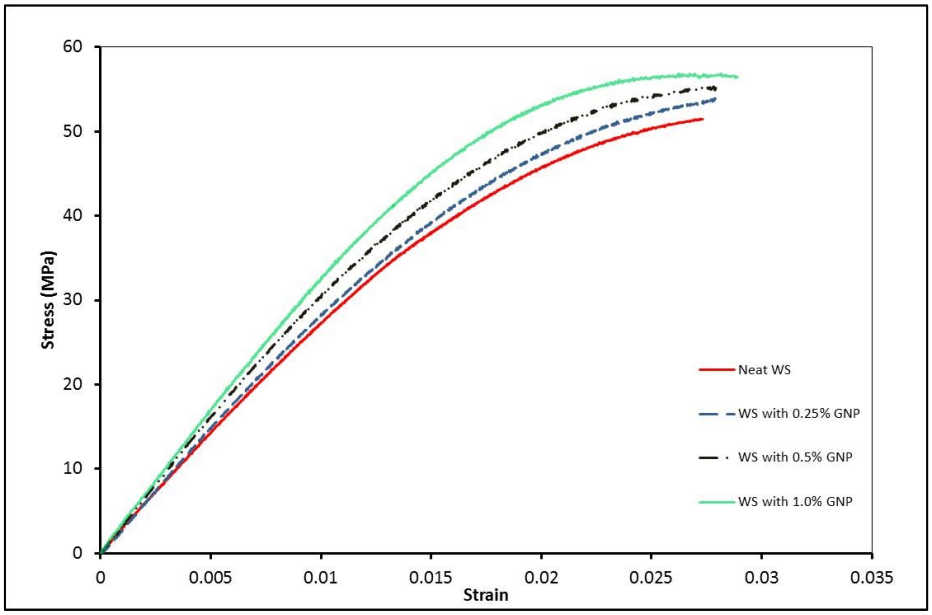

Fig. 4.14 Influence of GNP weight content on West System resin's mechanical response (Loading Rate = 1.5 mm/min).

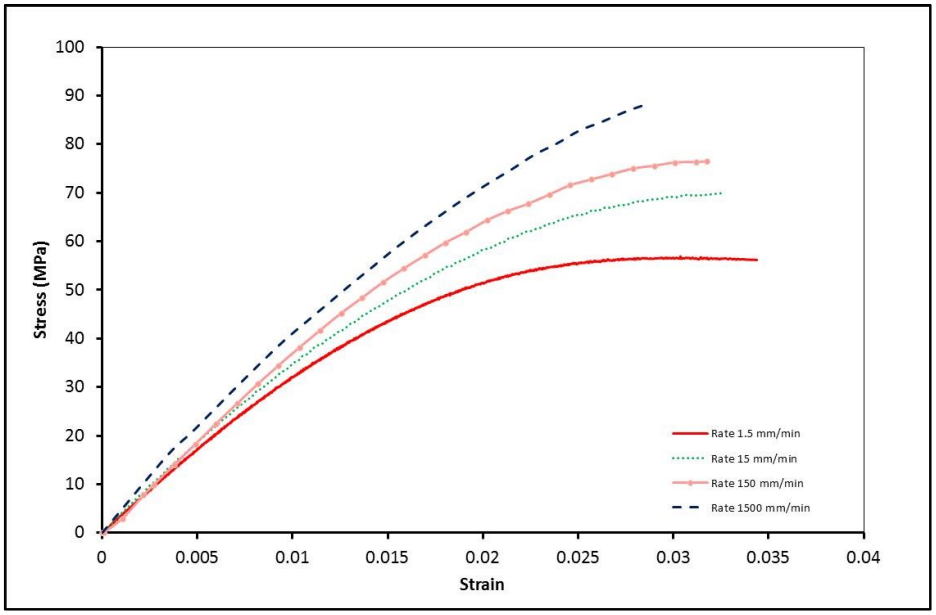

Fig. 4.15 Influence of loading rate on stress-strain responses of 1% wt GNP reinforced West System resin

4.7.2 Influence of loading rate on the mechanical response of nano-particle-reinforced SLJs

As discussed in the previous section (4.5.2.4), the prepared SLJ specimens were tested using a modified instrumented pendulum equipped with a specially designed impact load transfer apparatus, subjected to the HLR of 2.04×10^5 mm/min through the tensile impact apparatus.

The results showed that the inclusion of GNP in the resin could significantly improve the resin's stiffness and strength. The average ultimate shear strength of SLJs with carbon adherends was increased as much as 32% when SLJs were subjected to the HLR and by approximately 26% under quasi-static rate (see Fig. 4.16). It was observed that increase in the loading rate affected the average ultimate shear strength of the adhesive in a nonlinear manner. The level of enhancements changed in the case of SLJs with glass/epoxy adherends. In that case, the average ultimate shear strength was increased by 28% and 22% for the highest and static loading rates, respectively (see Fig. 4.17).

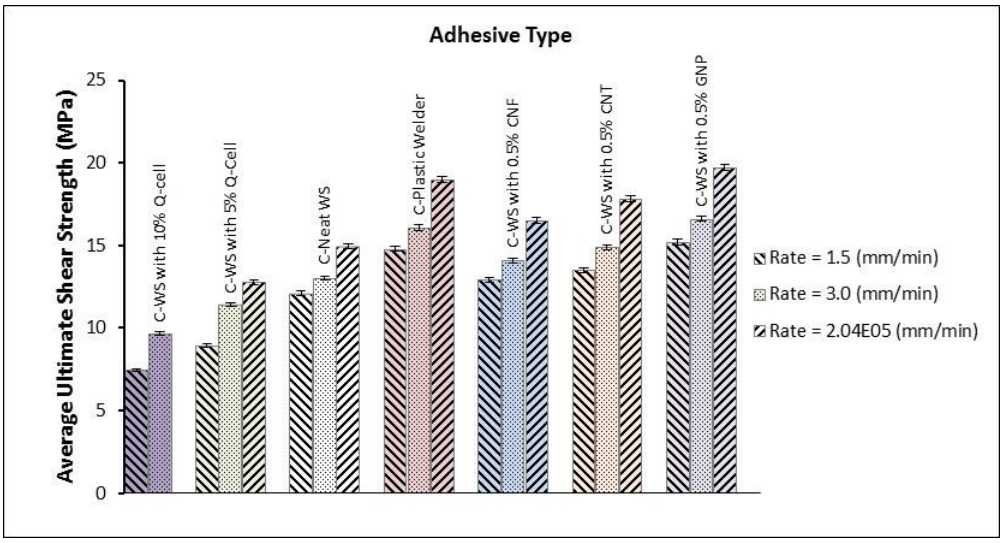

Fig. 4.16 Effect of loading rate on nano-reinforced SLJs with graphite/epoxy adherends.

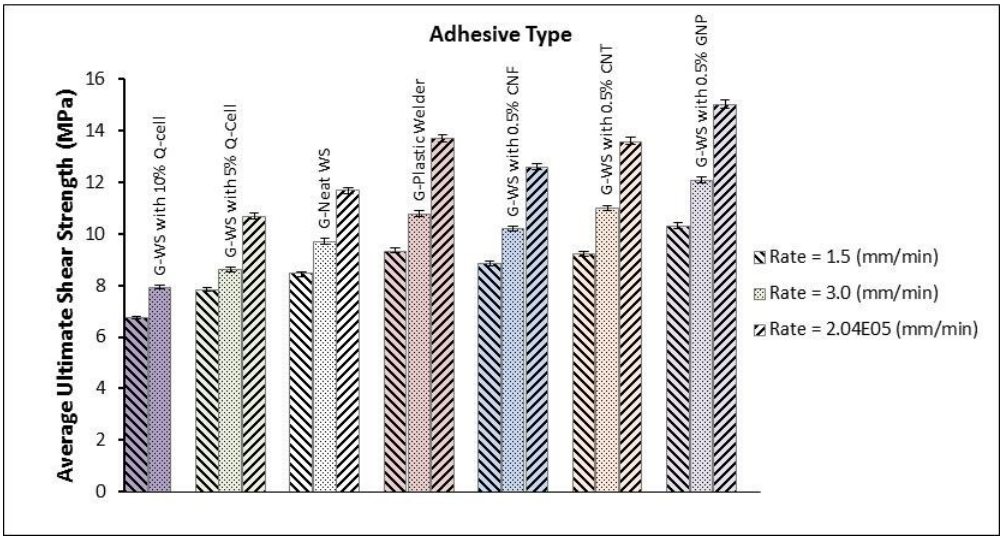

Fig. 4.17 Effect of loading rates on nano-reinforced SLJs with glass/epoxy adherends.

As noted, inclusion of GNP into the neat resin improved the stiffness and strength of the ABJs testes under different loading rates. Table 4.3 and 4.4 show that the apparent mechanical properties of ABJs (with different adherends) tested under different loading rates was improved by increasing the loading rate. Also, based on these results, one can conclude that the higher weight percentage (i.e., 1% GNP) results in higher stiffness, and strength.

Table 4.3 Effect of nano reinforcement and loading rate on Average ultimate shear strength (MPa) of SLJs with graphite/epoxy adherend tested under different loading rates.

Average ultimate shear strength (MPa) of C-SLJ*				
Loading Rate (mm/min)	Neat WS**	WS with 0.25% wt GNP	WS with 0.5% wt GNP	WS with 1.0% wt GNP
1.5	12.1	13.3	15.2	15.6
15	12.9	14.4	16.4	16.9
150	13.2	15.0	17.1	17.7
1500	13.8	15.8	17.9	18.6

* C-SLJ refers to the carbon/epoxy single-lap joints.
** WS stands for the West System.

Table 4.4 Effect of nano reinforcement and loading rate on Average ultimate shear strength (MPa) of SLJs with glass/epoxy adherend tested under different loading rates.

Average ultimate shear strength (MPa) of G-SLJ**				
Loading Rate (mm/min)	Neat WS*	WS with 0.25% wt GNP	WS with 0.5% wt GNP	WS with 1.0% wt GNP
1.5	8.4	9.7	10.3	11.7
15	10.3	12.2	13.8	15.3
150	10.8	12.9	14.4	16.1
1500	11.4	13.5	14.9	16.7

* C-SLJ refers to the carbon/epoxy single-lap joints.
** WS stands for the West System.

To gain a better understanding of the strength of nano-reinforced adhesives, the results were compared to the results of a two-part acrylic thermoplastic adhesive (Plastic Welder (PW) [Devcon, Danvers, MA]) which was used to form SLJ specimens.

In further illustrating the influence of nanoparticle type on the response of the ABJs, the stress-strain response of nano-reinforced ABJs with different adherends is shown in Fig. 4.18 and 4.21, for graphite/epoxy, and glass/epoxy adherends respectively. As seen GNP inclusion produces the most optimum enhancement. Moreover, the results illustrated in Fig. 4.19 and 4.22 indicate that the optimum %wt inclusion of GNP is at 1% wt. Finally, the influence of the loading rate on the stress-strain response and failure mode of GNP-reinforced ABJs can be seen in Fig. 4.20 and 4.23. Furthermore, as reported in Table 4.5, the average ultimate shear strengths of SLJs with carbon adherends are noticeably higher than those with E-glass adherends. This is due to the higher stiffness of carbon adherends, hence resistance to bending moments at the overlap region.

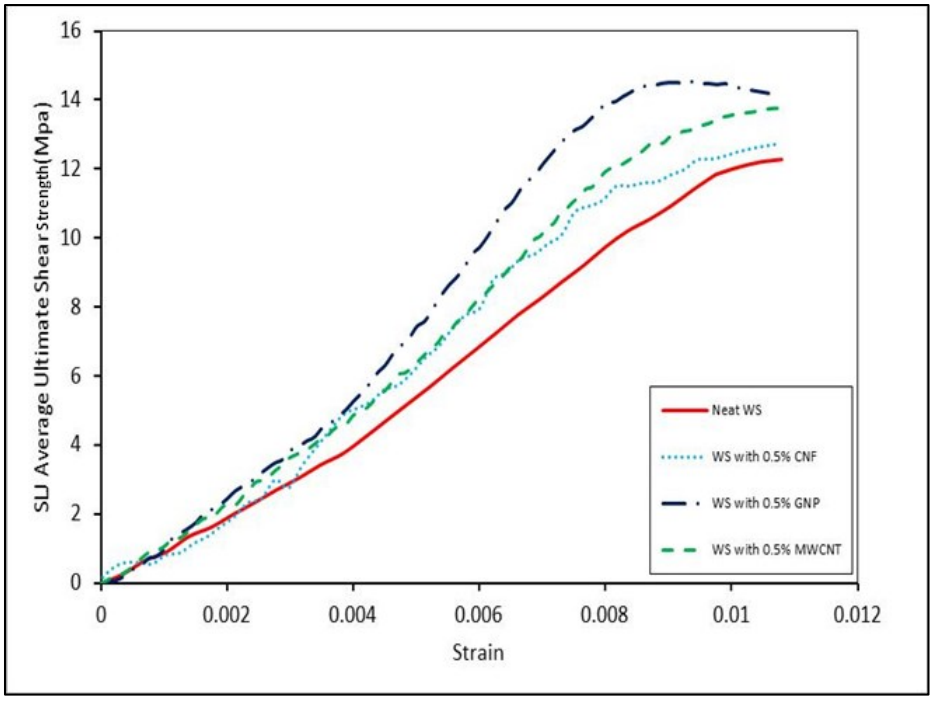

Fig. 4.18 Stress-strain curves of West System resins reinforced with various nanoparticles used to form ABJs with carbon/epoxy adherend (Loading Rate =1.5 mm/min)

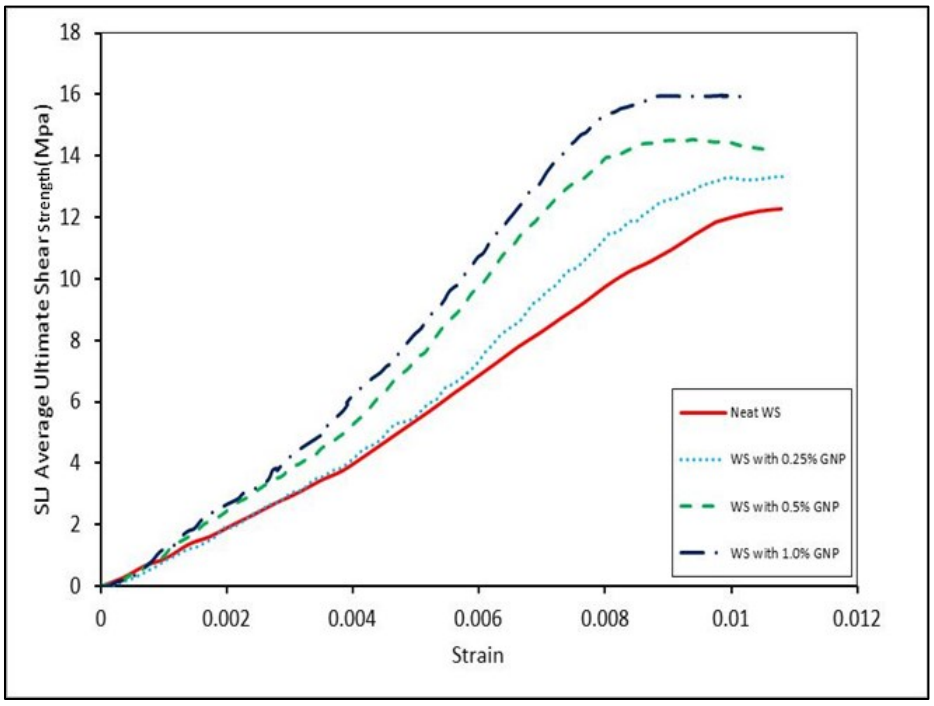

Fig. 4.19 Influence of GNP weight content on West System resin's mechanical response used to form ABJs with carbon/epoxy adherend (Loading Rate = 1.5 mm/min).

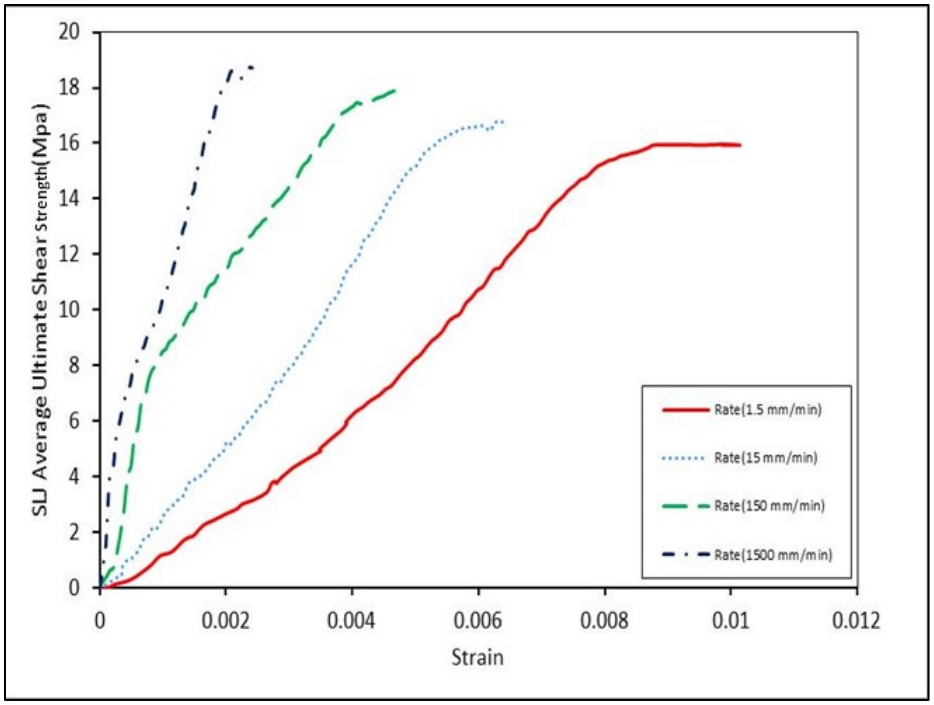

Fig. 4.20 Influence of loading rate on stress-strain responses, and failure mode of 1% wt GNP reinforced West System resin used to form ABJs with carbon/epoxy adherend.

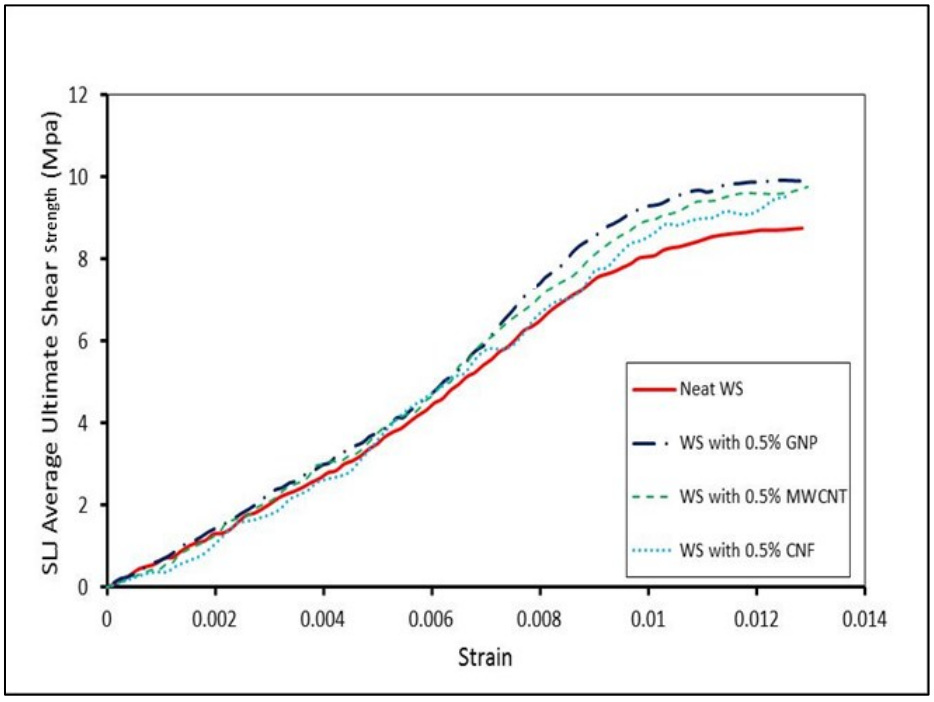

Fig. 4.21 Stress-strain curves of West System resins reinforced with various nanoparticles used to form ABJs with glass/epoxy adherend (Loading Rate =1.5 mm/min).

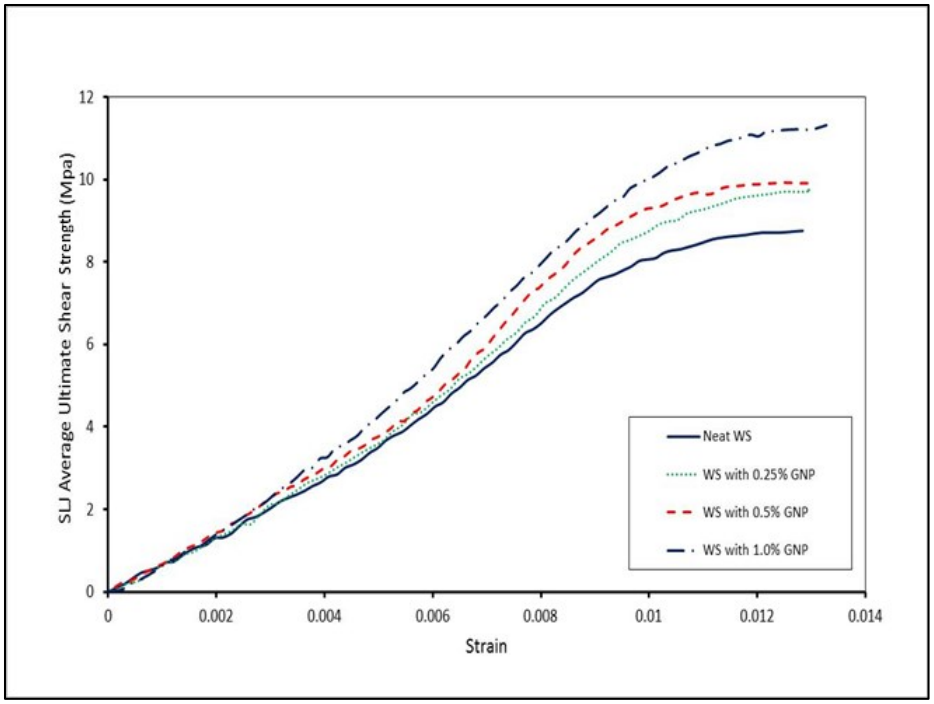

Fig. 4.22 Influence of GNP weight content on West System resin's mechanical response used to form ABJs with glass/epoxy adherend (Loading Rate = 1.5 mm/min).

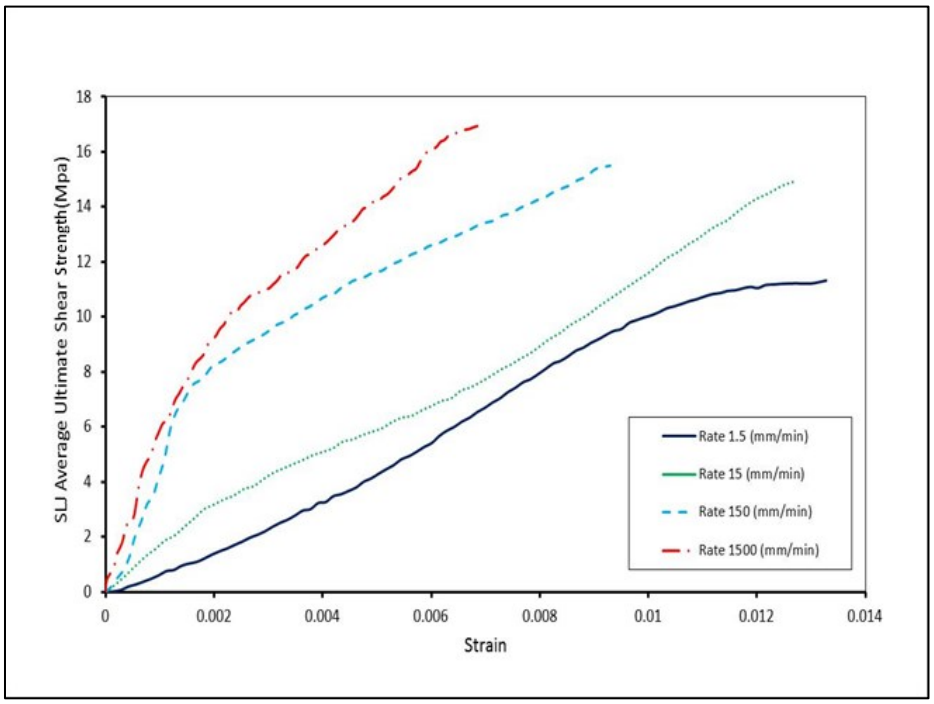

Fig. 4.23 Influence of loading rate on stress-strain responses, and failure mode of 1% wt GNP reinforced West System resin used to form ABJs with glass/epoxy adherend.

Table 4.5 Effect of adherend type on the average ultimate shear strength (MPa) of SLJs tested under different loading rates.

Adherend Type	Static loading rate (1.5 mm/min)					Impact loading rate (2.04E05 mm/min)				
	WS* with 5% wt Q-Cell	Neat WS	WS with 0.5% wt CNT	WS with 0.5% wt GNP	PW**	WS with 5% wt Q-Cell	Neat WS	WS with 0.5% wt CNT	WS with 0.5% wt GNP	PW
Graphite/Epoxy	8.9	12.1	13.5	15.2	14.9	14.9	14.9	17.8	19.7	18.2
Glass/Epoxy	7.8	8.4	9.2	10.3	9.3	10.7	11.7	13.6	15.0	13.7

*WS stands for the West System.
**PW stands for the Plastic Welder.

4.7.3 Failure Mechanism

Elastomeric particles (fillers or additives) would stretch as they bridge through a propagating crack, resulting in dissipating a portion of the energy required to develop the new surfaces of the growing crack. This, in turn, leads to increased strength under higher rate of loading. Fig. 4.24(a) illustrates the SEM images of the GNP powder. The remaining figures show the fractured surface of the GNP-reinforced resin as well as that of folded, exfoliated, and piled GNP-reinforced resins, respectively. The higher surface aspect ratio of the GNPs offers added strength to micro-cracking. Moreover, in the event of cracking, they effectively bridge the micro-cracks, in contrast to the MWCNTs dispersed in the resin, and are usually filamentous and furcated, or exfoliated and piled on top of one another, as can be seen in Figs. 4.24 (b, c) [33, 34].

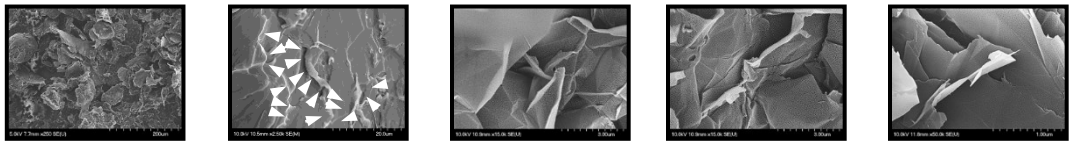

(a) (b) (c) (d) (e)

Fig. 4.24 SEM images of (a) GNP powder, (b) fractured surface of GNP-reinforced resin with GNPs identified by the arrows, and (c) folded, (d) exfoliated, and (e) piled GNP-reinforced resin.

It was observed that interfacial, and cohesive failure occurred in all specimens, regardless of loading rate. Hoeever, the failure mechanism was different, depending on the loading rate. Fig. 4.25 shows different modes of failure observed in nano-reinforced adhesives of SLJs when tested under different loading rates. Based on the statistical study of the geometric appearance of fractured surfaces of SLJs' adherends (shown at the left column

of Fig. 4.25), and of the tensile coupons (shown at the right column of Fig. 4.25). It can be seen that in specimens tested under the highest loading rates (HLR), micro cracks appeared in the form of straight lines, separating the failure zone borders into two parts (see Fig. 4.25(a)). In contrast, the failure in specimens tested under static and quasi-static rates appeared in the form of a jagged front (see Fig. 4.25(b)). Fiber imprints can also be seen in the failure zones of these SLJs. From these results, it can be surmised that although failure was in combined mode I and II, mode II was the primary cause of failure of the ABJs subjected to the HLR due to the existance of very high shear stress concentration. This is in contrast to the modes of failure observed in ABJs subjected to static, or quasi-static loading rates, which mostly occurred under mixed-mode with more significant contribution by mode I, due to the existance of relatively high peel stress. Fig. 4.25(c) illustrates typical failure surfaces of MWCNT-reinforced ABJs (on left) and MWCNT reinforced adhesive (on right).

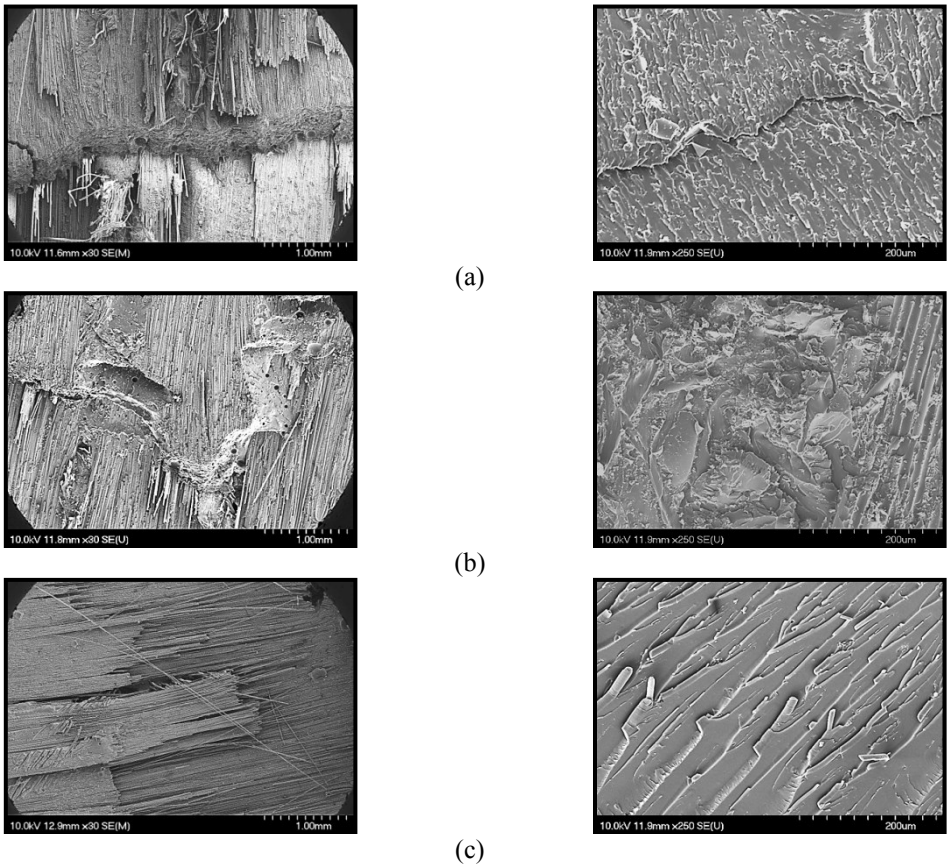

Fig. 4.25 SEM images of failure surfaces of nano-reinforced ABJs failed under different loading rates; (a) GNP, 2.04E+5 mm/min (b) GNP 1.5 mm/min (c) MWCNT 1.5 mm/min

It should be mentioned here that, from a macro-molecular point of view, loading rates also affected failure modes. Fig. 4.26 illustrates the differences between failure modes in static and HLR. As shown, in the specimens tested under static loading rate adhesive chunks remained on the adherends only the bonded zone almost two equal portions. Although, the failure of the specimens tested under static loading rate occurred under interfacial category of failure, and at the middle of the adhesive. However, in the case of HLR (impact), the failure occurred almost at the end of the bond-line, and almost in complete cohesive failure mode.

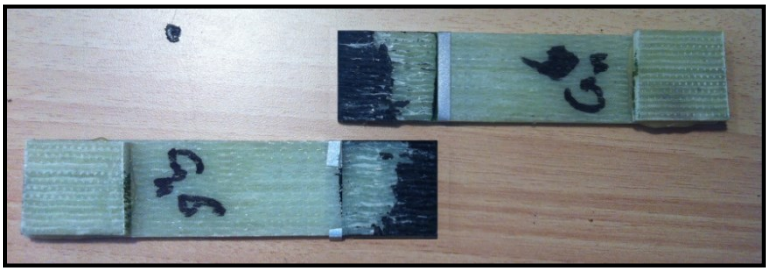

(a)

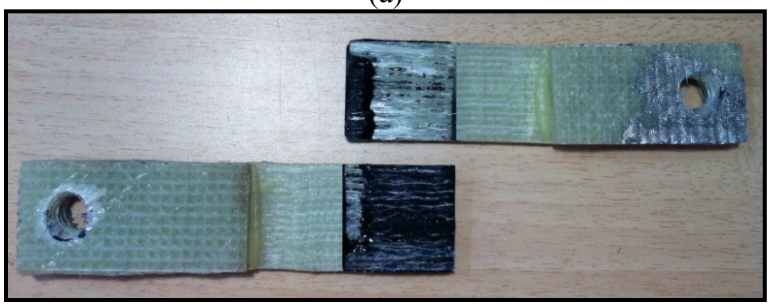

(b)

Fig. 4.26 The effects of loading rates on failure modes in SLJs (a) typical failure mode observed under static and quasi-static loading rate (b) at the highest loading rate (impact).

4.8 Conclusions

The results of the comprehensive experimental investigation on the influence of loading rate on SLJ indicated that ABJs tested under highest loading rate exhibited improved stiffness and strength. It was also observed that inclusion of 0.25 wt% GNP in the adhesive produced approximately the same mechanical properties as the inclusion of 0.5 wt% CNF and CNT in the adhesive did at the same loading rate. Moreover, SLJ specimens produced by 0.5 wt% GNP tested under lower loading rates exhibited similar behavior as did the SLJs prepared with 0.25 wt% GNP when tested under the highest loading rate. As well, it was determined that ABJs with carbon adherends produced

higher strength compared to ABJs with glass adherends. It was also observed that the increase in the loading rate increased the average ultimate shear and tensile strength and stiffness of the ABJs.

The other observations of this experimental investigation are as follows:

1. The results of the tensile tests on the adhesive coupons showed that although adding Q-Cell filler increased the adhesive's workability (viscosity), however, the mechanical properties of the adhesive were degraded. The observed decrease in Q-Cell-added adhesive renders the adhesive unsuitable for practical bonding.

2. In contrast to the above, very good results were obtained when the relatively inexpensive type nano-carbon (i.e., graphene nano-platelets - GNP) was added to the resin. It was also observed that the addition of Carbon Nano Fibers (CNF) or Multi-Walled Carbon Nano Tubes (MWCNTs) to resins improved the resin's mechanical properties, but not to the same degree as the GNP did.

3. It was demonstrated that the increase in loading rate resulted to higher apparent strength and stiffness of ABJs. This increase was even more significant than the enhancement obtained by inclusion of the nano-carbon particles. Moreover, the increase in stiffness was more significant compare to the strength.

4. ABJs with graphite/epoxy adherends showed higher strength and stiffness compare to the ones with glass/epoxy adherends. This increase is attributed to the fact that graphite/epoxy adherends are in general stiffer than glass/epoxy adherends, and consequently, the bending moments at the overlap region (hence the shear and peel stresses) are minimized.

5. In contrast to the failure mode observed in the specimens tested under the highest loading rate (i.e., straight cracking front), the failure in specimens tested under static and quasi-static rates appeared in the form of a jagged front. While, cohesive debonding, and mode II of failure (due to higher shear stress) were

observed in specimens tested under highest loading rate, interfacial failure, but with a more dominant mode I failure mode (due to higher peel stress) were observed in specimens tested under static and quasi-static loading rates.

4.9 Acknowledgement:

The Natural Science and Engineering Research Council of Canada's financial support for this research work is gratefully acknowledged.

4.10 References

[1] da Silva L. F. M., Ochsner A., and Adams R. D. [2011] Handbook of adhesion technology. Springer-Verlag, Berlin, Heidelberg.

[2] Petrie E. M. [2000] Handbook of adhesives and sealants. McGraw-Hill, New York.

[3] Kinloch A. J. [1987] Adhesion and adhesives: science and technology. Chapman & Hall, London.

[4] Adams R. D., Comyn J., and Wake W. C. [1997] Structural adhesive joints in engineering, 2nd edition. Chapman & Hall, London.

[5] Berthelot J.-M. [1999] Composite materials, Mechanical behavior and structural analysis. New York: Springer.

[6] Hyer M. W. [1998] Stress Analysis of Fiber-Reinforced Composite Materials. McGraw-Hill Inc., New York.

[7] Reddy J. N. [2006] Theory and Analysis of Elastic Plates and Shells CRC, 2nd edition. Taylor & Francis, Philadelphia, PA.

[8] Timoshenko S., and Woinowsky-Krieger S. [1959] Theory of Plates and Shells, 2nd Ed., McGraw-Hill, New York.

[9] Banea M. D., and da Silva L. F. M. [2008] Adhesively-bonded joints in composite materials: an overview, Journal of Materials: Design and Applications, vol. 233, pp. 1-18.

[10] Iijima S. [1991] Helical microtubules of graphitic carbon. Journal of Nature, vol. 354, pp. 56-58.

[11] Iijima S., and Ichihashi T. [1993] Single-shell carbon nanotubes of 1-nm diameter. Journal of Nature, vol. 363, pp. 603-605.

[12] Tjong S. C. [2006] Structural and mechanical properties of polymer nanocomposites. Journal of Material Science and Engineering, vol. 53, Issue (3-4), pp. 73-197.

[13] Lau K.T., Gu C., Gao G.H., Ling H.Y., and Reid S.R [2004] Stretching process of single- and multi-walled carbon nanotubes for nanocomposite applications. Journal of Carbon, vol. 42, Issue (2), pp. 426-429.

[14] Saito R., Dresselhaus G., and Dresselhaus M. S. [1998] Physical properties of carbon nanotubes. Imperial College Press, London.

[15] Demczyk B. G., Wang Y. M., Cumings J., Hetman M., Han W., Zettl A., and Ritchie R. O. [2002] Direct mechanical measurement of the tensile strength and elastic modulus of multiwalled carbon nanotubes. Journal of Material Science and Engineering, vol. 12, pp. 934-935.

[16] Alexandre M., and Dubois P. [2000] Polymer-layered silicate nanocomposites: preparation, properties and uses of a new class of materials. Journal of Material Science Engineering Reports, vol. 28, Issue (1-2), pp. 1-63.

[17] Hsiao K. T., Alms J., and Advani S. G. [2003] Use of epoxy/multiwalled carbon nanotubes as adhesives to join graphite fiber reinforced polymer composites. Nanotechnology, vol. 14, Issue (7), pp. 791-793.

[18] Harris J. A., and Adams R. [1985] An assessment of the impact performance of bonded joints for use in high energy absorbing structures. Proc International Mechanical Engineering, vol. 199(C2), pp. 121-131.

[19] Galliot C., Rousseau J., and Verchey G. [2012] Drop weight tensile impact testing of adhesively-bonded carbon/epoxy laminate joints. International Journal of Adhesion and Adhesives, vol. 35, pp. 68-75.

[20] Goglio L., and Rossetto M. [2008] Impact rupture of structural adhesive joints under different stress combinations. International Journal of Impact Engineering, vol. 35, Issue (7), pp. 635-643.

[21] Ger G.S., Kawata K., and Itabashi M. [1996] Dynamic tensile strength of composite laminate joints fastened mechanically. Journal of Theoretical and Applied Fracture Mechanics, vol. 24, Issue (2), pp. 147-155.

[22] Kevin A., Brown K. A., Brooks R., and Warrior N. A. [2010] The static and high strain rate behavior of a commingled E-glass/polypropylene woven fabric composite. Composites Science and Technology, vol. 70, Issue (2), pp. 272-283.

[23] Srivastava V. K., and Hogg P. J., Moisture [1998] Effects on the toughness, mode-I and mode-II of particles filled quasi-isotropic glass-fibre-reinforced polyester resin composites. Journal of Material Science. vol. 33, Issue (5), pp. 1129-1136.

[24] Srivastava V.K. [2011] Effect of carbon nanotubes on the strength of adhesive lap joints of C/C and C/C–SiC ceramic fibre composites. International Journal of Adhesion and Adhesives, vol. 31, Issue (6), pp. 486-489.

[25] Jacob G. C., Starbuck J. M., Fellers J. F., and Simunovic S. [2004] Strain rate effects on the mechanical properties of polymer composite materials. Journal of Applied Polymer Science, Vol. 94, pp. 296-301.

[26] Sierakowski R. L. [1999] Strain rate effects in composites. Journal of Applied Mechanics Review, vol. 50, pp. 741-761.

[27] Barre S., Chotard T., and Benzeggagh M. L. [1996] Comparative study of strain rate effects on mechanical properties of glass fiber-reinforced thermoset matrix composites. Journal of Composite: Applied Science Manufacturing, vol. 27, pp. 1169-1181.

[28] Hamouda M. S. and Hashmi M. S. J. [1998] Testing of composite materials at high rates of strain: advances and challenges. Journal of Material Processing Technology, vol. 7, pp. 327-336.

[29] Davis M. J. and Bond D. [1999] Principles and practice of adhesive bonded structural joints and repairs. International Journal of Adhesion and Adhesives, 19(3), 91-105.

[30] Molitor P., Barron V., and Young T. [2001] Surface treatment of titanium for adhesive bonding to polymer composites: a review. International Journal of Adhesion Adhesives, vol. 21, Issue (2), pp. 129-136.

[31] Kim J. S., and Reneker D. H. [1999] Mechanical properties of composites using ultrafine electrospun fibers. Journal of Polymer Composites, vol. 20, Issue (1), pp. 124-131.

[32] J. A. Chambers, [1995] Preloaded Joint Analysis Methodology for Space Flight Systems. NASA TM-106943, December 1995.

[33] Rothon R. N., and Hancock M. [1995] General principles guiding selection and use of particulate materials. In: Particulate-filled polymer composites. Rothon R. N. (ed) Longman Scientific and Technical, Harlow, P1.

[34] Senguptaa R., Bhattacharyaa M., Bandyopadhyayb S., and Bhowmicka A.K. [2011] A review on the mechanical and electrical properties of graphite and modified graphite reinforced polymer composites, Journal Polymer Science, vol. 36, pp. 638-670.

[35] ASTM D5868-01, Standard Test Method for Lap Shear Adhesion for Fiber Reinforced Plastic (FRP) Bonding, ASTM International, West Conshohocken.

[36] ASTM D638, Standard Test Method for Tensile Properties of Plastics, ASTM International, West Conshohocken.

[37] ASTM D907, Terminology of Adhesives, ASTM International, West Conshohocken.

[38] ASTM D4896, Guide for Use of Adhesive-Bonded Single-lap-Joint Specimen Test Results, ASTM International, West Conshohocken.

[39] ASTM D897, Test Method for Tensile Properties of Adhesive Bonds, ASTM International, West Conshohocken.

[40] ASTM D905, Test Method for Strength Properties of Adhesive Bonds in Shear by Compression Loading, ASTM International, West Conshohocken.

[41] ASTM D950, Test Method for Impact Strength of Adhesive Bonds, ASTM International, West Conshohocken.

[42] ASTM D1002, Test Method for Apparent Shear Strength of Single-Lap-Joint Adhesively-Bonded Metal Specimens by Tension Loading (Metal-to-Metal), ASTM International, West Conshohocken.

[43] Kaneka, http://www.kaneka.com. Retrieved 9 April 2012.

[44] Sigma Aldrich, http//www.sigmaaldrich.com. Retrieved 9 October 2012.

[45] Volkersen O., [1938] The rivet load distribution in lap-joints with member of constant thickness subjected to tension. Luftfahrtforschung, 15, 41-47.

[46] Goland M., and Reissner E. [1944] The stress in cemented joints. J Applied Mechanics, 11, A17-A27

[47] Hart-Smith L. J. [1973] Adhesive-bonded single-lap joints. NASA Langley Research Center, NASA CR-112235.

[48] Shahin K., and Taheri F. [2008] The strain energy release rates in adhesively bonded balanced and unbalanced specimens and lap joints. International J. Solids and Structures, 45, 6248-6300.

[49] Adams R. D., and Peppiatt N. A. [1973] Effects of Poisson's ratio strains in adherends on stresses of an idealized lap joint. J. Strain Analysis, 8(2), 134-139.

[50] Taheri F., and Zou G.P. [2004] Treatment of Unsymmetric Adhesively Bonded Composite Sandwich Panels-To-Flange Joints. International J. Mechanics of Advanced Materials and Structures, 11 (2), 175-196.

CHAPTER 5 SUMMARY AND CONCLUSION

5.1 Summary

In this thesis, the response of two types adhesives, as well as the response of adhesively bonded joints (ABJs) formed by epoxy adhesive reinforced with various type of nano-carbon particles were systematically investigated. ABJs made by graphite epoxy and E-glass epoxy adherends were considered. The study was divided into two separate, distinct, but complimentary parts, each dealing with specific aspect of the composite adhesive behavior in an adhesively bonded joint.

First an experimental investigation was conducted to study the influence of loading rate on nano reinforced composite adhesives use in forming adhesively bonded single-lap joints, with the specific concentration on the average ultimate tensile and shear strengths of the ABJ. This study is unique in that it considered the effect of very high loading rate (tensile impact) on graphene nano-reinforced adhesives.

In the second part of the investigation, the work was extended to study the effect of nano particles weight fraction on the response of ABJs. This work was undertaken primarily to determine the influence of various weight percentages of grapheme nano platelets utilized to reinforced ABJs under different loading rates. In addition, the failure mechanism and modes were carefully studied using scanning electron microscopic (SEM).

The investigation also aimed at establishing the mutual and relative influence of the nano reinforcements and loading rate.

5.2 Conclusions

While the overall aim of this thesis was to develop a relatively inexpensive and strong adhesive for common engineering applications where relatively thicker bond-lines are required (unlike the aerospace related applications), various aspects of nano composite adhesives utilized in the form of adhesively bonded single-lap joints were investigated. During the course of this study, it was deemed necessary to establish a comprehensive

database in regards with enhancement of the mechanical behavior of nano composite adhesives. The following conclusions can be made based on the results established through the experimental investigation carried out in this thesis:

1. The results of the tensile tests showed that although adding Q-Cell filler increased the adhesive's workability (viscosity), however, the mechanical properties of the adhesive were degraded. The observed decrease in Q-Cell-added adhesive renders the adhesive unsuitable for practical bonding.

2. In contrast to the above, very good results were obtained when the relatively inexpensive type nano-carbon (i.e., graphene nano-platelets - GNP) was added to the resin. It was also observed that the addition of carbon nano-fibers (CNF) or multi-walled carbon nano tubes (MWCNTs) to resins improved the resin's mechanical properties.

3. It was also discovered that using very small amount of GNP (0.25% in weight) to the epoxy adhesive produced almost similar improvement as that attained when higher amount of CNT (0.5% in weight) was utilized. In general, the comparison of the results obtained for adhesive reinforced with the various weight percentage of nano reinforcement considered in this study, it was observed that the larger the weight fraction of the GNP, the more improved the strength and stiffness of the adhesive.

4. It was shown that the increase in the loading rate, the increased the apparent mechanical properties of the adhesives. In fact the apparent increase attained due to higher loading rate was larger than the improvement resulting due to inclusion of the nano particles, especially, when graphene nano platelets were used.

5. Although, it was observed that increasing the strain rate, as well as inclusion of nano particles, results in improving the strength (average ultimate tensile and shear stresses), and stiffness (tensile and shear modulus) of the adhesives and ABJs, however, increase in stiffness was more significant.

6. ABJs with graphite/epoxy adherends showed higher strength and stiffness compare to the ones with glass/epoxy adherends. This increase is attributed to the fact that graphite/epoxy adherends are in general stiffer than glass/epoxy adherends, and consequently, the bending moments at the overlap region (hence the shear and peel stresses) are minimized.

7. In contrast to the failure mode observed in the specimens tested under the highest loading rate (i.e., straight cracking front), the failure in specimens tested under static and quasi-static rates appeared in the form of a jagged front. While, cohesive debonding, and mode II of failure (due to higher shear stress) were observed in specimens tested under highest loading rate, interfacial failure, but with a more dominant mode I failure mode (due to higher peel stress) observed in specimens tested under static and quasi-static loading rates.

5.3 Recommendations

The experimental studies discussed through this thesis with respect to the high loading rate response of composite adhesives do present difficulties. Review of the large volume of literature on loading rate effects on the mechanical properties of composites showed that most of the high loading rate characterization studies conducted thus far have focused on thermoset composites (i.e., epoxy and polyester matrices reinforced mainly with glass and carbon fibers). In contrast, few attempts have been made to study the influence of loading rate on mechanical properties of thermoplastic adhesives. Moreover, the mechanical properties of the GNP composite adhesives obtained through the experimental works carried out here could be used in conducting more precise finite element modeling, using the cohesive zone modeling approach. The suggested approach should enable one to model the actual performance of such reinforced adhesives, especially in the context of different joining configurations, in a more economical and effective manner. One should also explore the perspectives of crack initiation and propagation through such computational analysis.

BIBLIOGRAPHY

[1] Da Silva L. F. M., Ochsner A., Adams R. D. [2011] Handbook of adhesion technology. Springer-Verlag, Berlin, Heidelberg.

[2] Petrie E. M. [2000] Handbook of adhesives and sealants. McGraw-Hill, New York.

[3] Kinloch A. J. [1987] Adhesion and adhesives: science and technology. Chapman & Hall, London.

[4] Adams R. D., Comyn J., Wake W. C. [1997] Structural adhesive joints in engineering, 2nd edition. Chapman & Hall, London.

[5] Possart W. [1988] Experimental and theoretical description of the electrostatic component of adhesion at polymer/metal contact. International J Adhesion and Adhesives, 8(2), 77-83.

[6] Maheri M. R. and Adams R. D. [2002] Determination of dynamic shear modulus of structural adhesives in thick adherend shear test specimens. International J. Adhesion and Adhesives, 22(2), 119-127.

[7] Banea M. D. and da Silva L. F. M. [2009] Adhesively bonded joints in composite materials: an overview. J. Material Design and Applications, 223(L).

[8] Baldan A. [2004] Adhesively-bonded joints and repairs in metallic alloys, polymers and composite materials: adhesives theories and surface pretreatment. J. Material Science, 39, 1-49.

[9] Davis M. J. and Bond D. [1999] Principles and practice of adhesive bonded structural joints and repairs. International J. Adhesion and Adhesives, 19(3), 91-105.

[10] Molitor P., Barron V., and Young T. [2001] Surface treatment of titanium for adhesive bonding to polymer composites: a review. International J. Adhesion and Adhesives, 21(2), 129-136.

[11] Kim J. S. and Reneker D. H. [1999] Mechanical properties of composites using ultrafine electrospun fibers. J. Polymer Composites, 20(1), 124-131.

[12] Sancaktar E. and Aussawasathien D. [2009] Nanocomposites of epoxy with electrospun carbon nanofibers: mechanical behavior. J. Adhesion, 85, 160-179.

[13] Qian D., Dickey E. C., Andrwes R., and Rantell T. [2000] Load transfer and deformation mechanisms in carbon nanotube-polystyrene composites. J. Applied Physics Letters, 76, 2868-2870.

[14] Yu M. F., Lourie O., Dyer M., Moloni K., Kelly T., Ruoff R. S. [2000] Strength and breaking mechanism of multiwalled carbon nanotubes under tensile load. J. Science, 287(5453), 637-640.

[15] Rothon R. N. and Hancock M. [1995] General principles guiding selection and use of particulate materials. In: Particulate-filled polymer composites. Rothon R. N. (ed) Longman Scientific and Technical, Harlow, P1.

[16] SigmaAldrich, http//www.sigmaaldrich.com. Retrieved 9 October 2012.

[17] Senguptaa R., Bhattacharyaa M., Bandyopadhyayb S., Bhowmicka A.K. [2011] A review on the mechanical and electrical properties of graphite and modified graphite reinforced polymer composites, J Polymer Science, 36, 638-670.

[18] Iijima S. [1991] Helical microtubules of graphitic carbon. J. Nature, 354, 56-58.

[19] Iijima S., Ichihashi T. [1993] Single-shell carbon nanotubes of 1-nm diameter. J. Nature, 363, 603-605.

[20] Tjong S. C. [2006] Structural and mechanical properties of polymer nanocomposites. J Material Science and Engineering, 53(3-4), 73-197.

[21] Lau K-T, Gu C. et al. [2004] Stretching process of single- and multi-walled carbon nanotubes for nanocomposite applications. J. Carbon, 42(2), 426-429.

[22] Demczyk B. G., Wang Y. M., Cumings J., Hetman M., Han W., Zettl A., Ritchie R. O. [2002] Direct mechanical measurement of the tensile strength and elastic modulus of multiwalled carbon nanotubes. J. Material Science and Engineering, 12, 934-935.

[23] Saito R., and Dresselhaus G., Dresselhaus M. S. [1998] Physical properties of carbon nanotubes. Imperial College Press, London, UK.

[24] Alexandre M., Dubois P. [2000] Polymer-layered silicate nanocomposites: preparation, properties and uses of a new class of materials. J. Material Science Engineering Reports,28 (1-2), 1-63.

[25] Hsiao K. T., Alms j., and Advani S. G. [2003] Use of epoxy/multiwalled carbon nanotubes as adhesives to join graphite fiber reinforced polymer composites. Nanotechnology, 14 (7), 791-793.

[26] Galliot C., Rousseau J., and Verchey G. [2012] Drop weight tensile impact testing of adhesively bonded carbon/epoxy laminate joints. International J of Adhesion and Adhesives, 35, 68-75.

[27] Harris J.A., Adams R. [1985] An assessment of the impact performance of bonded joints for use in high energy absorbing structures. Proc International Mechanical Engineering, 199(C2), 121-131.

[28] Goglio L., Rossetto M. [2008] Impact rupture of structural adhesive joints under different stress combinations. International J. Impact Engineering, 35(7), 635-643.

[29] Ger G.S., Kawata K., Itabashi M. [1996] Dynamic tensile strength of composite laminate joints fastened mechanically. J. Theoretical and Applied Fracture Mechanics, 24(2), 147–155.

[30] Kevin A. Brown K. A., Brooks R., Warrior N. A. [2010] The static and high strain rate behavior of a commingled E-glass/polypropylene woven fabric composite. Composites Science and Technology, 70(2), 272-283.

[31] Srivastava V. K., Hogg P. J. [1998] Moisture effects on the toughness, mode-I and mode-II of particles filled quasi-isotropic glass-fibre-reinforced polyester resin composites. J Mater Sci, 33 (5), 1129–1136.

[32] Srivastava V.K. [2011] Effect of carbon nanotubes on the strength of adhesive lap joints of C/C and C/C–SiC ceramic fibre composites. International J. of Adhesion and Adhesives, 31(6), 486–489.

[33] Yasmin A., Daniel I. M. [2004] Mechanical and thermal properties of graphite lapelet/epoxy composites. J Polymer, 45, 8211-8219.

[34] Yasmin A., Abot J. L. et al. [2006] Processing of clay/epoxy nanocomposites by shear mixing. Scripta Materialia, 49, 81-86.

[35] Volkersen O., [1938] The rivet load distribution in lap-joints with member of constant thickness subjected to tension. Luftfahrtforschung, 15, 41-47.

[36] Goland M., Reissner E. [1944] The stress in cemented joints. J Applied Mechanics, 11, A17-A27

[37] Ojalvo I. U., and Eidinoff H. L. [1978] Bond thickness upon stresses in single-lap adhesive joints. J. AIAA, 16(3), 204-211.

[38] Luo Q., and Tong I. [2004] Linear and higher order displacement theories for adhesive bonded lap joints. International J. Solids and Structures, 41 (22-23), 6351-6381.

[39] Allman D. J. [1977] A theory for the elastic stresses in adhesive bonded lap joints. Q J Mechanics and Applied Mathematics, 30(4), 415-436.

[40] Chen D. and Cheng S. [1983] An analysis of adhesive-bonded single-lap joints. J applied Mechanics, 50(1), 109-115.

[41] Carpenter W. [1980] Stresses in bonded connections using finite element. International J Numerical Methods in Engineering, 15(11), 1659-1680.

[42] Adams R. D. and Mallick V., A [1992] method for the stress analysis of lap joints. J Adhesives, 38(3-4), 219-242.

[43] Zhao B., and Lu Z. H. [2009] A two-dimensional approach of single-lap adhesive bonded joints. Mechanics of Advanced Materials and Structures, 16(2), 130-159.

[44] Hart-Smith L. J. [1973] Adhesive-bonded single-lap joints. NASA Langley Research Center, NASA CR-112235.

[45] Grant P. and Teig I. C. [1976] Strength and stress analysis of bonded joints, British Aircraft Corporation Ltd. Military Aircraft Division, Report no. SOR PJ 109.

[46] Delale F., Erdogan F., Aydinoglu M. N. [1981] Stresses in adhesively bonded joints-a closed form solution. J Composite Material, 15, 249-271.

[47] Bigwood D. A. and Crocombe A. D. [1990] Nonlinear adhesive bonded joint design analysis. International J Adhesion and Adhesives, 10(1), 31-41.

[48] Yang C. D., Huang H., Tomblin J. S., Sun W. J. [2004] Elastic-plastic model if adhesive-bonded single-lap composite joints. J Composite Material, 38(4), 293-309.

[49] Lee J. and Kim H. [2007] Elasto-plastic analysis of adhesively bonded symmetric single-lap joints under in-plane tension and edge moments. J adhesives, 83(9), 837-870.

[50] Blackman B. R. K., Hadavinia H., Kinloch A. J., and Williams J. G. [2003] The use of a cohesive zone model to study the fracture of fibre composites and adhesively-bonded joints. International J. Fracture, 119(1), 25–46.

[51] Li S., Thouless M. D., Waas A. M., Schroeder J. A., and Zavattieri P. D. [2005] Use of mode-I cohesive-zone models to describe the fracture of an adhesively-bonded polymer-matrix composite. Composites Science and Technology, 65(2), 281–293.

[52] Alfano G. and Crisfield M. A. [2001] Finite element interface models for the delamination analysis of composites: mechanical and computational issues. International J. Numerical Methods in Engineering, 50(7), 1701-1736.

[53] Xie D. and Biggers Jr S. B. [2006] Progressive crack growth analysis using interface element based on the virtual crack closure technique. Finite Element Analysis and Design, 42(11), 977-984.

[54] Karkkainen R. L. and Yen C. F. [2012] Dynamic modeling for rate-dependent and mode-dependent cohesive interface failure analysis. J. Composite Materials, 1-9.

[55] Shahin K., and Taheri F., The strain energy release rates in adhesively bonded balanced and unbalanced specimens and lap joints. International J. Solids and Structures, (2008), 45, 6248-6300.

[56] Mehrabadi F. A. [2012] Experimental and numerical failure analysis of adhesive composite joints. International J. Aerospace Engineering.

[57] Lundsgaard-Larsen C., Massabo R., and Cox B. N. [2009] The design of dynamic tests to infer rate dependence in large-scale crack bridging. Proceedings of the Society for Experimental Mechanics Annual Conference, June 2009, Albuquerque, NM.

[58] Anvari M., Scheider I. and Thaulow C. [2006] Simulation of dynamic ductile crack growth using strain-rate andtriaxiality-dependent cohesive elements. J. Engineering Fracture Mechanics, 73, 2210–2228.

[59] Zavattieri P. D., Hector L. G., and Bower A. F. [2008] Cohesive zone simulations of crack growth along a rough interface between two elastic-plastic solids J. Engineering Fracture Mechanics, 75, 4309–4332.

[60] Xu X. P. and Needleman A. [1994] Numerical simulation of fast crack growth in brittle solids. J Mechanics and Physics of Solids, 42(9), 187–218.

[61] Abaqus 6.10 Analysis user's manual [2010], DassaultSystèmesSimuliaCorp., Providence, RI.

[62] Ma J., Yan Y., and Yang L. [2012] Experimental and numerical investigations on the crashworthiness response of composite tubes. J Composite Materials. (In progress)

[63] Broughton W. R. and Hinopoulos G. [1999] Evaluation of the single-lap joint using finite element analysis. NPL Report CMMT(A) 206.

[64] Qin M. and Dznis Y. A. [2003] Analysis of single-lap adhesive composite joints with delaminated adherends. J. Composite Part B: Engineering, 34(2), 167-173.

[65] Adams R. D. and Peppiatt N. A. [1973] Effects of Poisson's ratio strains in adherends on stresses of an idealized lap joint J. Strain Analysis, 8(2), 134-139.

[66] Ward I. M., Sweeney J. [2004] An introduction to the mechanical properties of solid polymers. Wiley, Chichester.

[67] Crocombe A. D. [1989] Global yielding as a failure criterion for bonded joints. International J. Adhesion and Adhesives, 9(3), 145-153.

[68] Dorn L., Liu W. [1993] The stress state and failure properties of adhesive-bonded plastic/metal joints. International J. Adhesion and Adhesives, 13(1), 21-31.

[69] Wahab M. A., Ashcroft I. A., Crocombe A. D., Hughes D. J., Shaw S. J. [2001] The effect of environment on the fatigue of bonded composite joints. Part 2: Fatigue threshold prediction. Composite Part A, 32, 59-69.

[70] Liljedahl C. D. M. and Crocombe A. D. et al. [2007] Modelling the environmental degradation of adhesively bonded aluminium and composite joints using a CZM approach. International J Adhesion and Adhesives, 27(6),505-518.

[71] Hahn H. T., Choi O., and Wang Z. [2008] Development of nanoplatelet composites. University of California, Los Angeles. (technical report, ADA492125)

[72] Dowling N. [2007] Mechanical behavior of materials. Pearson Prentice Hall, Upper Saddle River.

[73] Prolongo S. G., Gude M. R., and Ureña A. [2010] Nanoreinforced Adhesives, Nanofibers, Ashok Kumar (Ed.): http://www.intechopen.com/books/nanofibers/ nanoreinforced-adhesives

[74] ASTM D3433-99 [2012] Standard Test Method for Fracture Strength in Cleavage of Adhesives in Bonded Metal Joints, ASTM International, West Conshohocken.

APPENDIX A EXPERIMENTAL TEST RESULTS

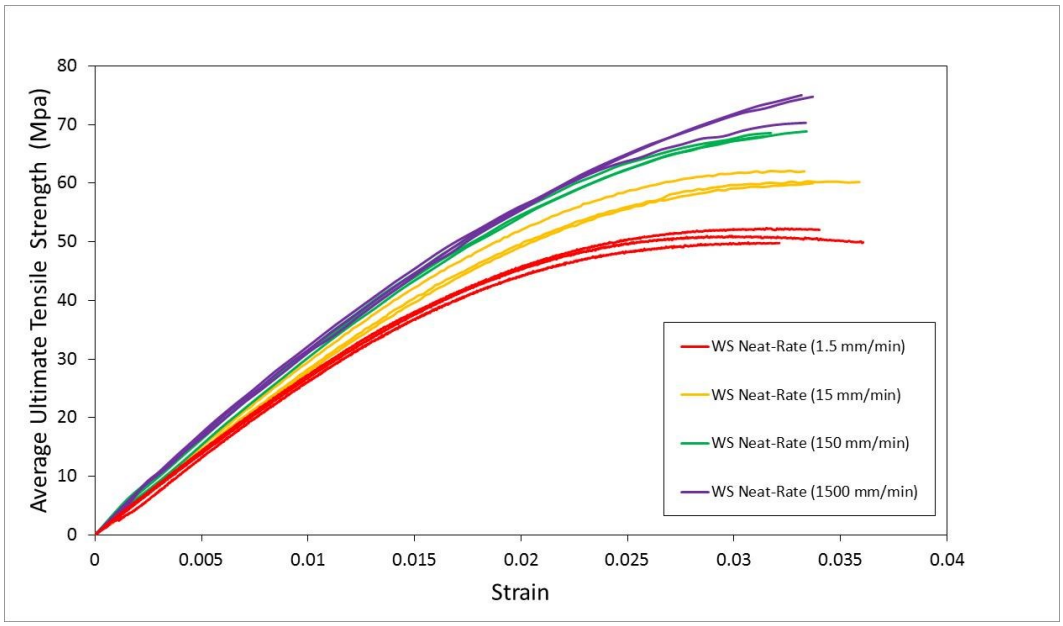

Fig. A.1 Loading rate effect on average ultimate tensile strength of neat West System resin.

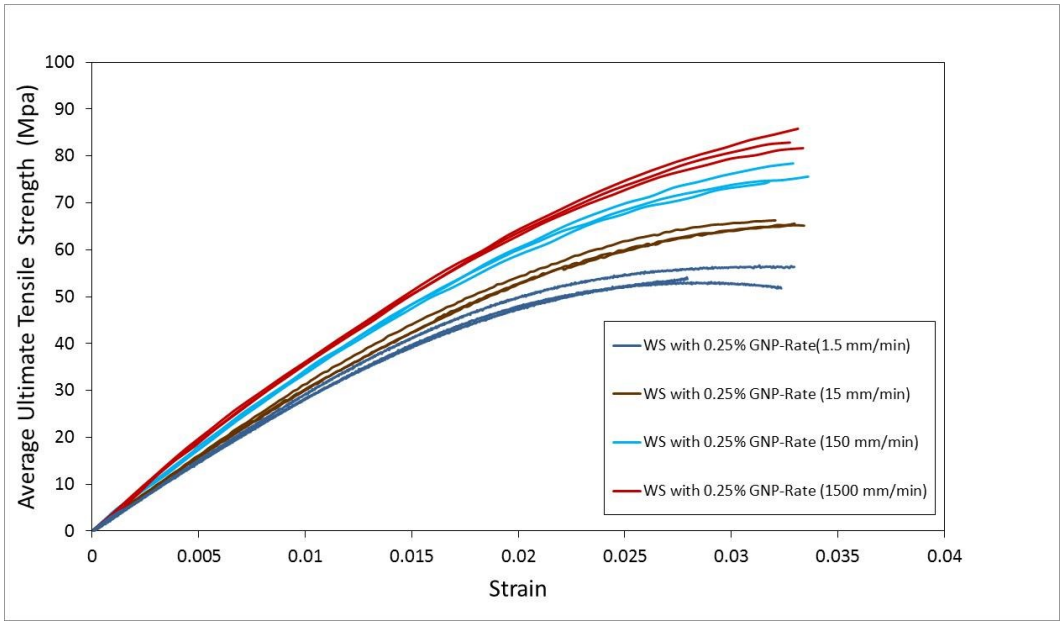

Fig. A.2 Loading rate effect on the average ultimate tensile strength of West System resin with 0.25% wt GNP.

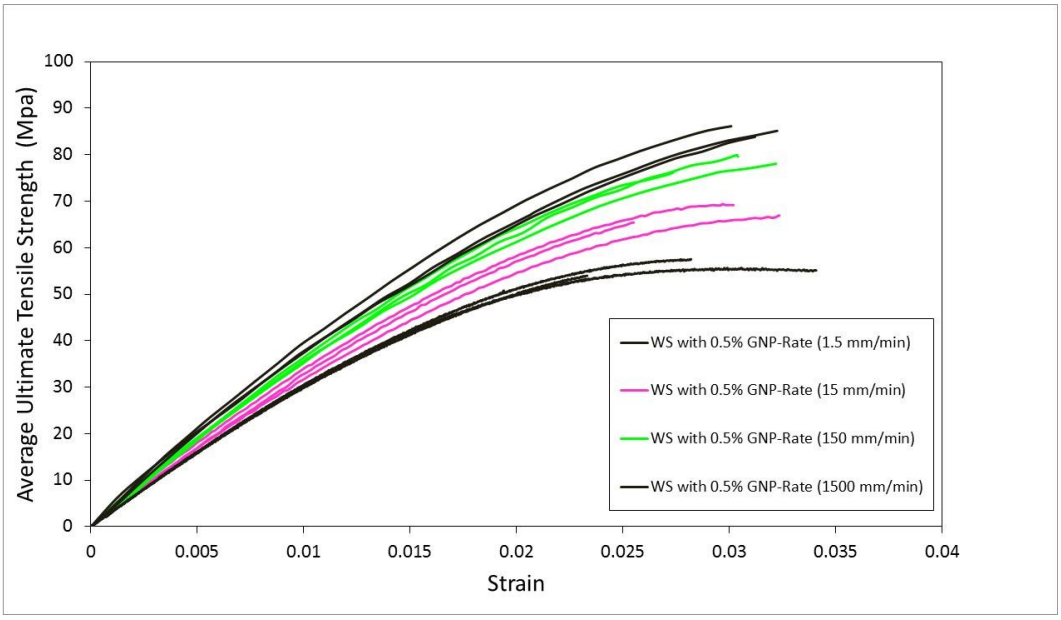

Fig. A.3 Loading rate effect on the average ultimate tensile strength of West System resin with 0.5% wt GNP.

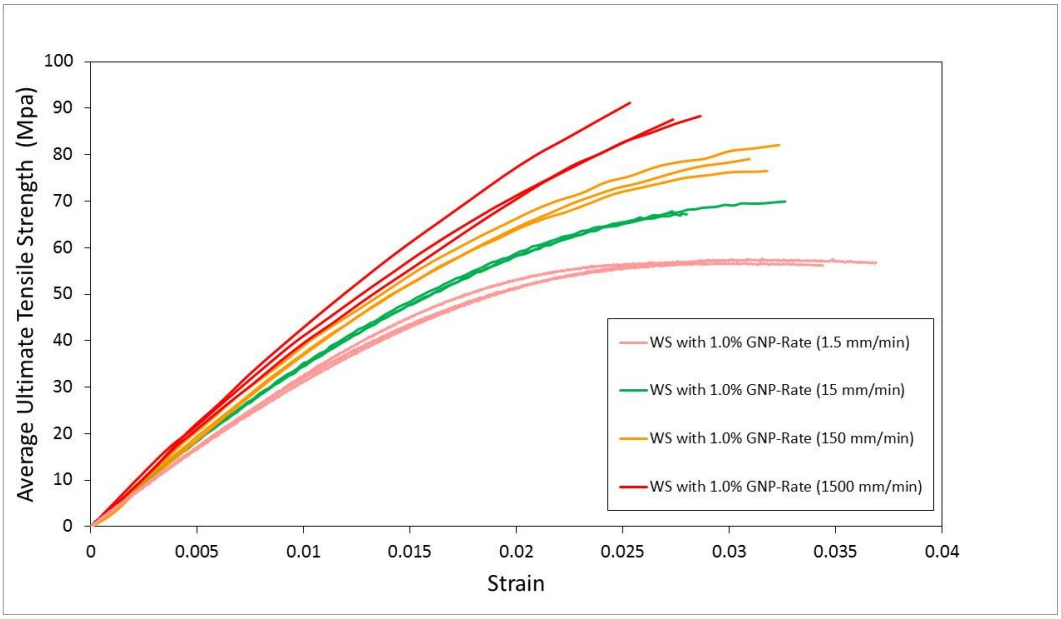

Fig. A.4 Loading rate effect on the average ultimate tensile strength of West System resin with 1.0% wt GNP.

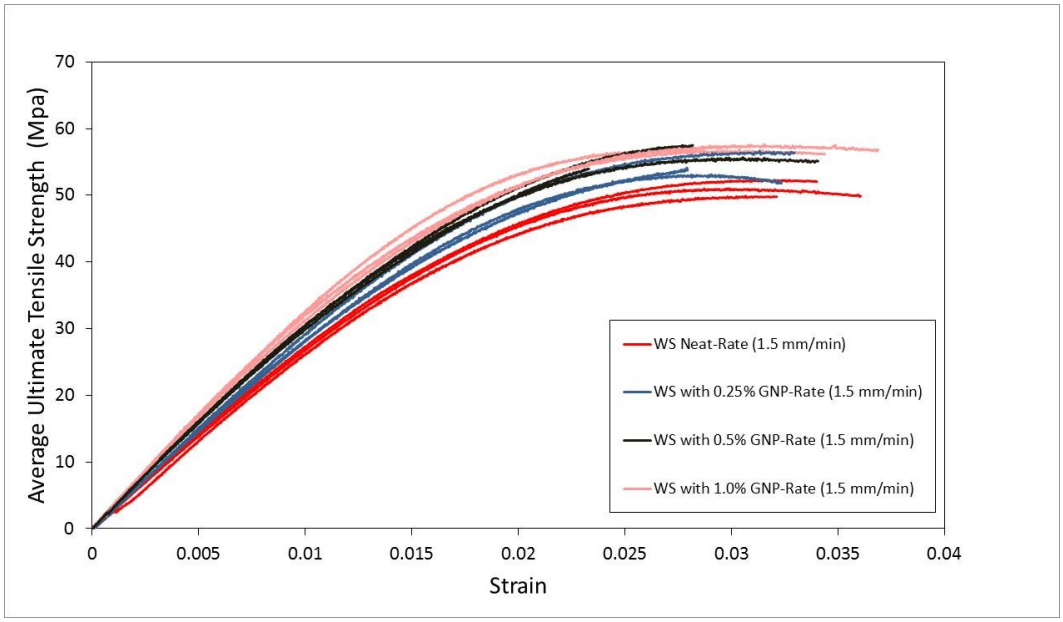

Fig. A.5 Influence of weight percentage of nano reinforcement on the average ultimate tensile strength of GNP reinforced West System resin (Rate=1.5 mm/min).

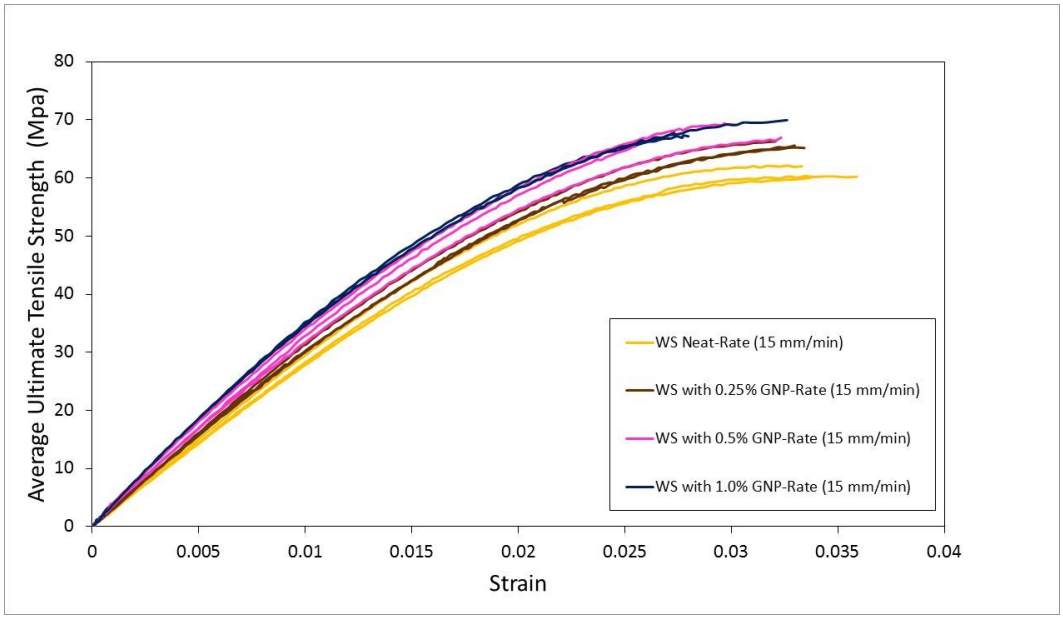

Fig. A.6 Influence of weight percentage of nano reinforcement on the average ultimate tensile strength of GNP reinforced West System resin (Rate=15 mm/min).

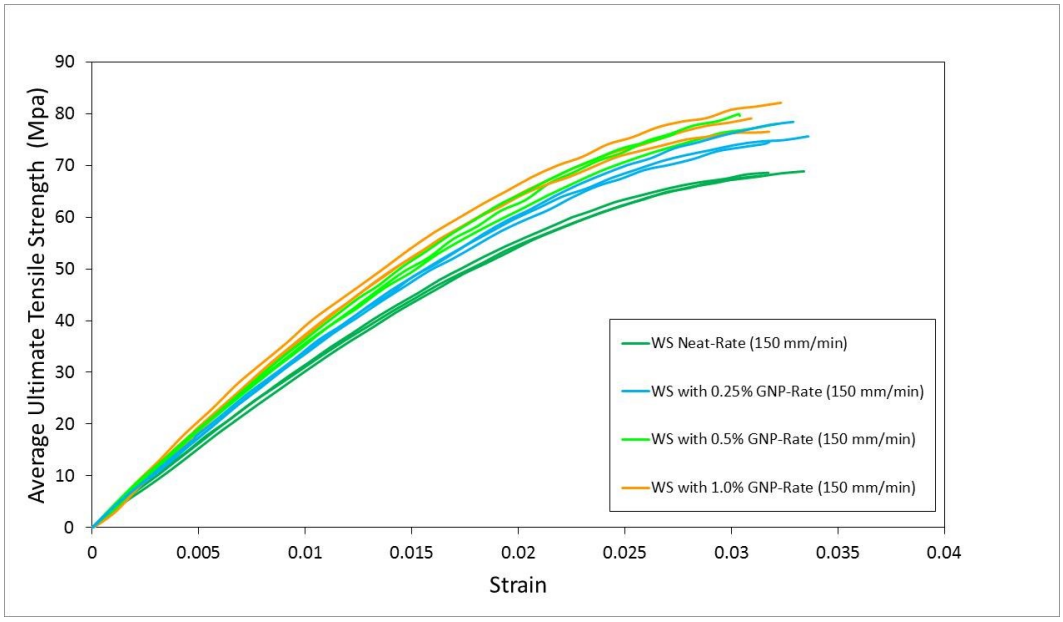

Fig. A.7 Influence of weight percentage of nano reinforcement on the average ultimate tensile strength of GNP reinforced West System resin (Rate=150 mm/min).

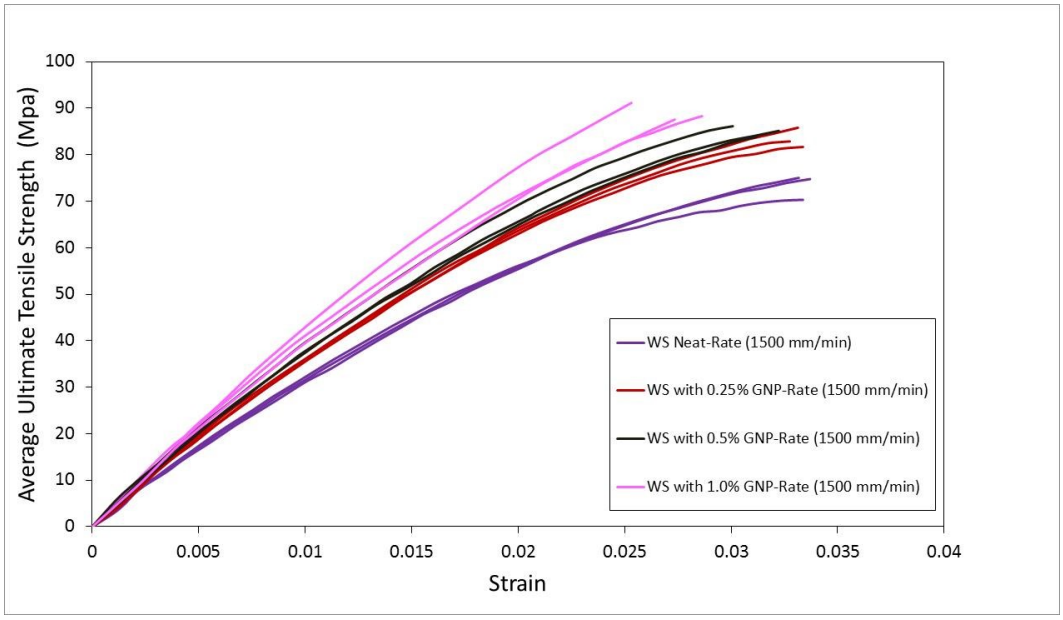

Fig. A.8 Influence of weight percentage of nano reinforcement on the average ultimate tensile strength of GNP reinforced West System resin (Rate=1500 mm/min).

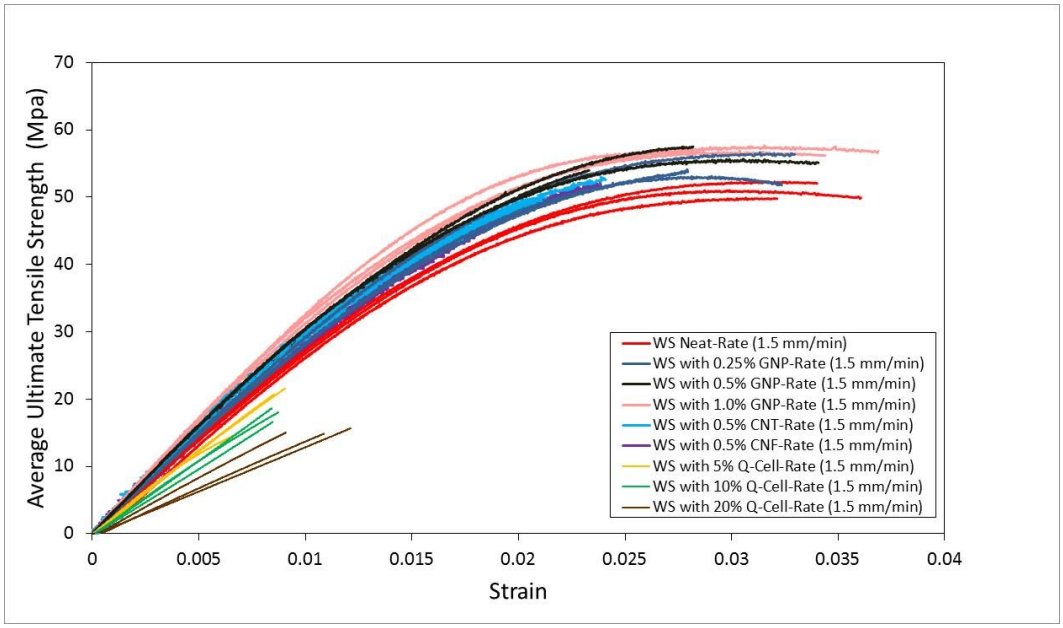

Fig. A.9 Influence of weight percentage and type of additives (Q-Cell filler, various nano particles) on the average ultimate tensile strength (Rate=1.5 mm/min).

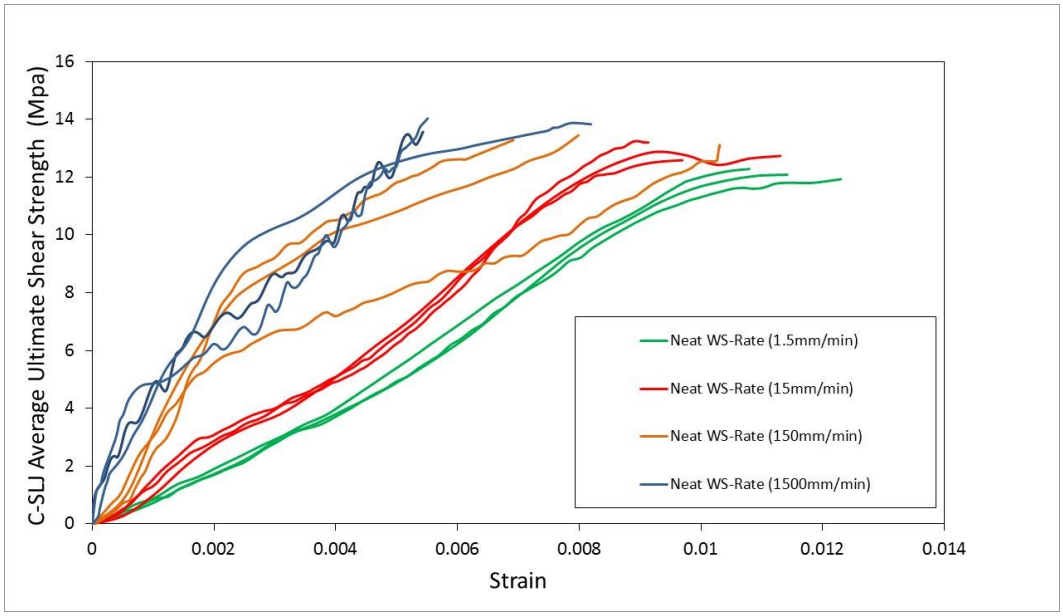

Fig. A.10 Loading rate effect on adhesively bonded single-lap joints with graphite/epoxy adherends.

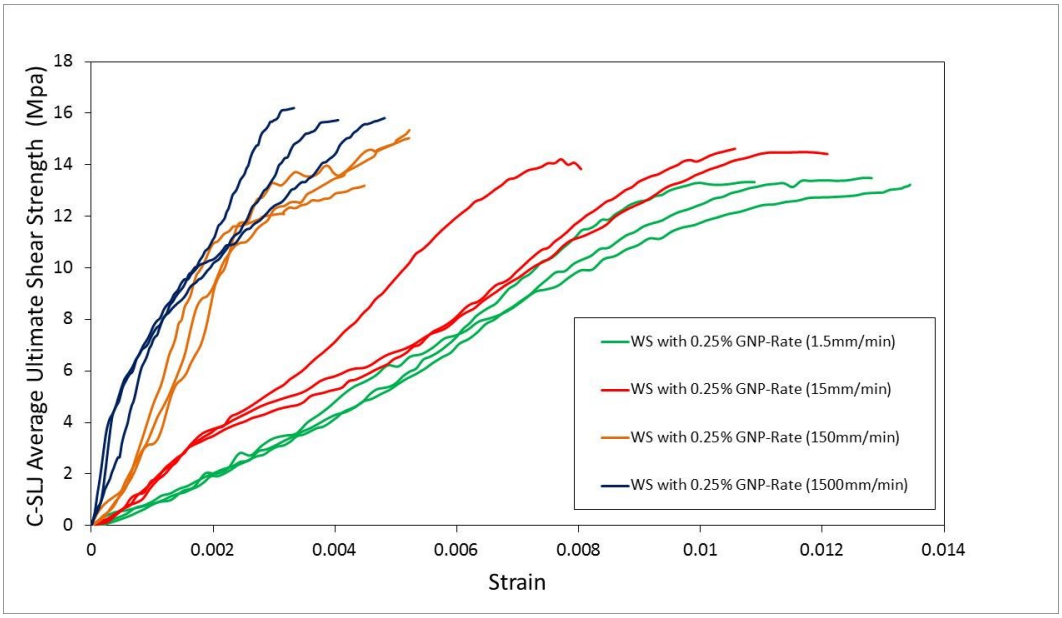

Fig. A.11 Loading rate effect on 0.25% wt GNP-reinforced adhesively bonded single-lap joints with graphite/epoxy adherends.

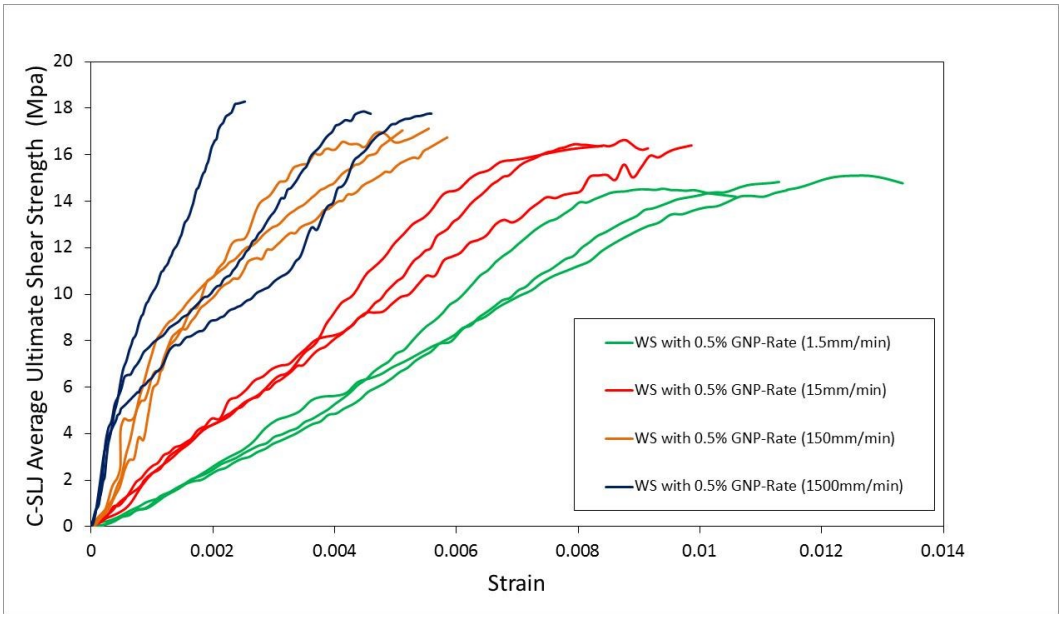

Fig. A.12 Loading rate effect on 0.5% wt GNP-reinforced adhesively bonded single-lap joints with graphite/epoxy adherends.

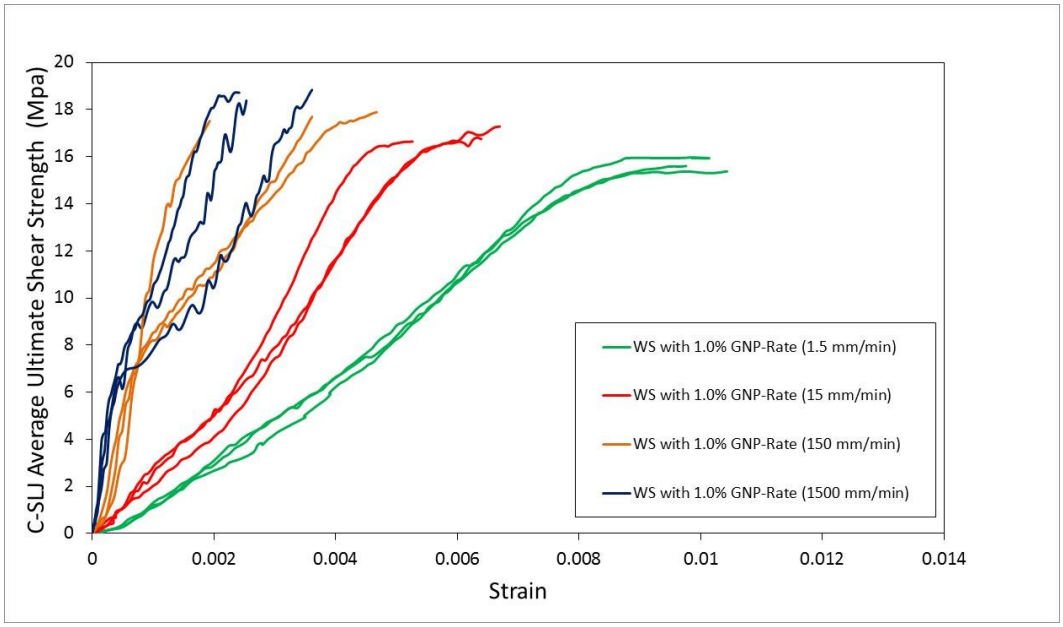

Fig. A.13 Loading rate effect on 1.0% wt GNP-reinforced adhesively bonded single-lap joints with graphite/epoxy adherends.

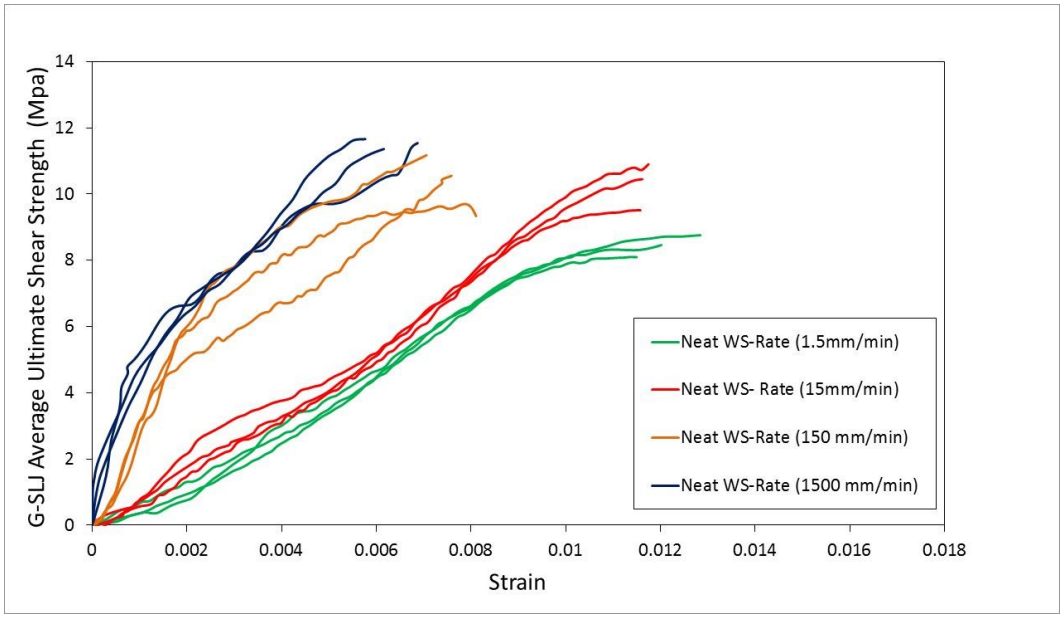

Fig. A.14 Loading rate effect on adhesively bonded single-lap joints with glass/epoxy adherends.

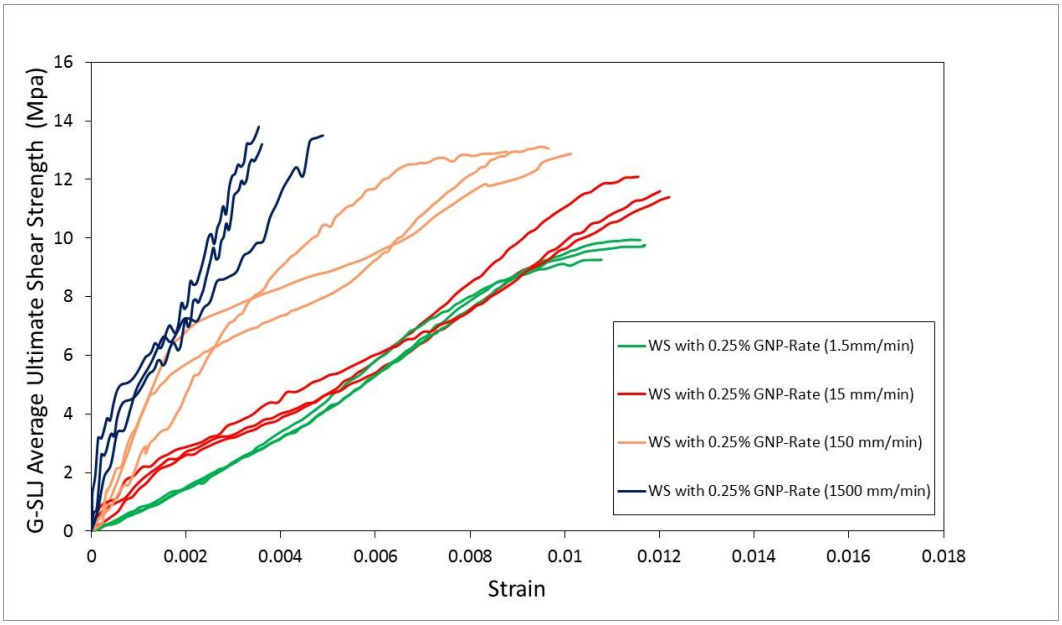

Fig. A.15 Loading rate effect on 0.25% wt GNP-reinforced adhesively bonded single-lap joints with glass/epoxy adherends.

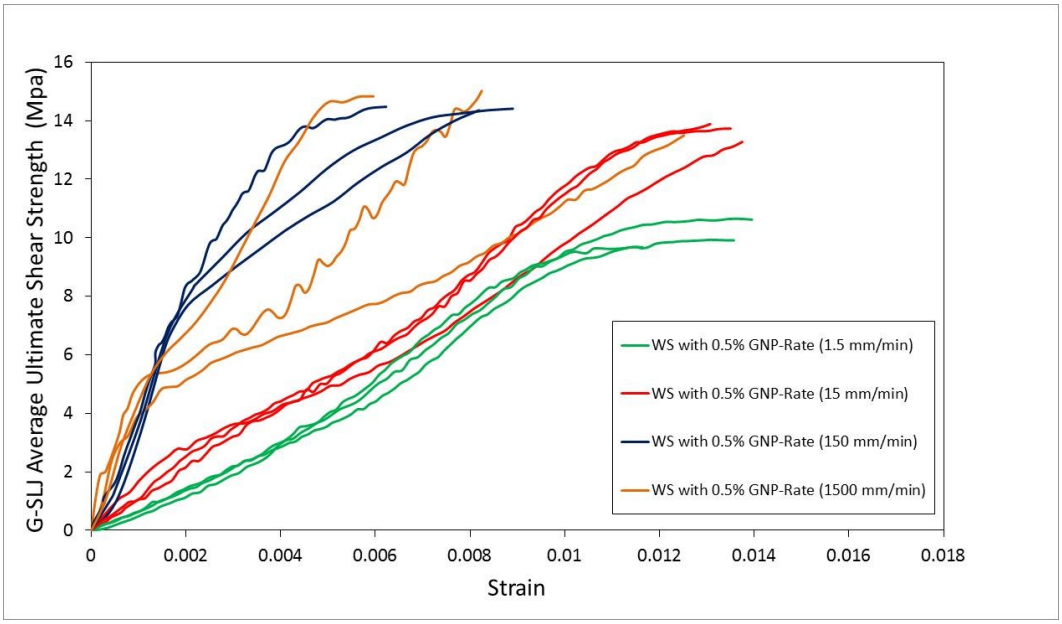

Fig. A.16 Loading rate effect on 0.5% wt GNP-reinforced adhesively bonded single-lap joints with glass/epoxy adherends.

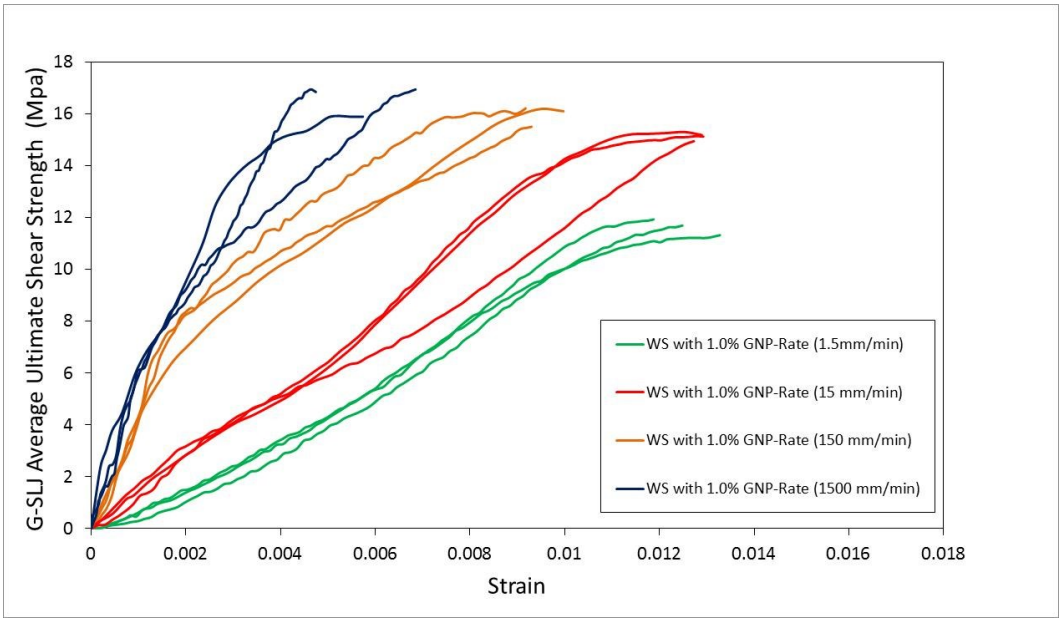

Fig. A.17 Loading rate effect on 1.0% wt GNP-reinforced adhesively bonded single-lap joints with glass/epoxy adherends.